5-28-2020 9:45 AM

Design, Fabrication and Applications of Efficient Conductive Polymers for Photocatalytic Antimicrobials

Chunbo Liu, *The University of Western Ontario*

Supervisor: Charpentier, Paul, *The University of Western Ontario*
A thesis submitted in partial fulfillment of the requirements for the Master of Engineering
Science degree in Chemical and Biochemical Engineering
© Chunbo Liu 2020

Abstract

Designing new antimicrobial surfaces which are effective under visible light irradiation without leaching toxic ions is a current challenge for effective disinfection. A new polymeric system poly[2,11'-thiophene-ethylene-thiophene-alt-2,5-(3-carboxyl) -thiophene] (PTET-T-COOH) with broad light absorption was synthesized. Its photocatalytic disinfection performance against staphylococcus aureus (*S. aureus*) and streptococcus suis (*S. suis*) was evaluated, showing over 99.999% inactivation (higher than 5-log inactivation) in 2 h for both bacteria, under visible light irradiation at a low concentration of PTET-T-COOH (0.1 mg/mL). In addition, a PTET-T-COOH/polyurethane (PU) polymeric coating was designed and fabricated. Chemical attachment was confirmed between PTET-T-COOH and PU using various thermophysical techniques (FTIR, XPS and UV-Vis absorption spectra). The coating was found to possess excellent photocatalytic disinfection effect on *S. aureus* (7-log inactivation) in 4 h under visible-light exposure. PTET-T-COOH and PTET-T-COOH/PU coating demonstrated good stability, showing excellent antibacterial activity after five runs. The chemical interaction was generated and confirmed between PTET-T-COOH and PU. The active species generated and responsible for the photocatalytic disinfection were confirmed to be singlet oxygen and free electrons by using scavengers and electron spin resonance spectroscopy (ESR) in PTET-T-COOH based systems. In addition, ultrathin graphitic carbon nitride (g-C_3N_4) nanosheets with rich amino groups (g-C_3N_4-NH_2) were also fabricated to inactivate more than 80 % of *S. aureus* in 2 h upon visible light exposure. The photocatalytic activities of g-C_3N_4-NH_2 and g-C_3N_4 were compared and the reasons for improved performance of g-C_3N_4-NH_2 were also analyzed. The results from this thesis will open a new strategy for exploring novel high-efficiency and durable disinfection coatings for living environmental and industrial applications.

Keywords

Summary for Lay Audience

Bacteria, viruses and fungi in our surroundings can lead to a variety of diseases. As the current COVID-19 pandemic is illustrating, it is of paramount importance to develop efficient antimicrobial materials which are both active and processable into various products. With the emergence of antibiotic-resistance, a range of conventional bactericides such as metal-based compounds, 2D antimicrobials, antibacterial polymers and chemical oxidizing agents have been extensively reported. However, some disadvantages of these materials are evident, including harmful heavy metals, hazardous by-products and side effects are always involved in the above materials. In addition, although ultraviolet irradiation as a disinfection technique was widely used in wastewater treatment, the cost is high, and the efficiency is limited when it was applied alone.

Photocatalytic technology has attracted tremendous attention and achieved a variety of successful applications in water splitting to produce H_2, CO_2 reduction and pollutants removal. Photocatalytic disinfection has also demonstrated effective inactivation of microbials. Compared with conventional antimicrobials and techniques, photocatalytic disinfection is more simple, environmental-friendly and sustainable. Under ambient condition with UV or visible light irradiation, electrons and holes can be generated in the photocatalysts and then react with water and oxygen to form a series of reactive oxygen species which can kill microbials efficiently.

A wide range of photocatalysts including inorganic and organic photoactive agents have been explored for disinfection applications. Compared to inorganic photocatalysts, organic photocatalytic antimicrobials such as polymers possess more potential for practical applications, needing the processability of the polymeric system. The objectives of this work are to explore efficient antibacterial polymers, including the following: (1) design and synthesis of polythiophene derivative (PTET-T-COOH) for efficient inactivation of bacteria upon visible light exposure, (2) fabrication of bilayer coating where polyurethane (PU) acts as protective layer and PTET-T-COOH/PU functions as a photoactive layer for efficient killing of bacteria. A robust chemical bonding was generated between PTET-T-COOH and PU which offered the excellent recycling stability of coating, (3) exploration of rich amino modified carbon nitride (g-C_3N_4) polymer with thin layers for efficient inactivation of bacteria.

Co-Authorship Statement

Title: Synthesis and photocatalytic antibacterial properties of poly [2,11'-thiophene-ethylene-thiophene-alt-2,5-(3-carboxyl)-thiophene]

Authors: Chunbo Liu, Paul A Charpentier, William Z. Xu

Chunbo Liu performed the experiment and carried out data analysis under the guidance Dr. William Xu. The draft of this manuscript was written by Chunbo Liu and revisions were carried out under the close supervision of Dr. Paul Charpentier (ACS Applied Polymer Materials, 2020, 2, 1886-1896.)

Acknowledgments

I would like to acknowledge that so many people, who have given me their encouragement & helps during the past two years in my academic pursuit.

First of all, I am really grateful to my supervisor, Dr. Paul A. Charpentier, who offered me the opportunity to work on this wonderful project, this project would not be completed without his guidance, support, and understanding.

I would like to thank my dear colleagues in the lab and at my work place, who helped me in finalizing this project within the limited time frame, chief among them I am so grateful to Dr. William Xu, who provided timely help whenever I am in need of one, and his valuable advice helped me moving forward with ease in my program.

My special thanks go to my friends, Dr. Haiyong Guo and Dr. Enwei Zhu, who helped me in the areas of photocatalytic disinfection and synthesizing polymers, respectively.

Finally, I would like to thank my family who gave me their love, understanding and support, which motivates me to carry this project to its fruition.

Table of Contents

List of Tables

List of Figures

List of Abbreviations

BMPO	3, 4-Dihydro-2-methyl-1,1-dimethylethyl ester-2H-pyrrole-2-carboxylic acid-1-oxide
CFU	Colony-Forming Units
DMPO	5,5-di-methyl-1-pyrroline N-oxide
EDTA-2Na	ethylenediaminetetraacetic acid disodium salt
E. coli	Escherichia coli
ESR	electron spin resonance
EIS	electrochemical impedance spectroscopy
g-C$_3$N$_4$	graphitic carbon nitride
IZ	inhibition zone
PEG2000	poly (ethylene glycol)2000
PTET-T-COOH	poly[2,11'-thiophene-ethylene-thiophene-alt-2,5-(3-carboxyl) - thiophene]
PTh	polythiophene
PU	polyurethane
ROS	reactive oxygen species
S. aureus	Staphylococcus aureus
S. suis	streptococcus suis
TBA	tertbutyl alcohol
TEMP	4-hydroxy-2,2,6,6-tetramethyl-1-piperidine

Chapter 1

1   Introduction

1.1   Background & Motivation

1.1.1   Urgency of exploring antimicrobials

Millions of people die from a variety of infectious diseases such as chickenpox, measles and typhoid globally every year. Pathogenic microorganisms including bacteria, viruses, spores and fungi can be transmitted by various routes to lead to infectious disease.[1] Although antibiotics play a vital role in defeating pathogens, antibiotic or multi-drug resistance arising from microbe evolution and abuse or overuse of broad-spectrum antibiotics in humans and animals have weakened their antimicrobial effects gradually. For example, some infections including gonorrhea, pneumonia, tuberculosis and salmonellosis are not as easy to treat as previously, as antibiotics are not effective. Antibiotic resistance is threatening our global health. In addition, antibiotic resistance will result in higher medical costs and increased death rate. Although many countries have adopted effective steps to control the use and dosage of antibiotics, efficient alternatives to kill or inhibit the multiplication of pathogenic microorganisms existing in our surroundings is of great urgency.

1.1.2   Classes of antimicrobials

Antimicrobials as efficient alternatives to antibiotics can be classified according to their spectrum of activity, effect on microbes and mode of action. Broad spectrum antimicrobials are those which are effective toward both Gram-positive and Gram-negative bacteria. However, some antimicrobials are only active against a particular species of microbe. Based on effects on microbes, antimicrobials can be divided into 1) bactericidal, which can kill bacteria and 2) bacteriostatic, which can only inhibit bacterial growth and replication. Based on modes of action, antimicrobials can be classified into cell wall synthesis inhibitors, cell membrane function inhibitors, protein synthesis inhibitors and metabolic process inhibitors.

1.1.3 Types and mechanisms of conventional antimicrobials and disinfection techniques

Metal-based antimicrobials

Nanomaterials based on metal elementals as antimicrobial agents are being regarded as a solution to the ever-growing problem of antibiotic resistance. Nanoparticles consisting of metal, metal oxides and carbon-based materials have been widely utilized for their antimicrobial activity. From ancient times, silver has been exploited as an efficient antimicrobials to treat infections resulting from bacteria, virus and other microorganisms.[2] The usage of silver nanoparticles underwent recession after the appearance of penicillin and revival with the increase of antibiotic-resistant microbes.[3, 4] Apart from silver, gold and copper metal nanoparticles have also been explored extensively.[5] Metal oxide antimicrobials with a primary focus on ZnO and TiO_2 nanoparticles have also received intensive investigation due to their low toxicity to human cells.[6-11]

The disinfection mechanisms of metal-based nanoparticles vary with the characteristics of microbes. In general, they can kill or inhibit microbes by the following mechanisms: (1) destruction of cell wall by binding or penetrating microbes; Inhabitation of cell wall synthesis by generation of reactive active species, (2) destruction of cell membranes of microbes or inhibition of their cell membrane function, (3) inhibition the syntheses of protein, enzyme and nucleic acid including DNA and RNA.

Although metal-based antimicrobials have been explored and applied to treat a range of infections, the study on toxicity of metal-based antimicrobials to human cells is still lacking. So, the appropriate use of metal-based nanoparticles in treating various infections should be necessary.

2D antimicrobials

A wide range of 2D antimicrobials and their action mechanisms were summarized.[12] These 2D antimicrobials mainly include graphene based materials, transition-metal dichalcogenides (TMDs) and transition-metal carbides/nitrides (MXenes). Graphene based materials consist of various graphene oxide (GO) and reduced graphene oxide (rGO) as

well as their derivatives. Graphene-based materials can kill or inhibit the growth of microbes by physical interaction with microbial cells and oxidative stress.[13, 14] However, toxicity raised by employment of graphene-based materials should not be ignored.[15] Similar to graphene materials, TMDs are also layered compounds consisting of transition metal elements (Mo, W, etc.) and chalcogen elements (S, Se, etc.) and can be formulated as MX_2.[16, 17] Among various TMDs, MoS_2[18-20] and WS_2[21] have been intensively explored due to their potential biomedical applications. Induction of oxidative stress by interaction and ions such as MoO_4^{2-} release are believed responsible for the mode of action of TMDs.[21] MXenes is a new class of 2D material which was reported in 2011[22] and examined as an antimicrobial in 2016.[23] Recent progress of MXenes in antimicrobial applications was surveyed.[24, 25] However, the research on MXenes used as antimicrobials is at a very early stage and systematic investigation on action mechanisms needs to be carried out.[24] Although the 2D materials mentioned above behave by their inactivation ability toward bacteria, the dosage of these materials is relatively high, likely resulting in safety concerns.

Antimicrobial polymers

A wide variety of antimicrobial polymers were summarized in several reviews.[26-28] Generally, these antimicrobial polymers can be divided into three classes: (1) polymers with intrinsic disinfection ability; (2) polymers modified by antimicrobial groups introduced in polymer structure; (3) polymer/antimicrobials composites. Here, polymers with intrinsic antimicrobial activity was emphasized including their types and antimicrobial applications.

Polymers with intrinsic disinfection ability can be classified into three categories including natural polymers, nitrogen-containing polymers and halogen-containing polymers. Chitosan and poly-ε-lysine are two common natural polymers and various composites based on these two materials have been reported.[29-32] Nitrogen-containing polymers mainly refer to linear quaternary ammonium compounds (QACs),[33-35] ring quaternary polymers, polyethylenimine and poly(ionic liquid)s.[36, 37] Among these nitrogen-containing polymers, linear quaternary ammonium salts have received the most attention. Halogen-containing polymers are referred to N-halamine polymers in which nitrogen and halogen atoms such

as fluorine, chlorine, bromine and iodine are covalently bonded to form imide, amide or amine groups.[37, 38]

These polymers summarized above all belong to cationic polymers. They can kill or inhibit the growth of microbes by similar action modes such as electrostatic interactions between positive charged polymer biocidal with negatively charged microorganism which can lead to the cell wall or membrane destruction. However, most cationic antimicrobial polymers can result in hemolysis which may be a detrimental side-effect.

Chemical oxidizing agents

Several common disinfection methods were utilized to remove pathogens. Among them, chemical oxidation by using chlorine, chlorine dioxide, hydrogen peroxide and ozone as strong oxidizing agents was widely employed due to their highly efficient disinfection ability.[39] In this process, oxidizing ingredients can destroy cell membrane of microorganisms and make protein, deoxyribonucleic acid (DNA) and ribonucleic acid (RNA) release. This can influence and disturb a series of enzymes and inhibit the glycometabolism finally resulting in the death of microbials. However, hidden safety danger originating from the formation of hazardous by-products such as trihalomethanes in this process limits its further practical applications.

Ultraviolet irradiation

Ultraviolet irradiation can denature DNA and RNA of microorganism cells and inhibit their replication. However, this method suffers due to its high operational costs. In addition, the application of UV irradiation technique alone may be ineffective for UV-resistant microbes and can damage polymeric systems.

Hence, an efficient, facile, recyclable, environment-friendly, low cost and non-toxic method which can be integrated into polymers to easily form coatings or parts is still required to deal with pathogenic microorganisms.

1.2   Thesis Objectives & Structure

The main target of this work is to explore novel, low cost, efficient, stable and environmentally friendly photocatalytic antimicrobials and fabricate stable antimicrobial coatings based on the as-prepared samples.

In this thesis, the first objective is to design and synthesize a novel polythiophene derivative PTET-T-COOH which is presented in chapter 3. By using staphylococcus aureus (*S. aureus*) and streptococcus suis (*S. suis*) as model bacteria, the photocatalytic activity of PTET-T-COOH is evaluated. PTET-T-COOH demonstrated excellent antibacterial capability toward these two bacteria under visible light irradiation in 2 h with very low concentration (0.1 mg mL^{-1}). The relationship between the chemical structure of PTET-T-COOH and its antibacterial performance is examined. In addition, the action mode of PTET-T-COOH is elucidated by rabbit plasma test, fluorescence microscopy observation of bacteria, active species trapping experiments, electron spin resonance (ESR) analysis and photochemical measurements such as photocurrent response.

The second target is to design and fabricate stable and effective photocatalytic coatings by combining PTET-T-COOH with polyurethane (PU) (chapter 4). Chemical bonding was confirmed to form successfully between the carboxyl groups of PTET-T-COOH and NCO-terminated pre-polyurethane by ATR-FTIR spectra and XPS analyses. By using *S. aureus* as a model bacterium, the photocatalytic activity and recycling stability of PTET-T-COOH/PU coating were conducted and discussed. PTET-T-COOH/PU coating possessed excellent photocatalytic bactericidal effect on *S. aureus* (7 log inactivation) in 4 h upon visible-light exposure. In addition, the coating fabrication process was optimized and transparent light yellow PTET-T-COOH/PU coating was obtained finally.

The last target in this work is to synthesize g-C$_3$N$_4$ nanosheets with rich amino groups (g-C$_3$N$_4$-NH$_2$). Using urea as raw material, thermal polymerization and exfoliation methods were applied to obtain g-C$_3$N$_4$-NH$_2$. *S. aureus* was also examined as a model microbe to evaluate the antimicrobial activities of g-C$_3$N$_4$-NH$_2$ and bulk g-C$_3$N$_4$ which was examined as a reference sample. Photoluminescence, photocurrent density and electrochemical

impedance spectra (EIS) were carried out to explore the reasons for the improvement of photocatalytic antibacterial performance of g-C_3N_4-NH_2 compared to bulk g-C_3N_4.

1.3   References

1. Machado‑Moreira, B.; Richards, K.; Brennan, F.; Abram, F.; Burgess, C. M., Microbial contamination of fresh produce: what, where, and how? *Comprehensive Reviews in Food Science and Food Safety* **2019,** *18* (6), 1727-1750.

2. Siddiqi, K. S.; Husen, A.; Rao, R. A., A review on biosynthesis of silver nanoparticles and their biocidal properties. *Journal of Nanobiotechnology* **2018,** *16* (1), 14.

3. Barabadi, H.; Vahidi, H.; Kamali, K. D.; Rashedi, M.; Hosseini, O.; Ghomi, A. R. G.; Saravanan, M., Emerging Theranostic silver nanomaterials to combat colorectal cancer: a systematic review. *Journal of Cluster Science* **2019**, 1-11.

4. Rahimi, M.; Noruzi, E. B.; Sheykhsaran, E.; Ebadi, B.; Kariminezhad, Z.; Molaparast, M.; Mehrabani, M. G.; Mehramouz, B.; Yousefi, M.; Ahmadi, R., Carbohydrate polymer-based silver nanocomposites: recent progress in the antimicrobial wound dressings. *Carbohydrate Polymers* **2019**, 115696.

5. Lee, K. X.; Shameli, K.; Yew, Y. P.; Teow, S.-Y.; Jahangirian, H.; Rafiee-Moghaddam, R.; Webster, T. J., Recent developments in the facile bio-synthesis of gold nanoparticles (AuNPs) and their biomedical applications. *International Journal of Nanomedicine* **2020,** *15*, 275.

6. Zhu, Y.; Wu, J.; Chen, M.; Liu, X.; Xiong, Y.; Wang, Y.; Feng, T.; Kang, S.; Wang, X., Recent advances in the biotoxicity of metal oxide nanoparticles: Impacts on plants, animals and microorganisms. *Chemosphere* **2019,** *237*, 124403.

7. Mahamuni-Badiger, P. P.; Patil, P. M.; Badiger, M. V.; Patel, P. R.; Thorat-Gadgil, B. S.; Pandit, A.; Bohara, R. A., Biofilm formation to inhibition: Role of zinc oxide-based nanoparticles. *Materials Science and Engineering: C* **2019**, 110319.

8. Akbar, S.; Tauseef, I.; Subhan, F.; Sultana, N.; Khan, I.; Ahmed, U.; Haleem, K. S., An overview of the plant-mediated synthesis of zinc oxide nanoparticles and their antimicrobial potential. *Inorganic and Nano-Metal Chemistry* **2020**, 1-15.

9. Maheswari, P.; Harish, S.; Navaneethan, M.; Muthamizhchelvan, C.; Ponnusamy, S.; Hayakawa, Y., Bio-modified TiO_2 nanoparticles with Withania somnifera, Eclipta prostrata and Glycyrrhiza glabra for anticancer and antibacterial applications. *Materials Science and Engineering: C* **2020,** *108*, 110457.

10. Mustapha, S.; Ndamitso, M.; Abdulkareem, A.; Tijani, J.; Shuaib, D.; Ajala, A.; Mohammed, A., Application of TiO_2 and ZnO nanoparticles immobilized on clay in wastewater treatment: a review. *Applied Water Science* **2020,** *10* (1), 1-36.

11. Bhattacharya, P.; Neogi, S., Antibacterial properties of doped nanoparticles. *Reviews in Chemical Engineering* **2019,** *35* (7), 861-876.

12. Sun, W.; Wu, F. G., Two‐dimensional materials for antimicrobial applications: graphene materials and beyond. *Chemistry – An Asian Journal* **2018,** *13* (22), 3378-3410.

13. Zou, X.; Zhang, L.; Wang, Z.; Luo, Y., Mechanisms of the antimicrobial activities of graphene materials. *Journal of the american chemical society* **2016,** *138* (7), 2064-2077.

14. Alimardani, V.; Abolmaali, S. S.; Borandeh, S., Antifungal and antibacterial properties of graphene-based nanomaterials: A Mini-review. *Journal of Nanostructures* **2019,** *9* (3), 402-413.

15. Syama, S.; Mohanan, P., Comprehensive application of graphene: emphasis on biomedical concerns. *Nano-Micro Letters* **2019,** *11* (1), 6.

16. Kim, T. I.; Kim, J.; Park, I.-J.; Cho, K.-O.; Choi, S.-Y., Chemically exfoliated 1T-phase transition metal dichalcogenide nanosheets for transparent antibacterial applications. *2D Materials* **2019,** *6* (2), 025025.

17. Li, X.; Shan, J.; Zhang, W.; Su, S.; Yuwen, L.; Wang, L., Recent advances in synthesis and biomedical applications of two‐dimensional transition metal dichalcogenide nanosheets. *Small* **2017,** *13* (5), 1602660.

18. Wu, R.; Ou, X.; Tian, R.; Zhang, J.; Jin, H.; Dong, M.; Li, J.; Liu, L., Membrane destruction and phospholipid extraction by using two-dimensional MoS_2 nanosheets. *Nanoscale* **2018,** *10* (43), 20162-20170.

19. Kaur, J.; Singh, M.; Dell'Aversana, C.; Benedetti, R.; Giardina, P.; Rossi, M.; Valadan, M.; Vergara, A.; Cutarelli, A.; Montone, A. M. I., Biological interactions of biocompatible and water-dispersed MoS_2 nanosheets with bacteria and human cells. *Scientific reports* **2018,** *8* (1), 1-15.

20. Kim, T. I.; Kwon, B.; Yoon, J.; Park, I.-J.; Bang, G. S.; Park, Y.; Seo, Y.-S.; Choi, S.-Y., Antibacterial activities of graphene oxide–molybdenum disulfide nanocomposite films. *ACS applied materials & interfaces* **2017,** *9* (9), 7908-7917.

21. Cheng, P.; Chen, Y.; Yan, X.; Wang, Y.; Lang, W. Z., Highly stable and antibacterial two‐dimensional tungsten disulfide lamellar membrane for water filtration. *ChemSusChem* **2019,** *12* (1), 275-282.

22. Naguib, M.; Kurtoglu, M.; Presser, V.; Lu, J.; Niu, J.; Heon, M.; Hultman, L.; Gogotsi, Y.; Barsoum, M. W., Two‐dimensional nanocrystals produced by exfoliation of Ti_3AlC_2. *Advanced Materials* **2011,** *23* (37), 4248-4253.

23. Rasool, K.; Helal, M.; Ali, A.; Ren, C. E.; Gogotsi, Y.; Mahmoud, K. A., Antibacterial activity of Ti_3C_2T x MXene. *Acs Nano* **2016,** *10* (3), 3674-3684.

24. Huang, H.; Jiang, R.; Feng, Y.; Ouyang, H.; Zhou, N.; Zhang, X.; Wei, Y., Recent development and prospects of surface modification and biomedical applications of MXenes. *Nanoscale* **2020,** *DOI: 10.1039/c9nr07616f.*

25. Huang, K.; Li, Z.; Lin, J.; Han, G.; Huang, P., Two-dimensional transition metal carbides and nitrides (MXenes) for biomedical applications. *Chemical Society Reviews* **2018,** *47* (14), 5109-5124.

26. Kenawy, E.-R.; Worley, S.; Broughton, R., The chemistry and applications of antimicrobial polymers: a state-of-the-art review. *Biomacromolecules* **2007,** *8* (5), 1359-1384.

27. Siedenbiedel, F.; Tiller, J. C., Antimicrobial polymers in solution and on surfaces: overview and functional principles. *Polymers* **2012,** *4* (1), 46-71.

28. Jain, A.; Duvvuri, L. S.; Farah, S.; Beyth, N.; Domb, A. J.; Khan, W., Antimicrobial polymers. *Advanced Healthcare Materials* **2014,** *3* (12), 1969-1985.

29. Ahmed, K. B. M.; Khan, M. M. A.; Siddiqui, H.; Jahan, A., Chitosan and its oligosaccharides, a promising option for sustainable crop production-a review. *Carbohydrate Polymers* **2019**, 115331.

30. Miguel, S. P.; Moreira, A. F.; Correia, I. J., Chitosan based-asymmetric membranes for wound healing: A review. *International Journal of Biological Macromolecules* **2019,** *127*, 460-475.

31. Perinelli, D. R.; Fagioli, L.; Campana, R.; Lam, J. K.; Baffone, W.; Palmieri, G. F.; Casettari, L.; Bonacucina, G., Chitosan-based nanosystems and their exploited antimicrobial activity. *European Journal of Pharmaceutical Sciences* **2018,** *117*, 8-20.

32. Hu, X.; Yang, L. L.; Wang, K.; Wei, Y. Z.; Deng, H.; Dong, J., Studies of mechanical properties of electrospun zein/poly (ε-caprolactone) composites and antibacterial properties against Listeria monocytogenes strains of zein/poly (ε-caprolactone)/poly (ε-lysine) films. *Textile Research Journal* **2018,** *88* (24), 2800-2809.

33. Obłąk, E.; Piecuch, A.; Rewak-Soroczyńska, J.; Paluch, E., Activity of gemini quaternary ammonium salts against microorganisms. *Applied Microbiology and Biotechnology* **2019,** *103* (2), 625-632.

34. Brycki, B. E.; Kowalczyk, I. H.; Szulc, A. M.; Brycka, J. A., Quaternary alkylammonium salts as cleaning and disinfectant agents. *Tenside Surfactants Detergents* **2018,** *55* (6), 432-438.

35. Jiao, Y.; Niu, L.-n.; Ma, S.; Li, J.; Tay, F. R.; Chen, J.-h., Quaternary ammonium-based biomedical materials: State-of-the-art, toxicological aspects and antimicrobial resistance. *Progress in Polymer Science* **2017,** *71*, 53-90.

36. Jin, L.; Shi, Z.; Zhang, X.; Liu, X.; Li, H.; Wang, J.; Liang, F.; Zhao, W.; Zhao, C., Intelligent antibacterial surface based on ionic liquid molecular brushes for bacterial killing and release. *Journal of Materials Chemistry B* **2019,** *7* (36), 5520-5527.

37. Wang, M.; Shi, J.; Mao, H.; Sun, Z.; Guo, S.; Guo, J.; Yan, F., Fluorescent imidazolium-type poly (ionic liquid) s for bacterial imaging and biofilm inhibition. *Biomacromolecules* **2019,** *20* (8), 3161-3170.

38. Liang, J.; Zeng, J.; Li, J.; She, J.; Tan, R.; Liu, B., Cationic antimicrobial polymers. *PROGRESS IN CHEMISTRY* **2019,** *31* (9), 1263-1282.

39. Ogunniyi, A. D.; Dandie, C. E.; Ferro, S.; Hall, B.; Drigo, B.; Brunetti, G.; Venter, H.; Myers, B.; Deo, P.; Donner, E., Comparative antibacterial activities of neutral electrolyzed oxidizing water and other chlorine-based sanitizers. *Scientific Reports* **2019,** *9* (1), 1-13.

Chapter 2

2 Literature Review

Photocatalytic antibacterial technology has attracted significant attention due to its promising applications in water disinfection and microbial killing.[1] The design and selection of photocatalysts are of great importance for efficient disinfection. Numerous photo-active antibacterial agents including organic photo-sensitizers[2, 3] and inorganic photo-catalysts such as TiO_2,[4] ZnO,[5] NiO,[6] $g\text{-}C_3N_4$[7] and bismuth based compounds[8] have been explored as antibiotic alternatives for bacterial infection treatment. In this thesis, an overview of the types of photocatalytic antibacterial agents is presented. The underlying inactivation mechanisms of these materials is also summarized. Moreover, this thesis emphasizes on the recent advances in design and fabrication of polythiophene (PTh) and $g\text{-}C_3N_4$ based antibacterial agents as well as polyurethane (PU) photocatalytic antibacterial coatings.

2.1 Photocatalytic disinfection

Infections by microbes is a large concern for human health in areas such as medical treatments, hygienic applications and health care products. The existence of detrimental microorganisms is known to produce numerous infections and illnesses. So, it is important to maintain these fields free from pollution. Traditional antibacterial agents including quaternary ammonium compounds, 2-D materials with sharp edge like graphene, hypochlorite, hydrogen peroxide, metal particles or film and other reactive oxygen species (ROS) have been investigated extensively. However, these techniques always involve low efficiency, high cost and harmful disinfection byproducts. Therefore, high efficiency, low cost and environment-friendly techniques are of interest.

Semiconductor photocatalytic techniques have been known to be successful in environmental remediation with a primary focus on pollutant removal and energy exploration such as water splitting to produce H_2 in the past 30 years.[9-12] The pioneering work of photocatalytic inactivation of bacteria using TiO_2 to kill various bacterial cells including *E.coli*, Lactobacillus acidophilus, and Saccharomyces cerevisiae was reported in

1985.[13] From these origins, photocatalytic antibacterial technology has attracted increasing attention. Under light irradiation, semiconductor photocatalysts can generate various active species such as h^+, e^-, $^1O_2$, $\cdot OH$, $\cdot O_2^-$ and H_2O_2 etc. for killing bacteria, fungi, virus, microalgae and other pathogens.[14] This technique has been known to be promising for developing next-generation green and sustainable environmental disinfection systems.

2.1.1   Materials of photocatalytic disinfection

Since the first report on bactericidal properties of anatase TiO_2,[13] various photocatalysts were explored for photocatalytic disinfection. According to the ingredients, these photocatalysts can be divided into five types including metal oxides (TiO_2, ZnO, Fe_3O_4, CuO),[15-17] metal sulfides (CdS, MoS, CuS),[18-20] metal particles,[21, 22] carbon nitride,[23] nanocarbon materials (fullerenes, nanodiamonds, carbon dots, carbon nanotubes, and graphene-family materials),[24-26] metal-organic frameworks[27] and conductive polymers.[28] During the past several decades, the photocatalytic disinfection field was dominated by TiO_2 and ZnO due to their high efficiency, stability and non-toxicity. However, TiO_2 and ZnO can only be conducted under UV light which will limit their further practical applications. In order to harvest solar light, visible light responsive photocatalysts has attracted much attention. Recently, Wang group surveyed various visible light responsive photocatalysts as antimicrobials[29] including nanoscale metal (Ag), metal oxide (doped TiO_2, WO_3), metal sulfide (MoS_2, CuS, Ag_2S), metal-containing complex compounds ($MnWO_4$, $BiVO_4$, Ag_3PO_4), carbon-based nanomaterials (carbon dots, graphene),[30] nitride compounds (g-C_3N_4) and conductive polymers (polyaniline, polythiophene).[28] For selection of a photocatalytic agent, those antimicrobials with strong visible light absorption ability, low cost, environment-friendly and non-toxicity are advocated. Compared to the above summarized photocatalysts, the conductive polymers can be processed easily to obtain various antibacterial coatings. In addition, they always possess broad visible light spectra response and have been incorporated with a range of nanoscale photocatalytic agents to increase their light absorption abilities and antibacterial performance.[28]

2.1.2 Mechanism of photocatalytic disinfection

Generally, the photocatalytic disinfection process starts with photogenerated electrons and holes. When a semiconductor is irradiated with UV-Visible light with energy higher than its band gap, the electrons (e^-) can be excited to its conduction band (CB), thus leaving a hole (h^+) in its valence band (VB). Then, these charge carriers (e^-/h^+ pair) separate from each other and migrate to the surface/interface of the photocatalyst. Afterwards, a series of redox reactions occur to form various active species involving $\bullet OH, \bullet O_2^-$, $^1O_2$, H_2O_2, etc.. Finally, these active species can oxidize or interact with cellular components resulting in disruption of the cell membrane and cell wall. Figure 2.1 illustrates the photocatalytic disinfection process by using TiO_2 as an example.[31]
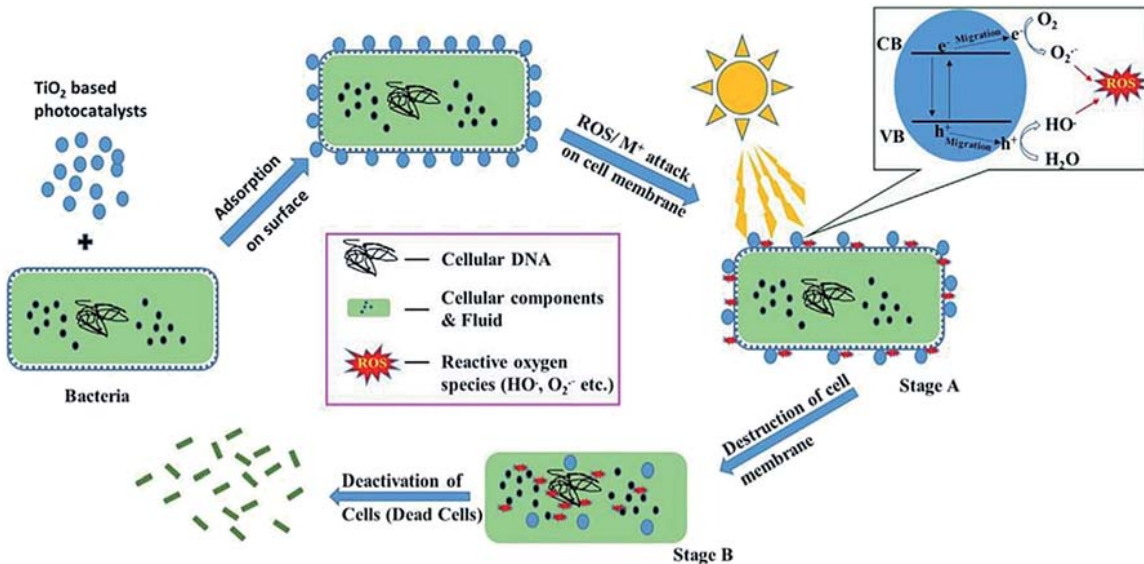
Figure 2.1. The disinfection process of photocatalysts by Reddy, P. A. K. et al. 2016.

2.2 Characterization of photocatalytic disinfection performance

Generally, there are several methods to characterize the photocatalytic activity of as-prepared samples.

Zone inhibition test is used to evaluate the antimicrobial property of photocatalysts. For zone of inhibition measurements, a suitable amount of photocatalyst is placed in the plate

with bacteria suspension. After the plate is incubated at 37 °C for 24 h, the zone area of inhibition without bacteria growth is measured which is the clear area surrounding the photocatalyst.[32]

The bacterial viability (survival ratio) is widely employed to express the inactivation efficiency of antimicrobials and can be calculated by the following equation, survival ratio $= (1-C_t/C_0) \times 100\%$ where C_t and C_0 are the concentration of bacteria cells at time t and time 0, respectively. The concentrations of bacteria cell (Colony-Forming Units, CFU/mL) can be obtained by counting the number of bacteria cells in the agar plate manually.[33] Change of CFU in the form of $\log_{10}$ with the reaction time is widely used and potent to demonstrate the disinfection efficiency of photoactive antimicrobials.[33]

The effects of photocatalytic agents on microbes' integrity can be investigated by scanning electron microscopy (SEM) or transmission electron microscopy (TEM). For example, the morphology of *S. aureus* cells changed with irradiation time in the presence of carbon-coated bismuth/cobalt nanoparticles (Figure 2.2).[34] Before the photocatalytic reaction, *S. aureus* is observed with round and plump shape with smooth membrane (a). After 5 min reaction, shrinkage of the cell membrane and pits on the surface of *S. aureus* cell are clearly observed (b). With increasing irradiation time, the extent of distortion of *S. aureus* cells was enhanced (c, d and e). Half an hour later, serious shrinkage of the cell membranes was observed, and many pores led to total distortion of *S. aureus* from round to a flat shape (f), indicating the cell membrane was seriously damaged.
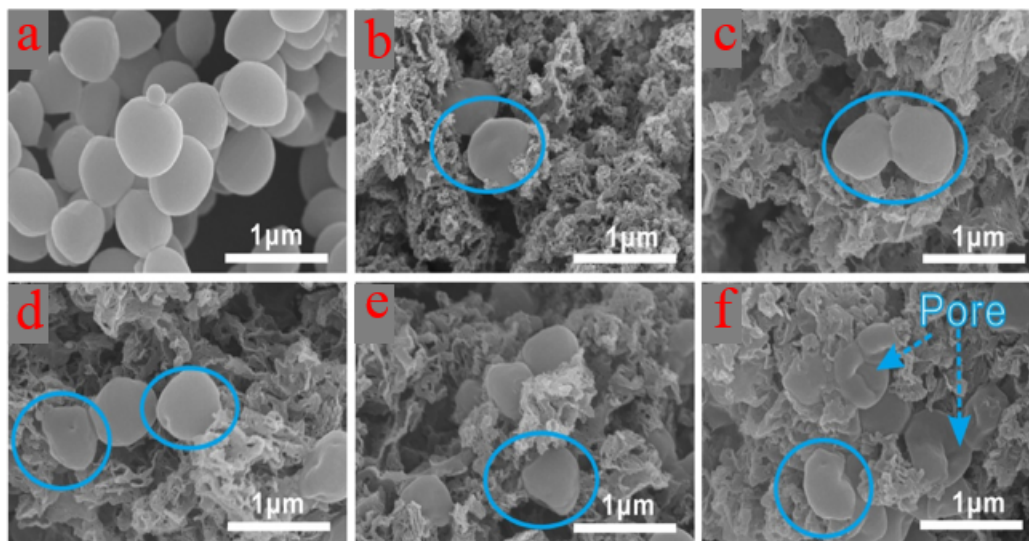
Figure 2.2. SEM images of *S. aureus* with the increase of irradiation time in the presence of photocatalyst by Wang, R. et al. 2019.

Compared to SEM, TEM images can show the change of cell inclusions before and after treatment with photocatalysts more clearly. As demonstrated in Figure 2.3, after disinfection, *S. aureus* and *E. coli* all presented obvious leakage of protein (red arrows) and rupture of cell membranes (dark arrows).[35]
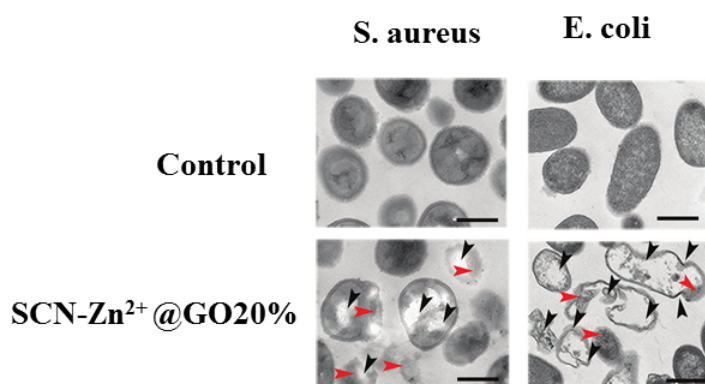
Figure 2.3. TEM images of *S. aureus* and *E. coli* without and with treatment by SCN-Zn^{2+}@GO20% after illumination for 10 min by Li, Y. et al. 2018.

To further confirm the effects of photocatalysts on microbes, cell live/dead test can be conducted by using laser scanning fluorescence microscopy. STYO9 and PI are common

stains used in this test. STYO9 is a green fluorescent nucleic acid dye which can pass through the cell membrane and thus can label live and dead cells including gram-positive and gram-negative bacteria. In contrast, PI cannot go through the cell membrane and only label dead cells. From the fluorescent images, the effects of disinfection can be observed intuitively. In addition, 4',6-diamidino-2-phenylindole (DAPI) can also penetrate the cell membrane and stain live cells with blue fluorescence. As shown in Figure 2.4, after 2 h treatment with GO/g-C$_3$N$_4$, more dead *E. coli* cells (red) were found, indicating *E. coli* cells were effectively inactivated by GO/g-C$_3$N$_4$. This is in agreement with the very low survival rate of 2.1 %.[36]
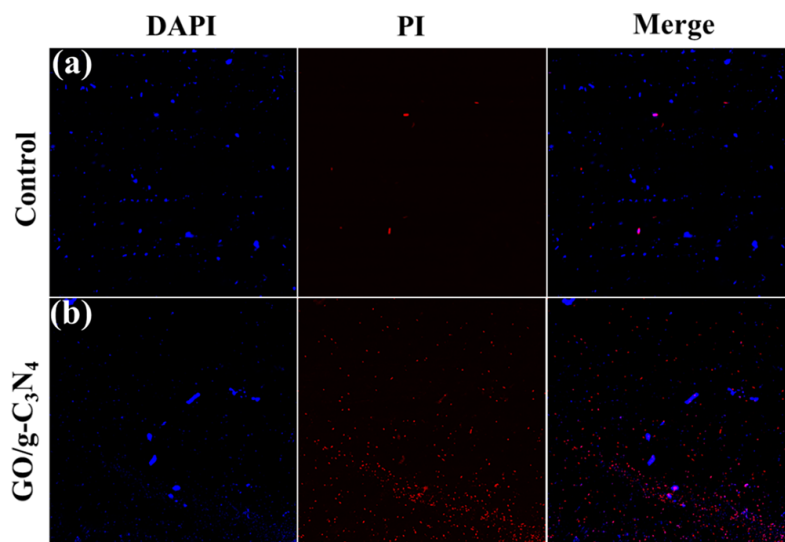
Figure 2.4. Fluorescent images of live and dead *E. coli* cells in control and treated by GO/g-C$_3$N$_4$ under illumination for 2 h by Sun, L. et al. 2017.

Stability of antimicrobials can be characterized by studying the survival ratio or cell density under the same conditions by using the recovered antimicrobials for several cycles, which is of great importance for practical applications of photoactive antimicrobials.

2.3 Study of photocatalytic disinfection mechanism

In order to elucidate the action modes of antimicrobials, the confirmation of active species killing or inhibiting microbes and discussion of dissociation of generated electron-hole pairs in disinfection process are essential.

Determination of active species

To confirm active species, two methods are widely used. One is active species trapping experiments in which various scavengers were added to a suspension of bacteria and photocatalyst individually and the disinfection efficiencies are compared. Generally, active species include holes (h^+), electrons (e^-), hydroxyl radicals (•OH), superoxide radicals (•O_2^-), singlet oxygen ($^1O_2$) and hydrogen peroxide (H_2O_2). Ethylenediaminetetraacetic acid disodium salt (EDTA-2Na), $K_2Cr_2O_7$, tertbutyl alcohol (TBA), L-ascorbic acid, NaN_3 and Fe (II) were applied as the scavengers for h^+, e^-, •OH, •O_2^-, $^1O_2$ and H_2O_2, respectively. The decrease of disinfection efficiency indicates that the active species trapped by corresponding scavengers plays vital roles in disinfection process.

Electron spin resonance measurements

Apart from trapping experiments, for confirming active species in photocatalytic reaction, another method is to measure the electron spin resonance (ESR) signals of photocatalyst solution in the presence of different scavengers under darkness and light irradiation. 5,5-di-methyl-1-pyrroline N-oxide (DMPO) and 3, 4-dihydro-2-methyl-1,1-dimethylethyl ester-2H-pyrrole-2-carboxylic acid-1-oxide (BMPO) are common scavengers for trapping •O_2^- and •OH. 4-hydroxy-2,2,6,6-tetramethyl-1-piperidine (TEMP) was used to consume $^1O_2$ in ESR measurements. As shown in Figure 2.5, under light illumination, GO/g-C_3N_4 showed stronger characteristic signals •OH (four peaks) and •O_2^- (six peaks) than g-C_3N_4, suggesting more active radicals were generated in GO/g-C_3N_4.[36]
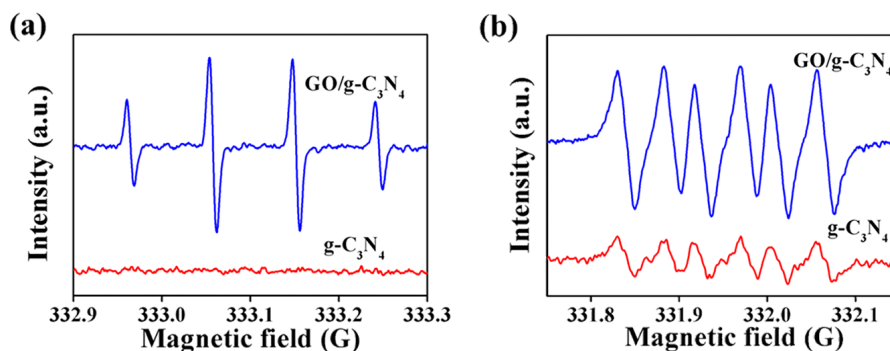
Figure 2.5. Comparison of ESR signals of (a) DMPO−•OH and (b) DMPO−•O_2^- between g-C_3N_4 and GO/g-C_3N_4 under visible light illumination by Sun, L. et al. 2017.

Photoelectrochemical measurements

Photocurrent signals and electrochemical impedance spectroscopy (EIS) are widely applied to evaluate the separation efficiency of photogenerated electron-hole pairs and charge transfer ability of photocatalysts. For example, as demonstrated in Figure 2.6, GO/g-C_3N_4 presented higher photocurrent response and lower electrochemical impedance than g-C_3N_4, indicating more free charge carriers were generated and transferred. This can account for the enhanced photocatalytic activity of photocatalysts.[36]
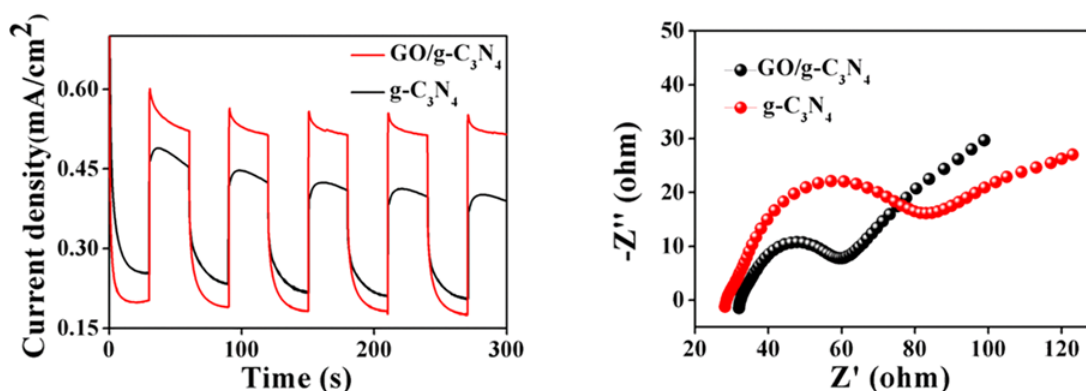
Figure 2.6. Comparison of (left) photocurrents and (right) electrochemical impedance spectroscopy of GO/g-C_3N_4 and g-C_3N_4 by Sun, L. et al. 2017.

2.4 Applications of polythiophene and its derivatives based photocatalysts in photocatalytic disinfection

Photodynamic antimicrobial polymers can produce reactive oxygen species (ROS) with oxygen in the surrounding and disinfect a range of pathogenic microorganisms when exposed to light illumination.[37] Various antibacterial coatings were explored by incorporating photosensitizers with polymer substrates or matrixes.[38, 39] In comparison with inorganic photocatalytic antibacterial agents, conductive polymers with delocalized structure possess many advantages including broad visible light absorption and easy processability. The first application of a series of water soluble cationic conjugated polyelectrolytes (CPEs) in photocatalytic antibacterial field was reported in 2008.[40] From then on, polyaniline (PANI), polypyrrole (PPy), poly(3,4-ethylenedioxythiophene) (PEDOT)) and polythiophene (PTh) have been incorporated with various semiconductor

nanomaterials to improve the photocatalytic activity of composites by extending their spectral responsive range and enhancing the separation efficiency of photogenerated electron-holes pairs.[28] Among these conductive polymers, PTh is of great interest. The pioneering work of photocatalytic inactivation of bactericides based on PTh was reported in 2006.[41] In this work, a novel composite photocatalyst was fabricated by incorporating thiophene with ZSM-5 zeolite. Under irradiation, reactive hydroxyl radicals were generated. The composite photocatalyst gives effective inactivation toward Staphylococcus aureus (*S. aureus*) and Escherichia coli (*E. coli*). In 2009, an anionic water-soluble polythiophene (PTP) was incorporated with a cationic porphyrin (TPPN) to form a complex via electrostatic interaction. Efficient energy transfer occurs between PTP and TPPN and singlet oxygen ($^1O_2$) kill the bacteria effectively (Figure 2.7).[42]
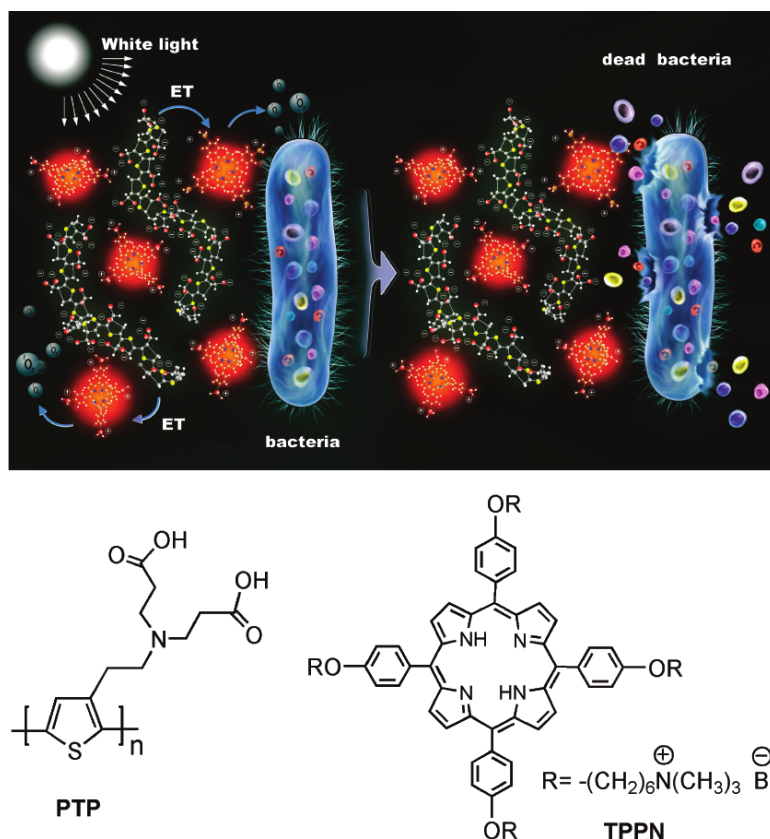
Figure 2.7. Schematic antibacterial mechanism of PTP/TPPN complex and chemical structures of PTP and TPPN by Xing, C. et al. 2009.

In 2010, a cationic polythiophene (PMNT) can act as a multifunctional agent for simultaneous killing cancer cells (cell carcinoma (A498)) and apoptosis imaging applications.[43] In 2011, a polythiophene/MnO$_2$ nanocomposite bactericide was reported. Under solar light irradiation, *E. coli* and *S. aureus* were killed efficiently. Almost all initial bacteria were killed in 6 h under solar light illumination. Hydroxyl radicals were found to play a vital role in the photocatalytic disinfection process.[44] In 2013, a flexible anti-microbial film was fabricated by incorporating polyterthiophene (PTTh) with porphyrin. Under white light, *E. coli* was efficiently killed by the singlet oxygen generated via fluorescence resonance energy transfer from PTTh to porphyrin.[45] In 2014, Cu doped ZnO/PTh composite was fabricated by in situ polymerization of thiophene in the presence of as-prepared Cu doped ZnO. The nanocomposite with 80 wt% of Cu doped ZnO showed the largest inhibition zone (IZ) diameter against three bacteria including *E. coli*, *S. aureus* and Candida albicans (C. albicans) compared to pure PTh, Cu-doped ZnO and other nanocomposites with different content of Cu doped ZnO.[46] In 2017, an imidazolium-functionalized PTh (P3HT-Im) was fabricated via Grignard metathesis controlled polymerization. Under visible light illumination, P3HT-Im was found to kill gram-positive and gram-negative bacteria efficiently. Furthermore, it showed non-toxicity to mammalian cells at a low concentration, as shown in Figure 2.8. [47]
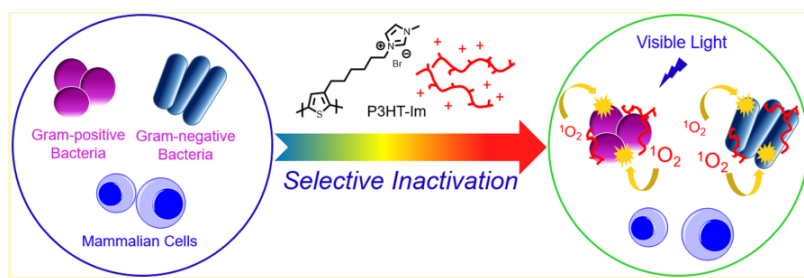
Figure 2.8. Chemical structure and photocatalytic disinfection mechanism of P3HT-Im by Huang, Y. et al. 2017.

In 2018, P3HT-Im and P3HT-T which are functionalized poly(3-hexylthiophene) (P3HT) by imidazolium and tertiary amines with different sizes were reported to kill *E. coli* and Bacillus atrophaeus efficiently both under dark and when illuminated. Figure 2.9 shows the chemical structures and synthetic process of P3HT-Im and P3HT-T. This work

compared the disinfection mechanisms of these two polymers and investigated the effects of size on photocatalytic performance.[48]
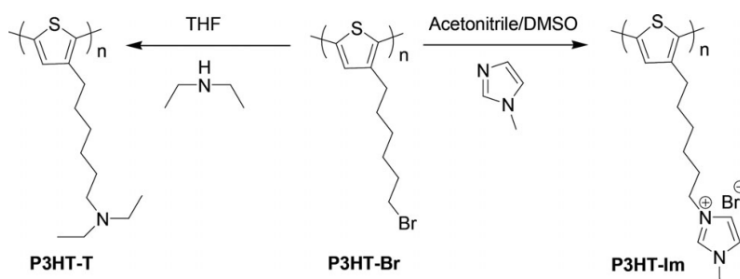
Figure 2.9. Synthetic route of P3HT-Im and P3HT-T by Brown, D. M. et al. 2018.

In 2019, enantiopure polythiophene nanoparticles with R or S chiral carbons (Figure 2.10) were reported to demonstrate opposite antibacterial abilities toward *E. coli* and *S. aureus*. In addition, these two materials showed non-toxicity to living mouse fibroblast cells. However, the antibacterial activities of these two materials were not satisfactory.[49]
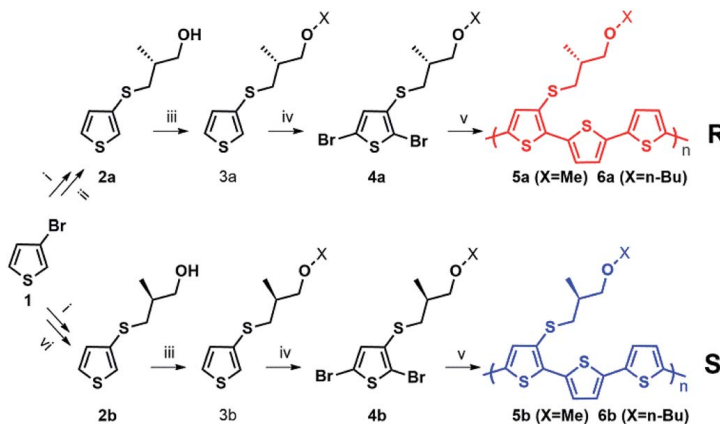
Figure 2.10. Synthetic routes of R and S chiral polythiophenes by Palamà, I. E. et al. 2019.

2.5 Fabrications and applications of PU coatings in photocatalytic disinfection

Polyurethane (PU) is a polymer consisting of a chain of repeating units connected by carbamate (urethane) links. It has been usually employed as biomaterials and matrix of photocatalysts thanks to its superior physical and mechanical properties and excellent

biocompatibility. Till now, TiO$_2$/PU composites dominated PU based photocatalytic antibacterial coatings. In 2012, a stable TiO$_2$/PU composite coating was fabricated by using 2,2-bis(hydroxymethyl) propionic acid (DMPA) as a binder which connects TiO$_2$ and PU by chemical bonding. Under solar light illumination, only 1 % of *E. coli* can survive within 60 min.[50] In 2013, Ag/TiO$_2$ was electro-sprayed on the PU composite nanofiber mat to form a photocatalytic coating which showed better inactivation toward *S. aureus* compared to Ag/TiO$_2$ and pure PU coating.[51] In 2014, TiO$_2$-fly ash/PU composite coating was fabricated by electrospinning the blend solution of TiO$_2$, fly ash and polyurethane. Compared to pure PU, fly ash/PU, and TiO$_2$/PU coatings protected mats, TiO$_2$-fly ash/PU composite coating behaved superior antibacterial activity, as depicted in Figure 2.11.[52]
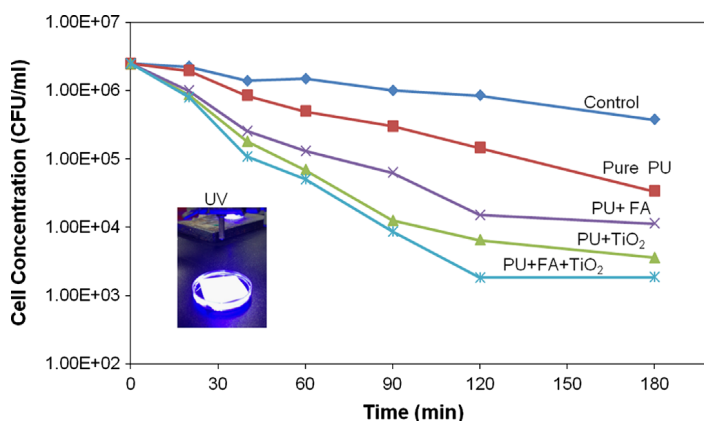
Figure 2.11. Antibacterial performance of mats protected by different coatings against *E. coli* bacteria under UV radiation by Kim, H. J. et al. 2014.

In 2015, waterborne PU/doped TiO$_2$ was obtained by deposition the mixture of doped TiO$_2$ and waterborne PU and then drying at room temperature. *E. coli* growth was efficiently inhibited compared to PU coating.[53] In addition, anatase and rutile TiO$_2$ were mixed with waterborne PU to obtain composites by conditioning the mixture at 50 ºC for several days. This work showed that anatase TiO$_2$/PU has better photocatalytic antifungal activity toward Aspergillus niger.[54] Another paper on PU based photocatalytic coating is also about TiO$_2$/PU coating which was fabricated by dipping stainless steel in a suspension of TiO$_2$ and PU. The composite coating demonstrated a reduction of 3.5-log CFU/cm^2 in 2 h against *E. coli*.[55] In 2016, rutile TiO$_2$ was used as a nanofiller of a styrene acrylic PU matrix to inhibit the growth of *E. coli*. The composite was fabricated by using ultrasonication. In

addition, the weight loss, impact strength and adhesion of the neat coating were greatly improved after the addition of TiO$_2$ nanoparticles.[56] In 2017, a PU-Acrylate-Ag/TiO$_2$ coating was made by in-situ polymerization in the presence of dispersed Ag/TiO$_2$ nanocomposites particles which can function as photoinitiator. In this case, only 3 % of *E.coli* cells can survive within 150 min. [57] In 2018, a hydrophobic carbon quantum dots (hCQDs)/PU coating was fabricated by dipping PU pieces into hCQDs solution and the hCQDs were encapsulated in PU matrix. Then the swelling PU containing hCQDs was dried at 80 °C for 12 h to obtain composite coating. Under blue light illumination, *S. aureus* and *E. coli* showed 5-log reduction within 60 min.[58] Dopamine/ZnO nanorod/PU ternary composite was obtained by immersing as-prepared electro-spun PU mats in the solutions of dopamine and precursor solution of ZnO in sequence. Then the composite was treated via a hydrothermal method to give dopamine/ZnO nanorod/PU ternary nanofiber, as illustrated in Figure 2.12. The composite nanofiber demonstrated better photocatalytic inactivation against *E. coli* and possessed excellent recycling stability. [59]
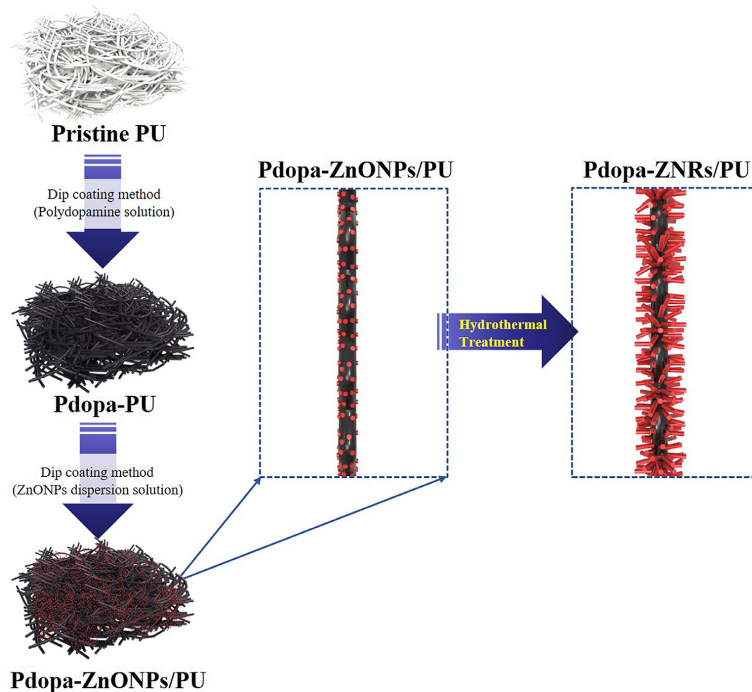
Figure 2.12. Fabrication process of Pdopa-ZnO/PU-coated nanofiber by Kim, J. H. et al 2018.

In 2019, a ternary composite of Ag/TiO$_2$/WPU was fabricated by a facile method where Ag nanoparticles, TiO$_2$ and waterborne were integrated together as the emulsion reaction finished. Over 99 % of K. pneumoniae and *S. aureus* cells were killed by the composite coating after 24 h. Importantly, this coating gave excellent mechanical properties and was found not harmful to mammalian cells.[60] RGO/TiO$_2$/PUA was fabricated via in-situ polymerization method as illustrated in Figure 2.13. Only 14 % of *S. aureus* can survive within 150 min under VU-Visible light. This result is better than that of any samples including pure PUA and TiO$_2$/PUA.[61] A series of visible responsive FeOx/PU coatings were fabricated by using PU as substrate. FeOx was grown on the surface of PU via various deposited methods such as spraying and dip coating. In addition, the PU substrate was pre-treated by using abrasion and acetone. Temperature, deposition time and pre-treatment methods on PU were investigated to be important factors in photocatalytic performance of antibacterial coatings.[62] Ag/AgCl/PU/SF composite coating was attained by two steps. Firstly, PU/silk fibroin (SF) composite films were made via a wet phase inversion method. Then, Ag@AgCl NPs were grown on the surface of PU/silk fibroin (SF) composite films by impregnation-precipitation-photoreduction technique. Ag/AgCl/PU/SF composite film showed moderate disinfection effect toward *E. coli* and *S. aureus* and the maximum inhibition diameter were 12.93 and 13.70 mm toward *S. aureus* and *E. coli*. In addition, the composite film gave excellent recycling stability after four runs.[63]
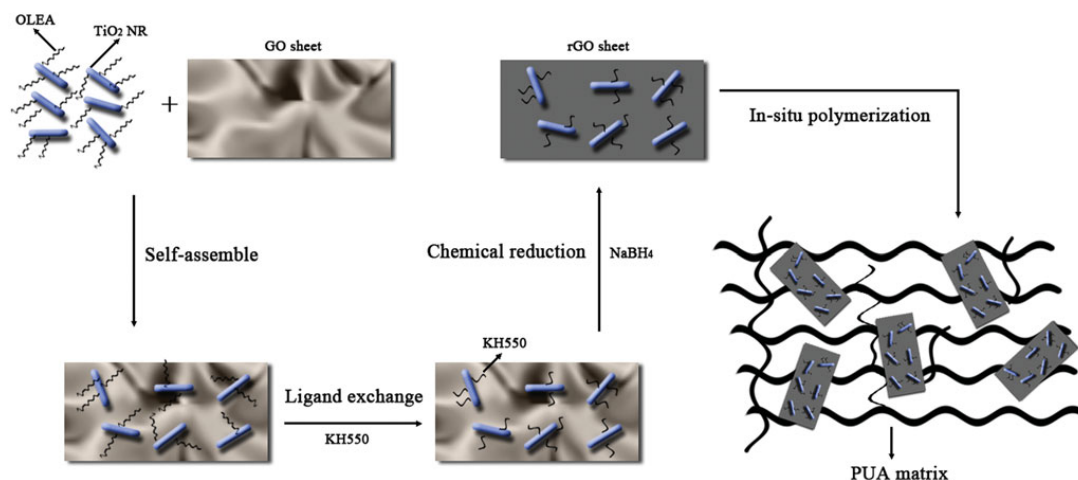
Figure 2.13. Scheme of formation of the rGO/TiO$_2$/PUA nanocomposites by Li, X. et al. 2019.

The achievements summarized above indicate the promising photocatalytic disinfection capability of PU/photocatalysts composite coatings. However, the majority of publications focused on TiO_2/PU composites which can only be conducted under UV light. In addition, most composites were synthesized by physical mixing PU matrix and photocatalysts which led to the unsatisfactory stability resulting from the leaching of photocatalysts. So, visible responsive and stable photocatalytic PU coatings are still active goals of scientific interest.

2.6 Applications of g-C$_3$N$_4$ and its composites in photocatalytic disinfection

Graphitic carbon nitride (g-C$_3$N$_4$) is a conjugative polymeric mainly containing carbon and nitrogen elements and consisting of triazine or heptazine building units (Figure 2.14).[64]
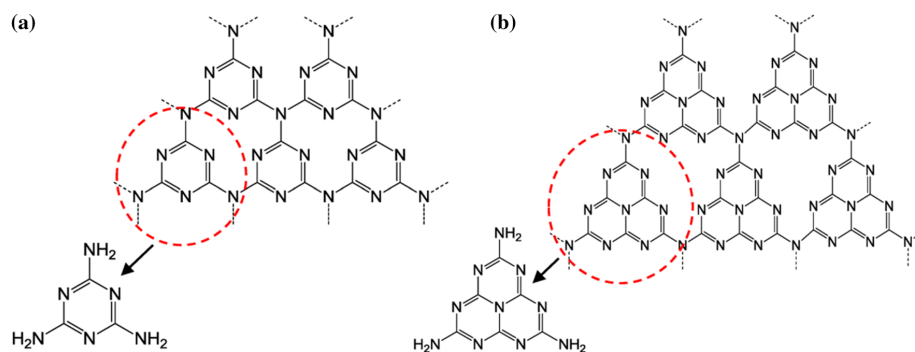
Figure 2.14. (a) Triazine and (b) heptazine structures of g-C$_3$N$_4$ by Ong, W.-J. et al. 2016.

Metal-free and non-toxic g-C$_3$N$_4$ as a visible responsive and robust photocatalyst has attracted significant attention due to its appropriate energy band gap (~2.7 eV), suitable positions of valence and conduction bands, and high thermal and chemical stability.[65] In addition, g-C$_3$N$_4$ can be synthesized easily via thermal polymerization from low-cost raw materials such as melamine, urea, cyanamide, thiourea and dicyandiamide.[66] G-C$_3$N$_4$ acting as a popular photocatalyst has obtained widespread applications in environmental renovation and energy exploration including pollutants removal, water splitting, CO_2 reduction and N_2 fixation since the pioneering work reported in 2009 for photocatalytic hydrogen production.[67] The first report of g-C$_3$N$_4$ in photocatalytic antibacterial field was reported in 2013. In this work, g-C$_3$N$_4$ nanosheets were incorporated with α-S$_8$ and reduced graphene oxide (RGO) to form a ternary composite which gave enhanced inactivation

against *E. coli* compared to any binary composites under aerobic and anaerobic conditions using visible light irradiation.[68] From then on, the interest in the photocatalytic inactivation against bacteria, viruses and algae has been increasing every year, as shown in Figure 2.15.
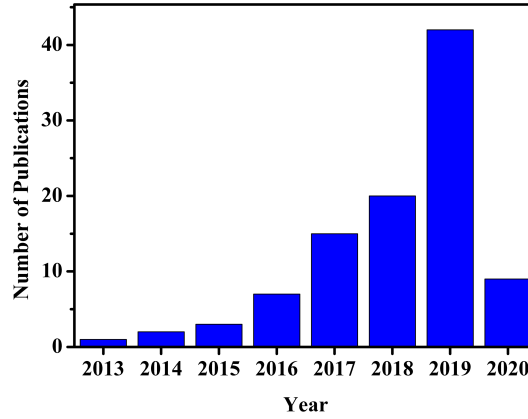
Figure 2.15. Number of annual publications on g-C$_3$N$_4$-based antimicrobials in recent years.

Similar to the mechanisms of g-C$_3$N$_4$ in other photocatalytic fields, the active species such as e$^-$, h$^+$, •OH, •O$_2^-$ and H$_2$O$_2$, are summarized in the following equations (1-7).[69] Similarly, the photocatalytic inactivation efficiency is dependent on the number and types of active species which further rely on the light absorption ability and dissociation efficiency of electron-hole pairs photo-generated when g-C$_3$N$_4$ was exposed to light.

$$\text{g-C}_3\text{N}_4 + h\upsilon \rightarrow \text{g-C}_3\text{N}_4(e_{\text{CB}}^- + h_{\text{VB}}^+) \tag{1}$$

$$\text{g-C}_3\text{N}_4(h_{\text{VB}}^+) + \text{H}_2\text{O} \rightarrow \text{g-C}_3\text{N}_4 + \cdot\text{OH} + \text{H}^+ \tag{2}$$

$$\text{g-C}_3\text{N}_4(h_{\text{VB}}^+) + \text{OH}^- \rightarrow \text{g-C}_3\text{N}_4 + \cdot\text{OH} \tag{3}$$

$$\text{g-C}_3\text{N}_4(e_{\text{VB}}^-) + \text{O}_2 \rightarrow \text{g-C}_3\text{N}_4 + \cdot\text{O}_2^- \tag{4}$$

$$\cdot\text{O}_2^- + \cdot\text{HO}_2 \rightarrow \cdot\text{OH} + \text{O}_2 + \text{H}_2\text{O}_2 \tag{5}$$

$$\cdot 2\text{HO}_2^- \rightarrow \text{O}_2 + \text{H}_2\text{O}_2 \tag{6}$$

$$\text{g-C}_3\text{N}_4(e_{\text{VB}}^-) + \text{H}_2\text{O}_2 \rightarrow \text{g-C}_3\text{N}_4 + \text{OH}^- + \cdot\text{OH} \tag{7}$$
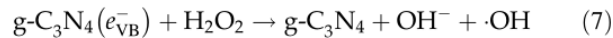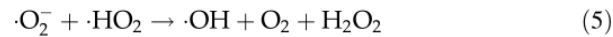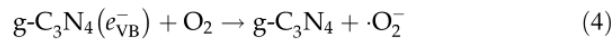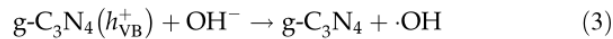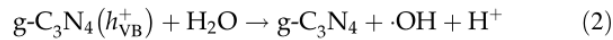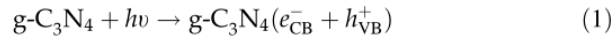
In order to overcome the bottlenecks of low separation efficiency of charge carriers and inadequate light absorption of bulk g-C$_3$N$_4$, various techniques such as modification of morphology, formation of heterojunctions, doping metal or nonmetal elements have been

shown to be successful for achieving this goal, as summarized in these reviews.[69, 70] Basically, there are two main methods to improve the photocatalytic performance of bulk g-C$_3$N$_4$. One is modification of bulk g-C$_3$N$_4$ by introducing porous structure or making ultrathin g-C$_3$N$_4$ nanosheets for increasing the surface area and active sites.[71-75] Because ultrathin g-C$_3$N$_4$ nanosheets can shorten the migration distance of free charge carriers from the interior to the surface of the catalyst, which are involved in a series of chemical reactions to form active species. In addition, elemental doping is also an effective way to improve the photocatalytic performance of bulk g-C$_3$N$_4$ by extending the visible light absorption range and enhancing the separation efficiency of charge carriers.[34] Design and fabricating heterojunctions systems such as binary and ternary composites by incorporating g-C$_3$N$_4$ with other photocatalysts is commonly utilized to enhance the photocatalytic antimicrobial activity. The synergistic effects of ingredients of composites can favor in harvesting solar light, facilitating dissociation of charge carriers and their transportation. Various composites based on g-C$_3$N$_4$ for photocatalytic antibacterial applications were previously summarized.[76] Composites based on elemental Ag and g-C$_3$N$_4$ include Ag/g-C$_3$N$_4$, AgBr/g-C$_3$N$_4$, AgCl/g-C$_3$N$_4$, Ag$_2$WO$_4$/mesoporous g-C$_3$N$_4$.[32, 77-79] Generally, Ag based g-C$_3$N$_4$ composites demonstrated excellent antibacterial performance originating from the surface plasmon resonance (SPR) effect of Ag nanoparticles and the synergistic effect between them. Additionally, Ag for Ag$^+$ can also kill bacteria efficiently in the dark. However, it should be noted that the leaching of Ag for Ag$^+$ is an inevitable issue for the sake of practical application. TiO$_2$ as a classical photocatalyst was used to fabricate a series of g-C$_3$N$_4$/TiO$_2$ hybrids which demonstrate better antibacterial capabilities than that of any pure counterparts.[80, 81] Additionally, bismuth based photocatalysts have gained significant attention due to their visible light absorption, low cost, non-toxicity and high stability in photocatalytic pollutants removal, hydrogen production and CO$_2$ reduction. g-C$_3$N$_4$/m-Bi$_2$O$_4$, Bi$_2$MoO$_6$/g-C$_3$N$_4$ NSs, BiVO$_4$ QDs/g-C$_3$N$_4$, BiOBr/BiOI/g-C$_3$N$_4$ and g-C$_3$N$_4$/Bi$_2$MoO$_6$ demonstrated superior antibacterial performance than those of their pure ingredients.[82-85] As far as water safety is concerned, perspective, metal-free photoactive agents as antimicrobials can avoid the issue of metal leaching into environmental surroundings and are desirable. Carbon materials, C60 and C70 which were widely used in organic solar cells as acceptors were also reported to combine with g-C$_3$N$_4$ to fabricate

metal-free photocatalysts.[86] In addition, GO as a layer material was extensively applied in the photocatalytic field was also used to construct g-C_3N_4 composites to improve antimicrobial activity owing to its large surface area and excellent transportation ability of electrons.[87] These metal-free photoactive agents can function as candidates for removing pathogens from our polluted surroundings.

Most model pathogens commonly used for evaluating the photocatalytic antimicrobial activity focused on *E. coli, S. aureus*, Bacillus anthracis (*B. anthracis*), and Salmonella. In addition, virus Bacteriophage MS2 and microalgae Microcystis aeruginosa were also used as models in several publications.[76, 88-91] Up to now, there are no reports on photocatalytic killing of Protozoa and fungi.

Although g-C_3N_4-based photocatalysts have obtained many achievements in antimicrobials, the exploration and research are still at an early stage yet and more endeavors are expected. In addition, *E. coli* dominated the model pathogens and some positive-gram bacterial cells were less investigated comparatively.

2.7   References

1. Wang, W.; Li, G.; Xia, D.; An, T.; Zhao, H.; Wong, P. K., Photocatalytic nanomaterials for solar-driven bacterial inactivation: recent progress and challenges. *Environmental Science: Nano* **2017,** *4* (4), 782-799.

2. Das, K. K.; Patnaik, S.; Mansingh, S.; Behera, A.; Mohanty, A.; Acharya, C.; Parida, K., Enhanced photocatalytic activities of polypyrrole sensitized zinc ferrite/graphitic carbon nitride nn heterojunction towards ciprofloxacin degradation, hydrogen evolution and antibacterial studies. *Journal of Colloid and Interface Science* **2020,** *561*, 551-567.

3. Bayat, F.; Karimi, A. R., Design of photodynamic chitosan hydrogels bearing phthalocyanine-colistin conjugate as an antibacterial agent. *International Journal of Biological Macromolecules* **2019,** *129*, 927-935.

4. Pedroza-Herrera, G.; Medina-Ramírez, I. E.; Lozano-Álvarez, J. A.; Rodil, S. E., Evaluation of the photocatalytic activity of copper doped TiO_2 nanoparticles for the purification and/or disinfection of industrial effluents. *Catalysis Today* **2020,** *341*, 37-48.

5. Wang, J.; Chen, R.; Xiang, L.; Komarneni, S., Synthesis, properties and applications of ZnO nanomaterials with oxygen vacancies: A review. *Ceramics International* **2018,** *44* (7), 7357-7377.

6. Hou, Y.-X.; Abdullah, H.; Kuo, D.-H.; Leu, S.-J.; Gultom, N. S.; Su, C.-H., A comparison study of SiO_2/nano metal oxide composite sphere for antibacterial application. *Composites Part B: Engineering* **2018,** *133*, 166-176.

7. Li, Y.; Liu, X.; Tan, L.; Cui, Z.; Jing, D.; Yang, X.; Liang, Y.; Li, Z.; Zhu, S.; Zheng, Y., Eradicating multidrug‑resistant bacteria rapidly using a multi functional g‑C_3N_4@Bi_2S_3 nanorod heterojunction with or without antibiotics. *Advanced Functional Materials* **2019,** *29* (20), 1900946.

8. Shtarev, D. S.; Shtareva, A.; Ryabchuk, V.; Rudakova, A.; Murzin, P.; Molokeev, M.; Koroleva, A.; Blokh, A.; Serpone, N., Solid-state synthesis, characterization, UV-induced coloration and photocatalytic activity–The $Sr_6Bi_2O_{11}$, $Sr_3Bi_2O_6$ and $Sr_2Bi_2O_5$ bismuthates. *Catalysis Today* **2020,** *340*, 70-85.

9. Prasannamedha, G.; Kumar, P. S., A Review on contamination and removal of sulfamethoxazole from aqueous solution using cleaner techniques: present and future perspective. *Journal of Cleaner Production* **2019**, 119553.

10. Zhang, X.; Wang, J.; Dong, X.-X.; Lv, Y.-K., Functionalized metal-organic frameworks for photocatalytic degradation of organic pollutants in environment. *Chemosphere* **2019**, 125144.

11. Sundar, K. P.; Kanmani, S., Progression of photocatalytic reactors and it's comparison: A Review. *Chemical Engineering Research and Design* **2020,** *154*, 135-150.

12. Ng, B. J.; Putri, L. K.; Kong, X. Y.; Teh, Y. W.; Pasbakhsh, P.; Chai, S. P., Z‑scheme photocatalytic systems for solar water splitting. *Advanced Science* **2020**, 1903171.

13. Matsunaga, T.; Tomoda, R.; Nakajima, T.; Wake, H., Photoelectrochemical sterilization of microbial cells by semiconductor powders. *FEMS Microbiology letters* **1985,** *29* (1-2), 211-214.

14. You, J.; Guo, Y.; Guo, R.; Liu, X., A review of visible light-active photocatalysts for water disinfection: Features and prospects. *Chemical Engineering Journal* **2019,** *373*, 624-641.

15. Lebedev, A.; Anariba, F.; Tan, J. C.; Li, X.; Wu, P., A review of physiochemical and photocatalytic properties of metal oxides against Escherichia coli. *Journal of Photochemistry and Photobiology A: Chemistry* **2018,** *360*, 306-315.

16. Anjana, P.; Bindhu, M.; Umadevi, M.; Rakhi, R., Antimicrobial, electrochemical and photo catalytic activities of Zn doped Fe_3O_4 nanoparticles. *Journal of Materials Science: Materials in Electronics* **2018,** *29* (7), 6040-6050.

17. Haseena, S.; Shanavas, S.; Duraimurugan, J.; Ahamad, T.; Alshehri, S.; Acevedo, R.; Jayamani, N., Investigation on photocatalytic and antibacterial ability of green treated copper oxide nanoparticles using Artabotrys Hexapetalus and Bambusa Vulgaris plant extract. *Materials Research Express* **2019,** *6* (12), 125064.

18. Raouf Hosseini, M.; Nasiri Sarvi, M., Recent achievements in the microbial synthesis of semiconductor metal sulfide nanoparticles. *Materials Science in Semiconductor Processing* **2015,** *40*, 293-301.

19. Ayodhya, D.; Veerabhadram, G., One-pot green synthesis, characterization, photocatalytic, sensing and antimicrobial studies of Calotropis gigantea leaf extract capped CdS NPs. *Materials Science and Engineering: B* **2017,** *225*, 33-44.

20. Ayodhya, D.; Veerabhadram, G., Preparation, characterization, photocatalytic, sensing and antimicrobial studies of Calotropis gigantea leaf extract capped CuS NPs by a green approach. *Journal of Inorganic and Organometallic Polymers and Materials* **2017,** *27* (1), 215-230.

21. Sharma, G.; Kumar, A.; Sharma, S.; Naushad, M.; Dwivedi, R. P.; ALOthman, Z. A.; Mola, G. T., Novel development of nanoparticles to bimetallic nanoparticles and their composites: a review. *Journal of King Saud University-Science* **2019,** *31* (2), 257-269.

22. Khan, Z. U. H.; Khan, A.; Chen, Y.; Shah, N. S.; Muhammad, N.; Khan, A. U.; Tahir, K.; Khan, F. U.; Murtaza, B.; Hassan, S. U., Biomedical applications of green synthesized Nobel metal nanoparticles. *Journal of Photochemistry and Photobiology B: Biology* **2017,** *173*, 150-164.

23. Xie, Z.; Peng, Y.-P.; Yu, L.; Xing, C.; Qiu, M.; Hu, J.; Zhang, H., Solar-inspired water purification based on emerging 2D materials: status and challenges. *SOLAR RRL* **2020,** *https://doi.org/10.1002/solr.201900400*.

24. Wang, L.; Yuan, Z.; Karahan, H. E.; Wang, Y.; Sui, X.; Liu, F.; Chen, Y., Nanocarbon materials in water disinfection: state-of-the-art and future directions. *Nanoscale* **2019,** *11* (20), 9819-9839.

25. Han, D.; Ma, M.; Han, Y.; Cui, Z.; Liang, Y.; Liu, X.; Li, Z.; Zhu, S.; Wu, S., Eco-friendly hybrids of carbon quantum dots modified MoS_2 for rapid microbial inactivation by strengthened photocatalysis. *ACS Sustainable Chemistry & Engineering* **2020,** *8*, 534-542.

26. Xin, Q.; Shah, H.; Nawaz, A.; Xie, W.; Akram, M. Z.; Batool, A.; Tian, L.; Jan, S. U.; Boddula, R.; Guo, B., Antibacterial carbon‐based nanomaterials. *Advanced Materials* **2019,** *31* (45), 1804838.

27. Li, P.; Li, J.; Feng, X.; Li, J.; Hao, Y.; Zhang, J.; Wang, H.; Yin, A.; Zhou, J.; Ma, X., Metal-organic frameworks with photocatalytic bactericidal activity for integrated air cleaning. *Nature Communications* **2019,** *10* (1), 2177.

28. Lee, S. L.; Chang, C.-J., Recent developments about conductive polymer based composite photocatalysts. *Polymers* **2019,** *11* (2), 206.

29. Miao, H.; Teng, Z.; Wang, S.; Xu, L.; Wang, C.; Chong, H., Recent advances in the disinfection of water using nanoscale antimicrobial materials. *Advanced Materials Technologies* **2019,** *4* (5), 1800213.

30. Dong, X.; Liang, W.; Meziani, M. J.; Sun, Y.-P.; Yang, L., Carbon Dots as Potent Antimicrobial Agents. *Theranostics* **2020,** *10* (2), 671-686.

31. Reddy, P. A. K.; Reddy, P. V. L.; Kwon, E.; Kim, K.-H.; Akter, T.; Kalagara, S., Recent advances in photocatalytic treatment of pollutants in aqueous media. *Environment International* **2016,** *91*, 94-103.

32. Adhikari, S. P.; Pant, H. R.; Kim, J. H.; Kim, H. J.; Park, C. H.; Kim, C. S., One pot synthesis and characterization of Ag-ZnO/g-C_3N_4 photocatalyst with improved photoactivity and antibacterial properties. *Colloids and Surfaces A: Physicochemical and Engineering Aspects* **2015,** *482*, 477-484.

33. Liu, H.; Ma, S.; Shao, L.; Liu, H.; Gao, Q.; Li, B.; Fu, H.; Fu, S.; Ye, H.; Zhao, F.; Zhou, J., Defective engineering in graphitic carbon nitride nanosheet for efficient photocatalytic pathogenic bacteria disinfection. *Applied Catalysis B: Environmental* **2020,** *261*, 118201.

34. Wang, R.; Zhang, B.; Liang, Z.; He, Y.; Wang, Z.; Ma, X.; Yao, X.; Sun, J.; Wang, J., Insights into rapid photodynamic inactivation mechanism of Staphylococcus aureus via rational design of multifunctional nitrogen-rich carbon-coated bismuth/cobalt nanoparticles. *Applied Catalysis B: Environmental* **2019,** *241*, 167-177.

35. Li, Y.; Liu, X.; Tan, L.; Cui, Z.; Yang, X.; Zheng, Y.; Yeung, K. W. K.; Chu, P. K.; Wu, S., Rapid sterilization and accelerated wound healing using Zn^{2+} and graphene oxide modified g‐C_3N_4 under dual light irradiation. *Advanced Functional Materials* **2018,** *28* (30), 1800299.

36. Sun, L.; Du, T.; Hu, C.; Chen, J.; Lu, J.; Lu, Z.; Han, H., Antibacterial activity of graphene oxide/g-C_3N_4 composite through photocatalytic disinfection under visible light. *ACS Sustainable Chemistry & Engineering* **2017,** *5* (10), 8693-8701.

37. Yuan, H.; Zhan, Y.; Rowan, A. E.; Xing, C.; Kouwer, P. H., Biomimetic networks with enhanced photodynamic antimicrobial activity from conjugated polythiophene/polyisocyanide hybrid hydrogels. *Angewandte Chemie International Edition* **2020**.

38. Yao, T.-t.; Wang, J.; Xue, Y.-f.; Yu, W.-j.; Gao, Q.; Ferreira, L.; Ren, K.-F.; Ji, J., A photodynamic antibacterial spray-coating based on the host–guest immobilization of the photosensitizer methylene blue. *Journal of Materials Chemistry B* **2019,** *7* (33), 5089-5095.

39. Jia, R.; Tian, W.; Bai, H.; Zhang, J.; Wang, S.; Zhang, J., Sunlight‐Driven Wearable and Robust Antibacterial Coatings with Water‐Soluble Cellulose‐Based Photosensitizers. *Advanced Healthcare Materials* **2019,** *8* (5), 1801591.

40. Chemburu, S.; Corbitt, T. S.; Ista, L. K.; Ji, E.; Fulghum, J.; Lopez, G. P.; Ogawa, K.; Schanze, K. S.; Whitten, D. G., Light-induced biocidal action of conjugated polyelectrolytes supported on colloids. *Langmuir* **2008,** *24* (19), 11053-11062.

41. Čík, G.; Priesolová, S.; Bujdáková, H.; Šeršeň, F.; Potheöová, T.; Krištín, J., Inactivation of bacteria G+-S. aureus and G−-E. coli by phototoxic polythiophene incorporated in ZSM-5 zeolite. *Chemosphere* **2006,** *63* (9), 1419-1426.

42. Xing, C.; Xu, Q.; Tang, H.; Liu, L.; Wang, S., Conjugated polymer/porphyrin complexes for efficient energy transfer and improving light-activated antibacterial activity. *Journal of the American Chemical Society* **2009,** *131* (36), 13117-13124.

43. Liu, L.; Yu, M.; Duan, X.; Wang, S., Conjugated polymers as multifunctional biomedical platforms: Anticancer activity and apoptosis imaging. *Journal of Materials Chemistry* **2010,** *20* (33), 6942-6947.

44. Shang, K.; Ai, S.; Ma, Q.; Tang, T.; Yin, H.; Han, H., Effective photocatalytic disinfection of E. coli and S. aureus using polythiophene/MnO_2 nanocomposite photocatalyst under solar light irradiation. *Desalination* **2011,** *278* (1-3), 173-178.

45. Liu, L.; Chen, J.; Wang, S., Flexible antibacterial film deposited with polythiophene–porphyrin composite. *Advanced Healthcare Materials* **2013,** *2* (12), 1582-1585.

46. Ma, G.; Liang, X.; Li, L.; Qiao, R.; Jiang, D.; Ding, Y.; Chen, H., Cu-doped zinc oxide and its polythiophene composites: Preparation and antibacterial properties. *Chemosphere* **2014,** *100*, 146-151.

47. Huang, Y.; Pappas, H. C.; Zhang, L.; Wang, S.; Cai, R.; Tan, W.; Wang, S.; Whitten, D. G.; Schanze, K. S., Selective imaging and inactivation of bacteria over mammalian cells by imidazolium-substituted polythiophene. *Chemistry of Materials* **2017,** *29* (15), 6389-6395.

48. Brown, D. M.; Yang, J.; Strach, E. W.; Khalil, M. I.; Whitten, D. G., Size and substitution effect on antimicrobial activity of polythiophene polyelectrolyte derivatives under photolysis and dark conditions. *Photochemistry and Photobiology* **2018,** *94* (6), 1116-1123.

49. Palamà, I. E.; Di Maria, F.; Zangoli, M.; D'Amone, S.; Manfredi, G.; Barsotti, J.; Lanzani, G.; Ortolani, L.; Salatelli, E.; Gigli, G., Enantiopure polythiophene nanoparticles. Chirality dependence of cellular uptake, intracellular distribution and antimicrobial activity. *RSC advances* **2019,** *9* (40), 23036-23044.

50. Charpentier, P.; Burgess, K.; Wang, L.; Chowdhury, R.; Lotus, A.; Moula, G., Nano-TiO$_2$/polyurethane composites for antibacterial and self-cleaning coatings. *Nanotechnology* **2012,** *23* (42), 425606.

51. Ryu, S.-Y.; Park, M.-K.; Kwak, S.-Y., Silver-titania-polyurethane composite nanofibre mat for chemical and biological warfare protection. *International Journal of Nanotechnology* **2013,** *10* (8-9), 771-788.

52. Kim, H. J.; Pant, H. R.; Kim, J. H.; Choi, N. J.; Kim, C. S., Fabrication of multifunctional TiO$_2$–fly ash/polyurethane nanocomposite membrane via electrospinning. *Ceramics International* **2014,** *40* (2), 3023-3029.

53. Qiu, S.; Deng, F.; Xu, S.; Liu, P.; Min, X.; Ma, F., Degradation of pollutant and antibacterial activity of waterborne polyurethane/doped TiO$_2$ nanoparticle hybrid films. *Journal of Wuhan University of Technology-Mater. Sci. Ed.* **2015,** *30* (3), 447-451.

54. Li, K.; Peng, J.; Zhang, M.; Heng, J.; Li, D.; Mu, C., Comparative study of the effects of anatase and rutile titanium dioxide nanoparticles on the structure and properties of waterborne polyurethane. *Colloids and Surfaces A: Physicochemical and Engineering Aspects* **2015,** *470*, 92-99.

55. Yemmireddy, V. K.; Farrell, G. D.; Hung, Y. C., Development of titanium dioxide (TiO$_2$) nanocoatings on food contact surfaces and method to evaluate their durability and photocatalytic bactericidal property. *Journal of Food Science* **2015,** *80* (8), N1903-N1911.

56. Nguyen, T. V.; Nguyen, T. A.; Dao, P. H.; Nguyen, A. H.; Do, M. T., Effect of rutile titania dioxide nanoparticles on the mechanical property, thermal stability, weathering resistance and antibacterial property of styrene acrylic polyurethane coating. *Advances in Natural Sciences: Nanoscience and Nanotechnology* **2016,** *7* (4), 045015.

57. Li, X.; Xie, J.; Liao, L.; Jiang, X.; Fu, H., UV-curable polyurethane acrylate–Ag/TiO$_2$ nanocomposites with superior UV light antibacterial activity. *International Journal of Polymeric Materials and Polymeric Biomaterials* **2017,** *66* (16), 835-843.

58. Kováčová, M. r.; Marković, Z. M.; Humpolíček, P.; Mičušík, M.; Švajdlenková, H.; Kleinová, A.; Danko, M.; Kubát, P.; Vajďák, J.; Capakova, Z., Carbon quantum dots

modified polyurethane nanocomposite as effective photocatalytic and antibacterial agents. *ACS Biomaterials Science & Engineering* **2018,** *4* (12), 3983-3993.

59. Kim, J. H.; Joshi, M. K.; Lee, J.; Park, C. H.; Kim, C. S., Polydopamine-assisted immobilization of hierarchical zinc oxide nanostructures on electrospun nanofibrous membrane for photocatalysis and antimicrobial activity. *Journal of Colloid and Interface Science* **2018,** *513*, 566-574.

60. Chitichotpanya, P.; Inprasit, T.; Chitichotpanya, C., In vitro assessment of antibacterial potential and mechanical properties of Ag-TiO$_2$/WPU on medical cotton optimized with response surface methodology. *Journal of Natural Fibers* **2019,** *16* (1), 88-99.

61. Li, X.; Wang, S.; Xie, J.; Hu, J.; Fu, H., Polyurethane acrylate-supported rGO/TiO$_2$ electrical conductive and antibacterial nanocomposites. *International Journal of Polymeric Materials and Polymeric Biomaterials* **2019,** *68* (6), 319-327.

62. Suárez Murillo, L. V.; Schärer, A.; Giannakis, S.; Rtimi, S.; Pulgarín, C., Iron-coated polymer films with high antibacterial activity under indoor and outdoor light, prepared by different facile pre-treatment and deposition methods. *Applied Catalysis B: Environmental* **2019,** *243*, 161-174.

63. Zhou, H.; Wang, X.; Wang, T.; Zeng, J.; Yuan, Z.; Jian, J.; Zhou, Z.; Zeng, L.; Yang, H., In situ decoration of Ag@ AgCl nanoparticles on polyurethane/silk fibroin composite porous films for photocatalytic and antibacterial applications. *European Polymer Journal* **2019,** *118*, 153-162.

64. Ong, W.-J.; Tan, L.-L.; Ng, Y. H.; Yong, S.-T.; Chai, S.-P., Graphitic carbon nitride (g-C$_3$N$_4$)-based photocatalysts for artificial photosynthesis and environmental remediation: are we a step closer to achieving sustainability? *Chemical reviews* **2016,** *116* (12), 7159-7329.

65. Jiang, L.; Yuan, X.; Pan, Y.; Liang, J.; Zeng, G.; Wu, Z.; Wang, H., Doping of graphitic carbon nitride for photocatalysis: a reveiw. *Applied Catalysis B: Environmental* **2017,** *217*, 388-406.

66. Lin, L.; Yu, Z.; Wang, X., Crystalline carbon nitride semiconductors for photocatalytic water splitting. *Angewandte Chemie International Edition* **2019,** *58* (19), 6164-6175.

67. Wang, X.; Maeda, K.; Thomas, A.; Takanabe, K.; Xin, G.; Carlsson, J. M.; Domen, K.; Antonietti, M., A metal-free polymeric photocatalyst for hydrogen production from water under visible light. *Nature Materials* **2009,** *8* (1), 76-80.

68. Wang, W.; Yu, J. C.; Xia, D.; Wong, P. K.; Li, Y., Graphene and g-C$_3$N$_4$ nanosheets cowrapped elemental α-sulfur as a novel metal-free heterojunction photocatalyst for bacterial inactivation under visible-light. *Environmental science & technology* **2013,** *47* (15), 8724-8732.

69. Murugesan, P.; Moses, J. A.; Anandharamakrishnan, C., Photocatalytic disinfection efficiency of 2D structure graphitic carbon nitride-based nanocomposites: a review. *Journal of Materials Science* **2019,** *54* (19), 12206-12235.

70. Zhang, C.; Li, Y.; Shuai, D.; Shen, Y.; Xiong, W.; Wang, L., Graphitic carbon nitride (g-C$_3$N$_4$)-based photocatalysts for water disinfection and microbial control: A review. *Chemosphere* **2019,** *214*, 462-479.

71. Huang, J.; Ho, W.; Wang, X., Metal-free disinfection effects induced by graphitic carbon nitride polymers under visible light illumination. *Chemical Communications* **2014,** *50* (33), 4338-4340.

72. Zhao, H.; Yu, H.; Quan, X.; Chen, S.; Zhang, Y.; Zhao, H.; Wang, H., Fabrication of atomic single layer graphitic-C$_3$N$_4$ and its high performance of photocatalytic disinfection under visible light irradiation. *Applied Catalysis B: Environmental* **2014,** *152*, 46-50.

73. Xu, J.; Wang, Z.; Zhu, Y., Enhanced visible-light-driven photocatalytic disinfection performance and organic pollutant degradation activity of porous g-C$_3$N$_4$ nanosheets. *ACS Applied Materials & Interfaces* **2017,** *9* (33), 27727-27735.

74. Kang, S.; Huang, W.; Zhang, L.; He, M.; Xu, S.; Sun, D.; Jiang, X., Moderate bacterial etching allows scalable and clean delamination of g-C$_3$N$_4$ with enriched unpaired electrons for highly improved photocatalytic water disinfection. *ACS Applied Materials & Interfaces* **2018,** *10* (16), 13796-13804.

75. Kang, S.; Zhang, L.; He, M.; Zheng, Y.; Cui, L.; Sun, D.; Hu, B., " Alternated cooling and heating" strategy enables rapid fabrication of highly-crystalline g-C$_3$N$_4$ nanosheets for efficient photocatalytic water purification under visible light irradiation. *Carbon* **2018,** *137*, 19-30.

76. Zhang, C.; Li, Y.; Zhang, W.; Wang, P.; Wang, C., Metal-free virucidal effects induced by g-C$_3$N$_4$ under visible light irradiation: Statistical analysis and parameter optimization. *Chemosphere* **2018,** *195*, 551-558.

77. Adhikari, S. P.; Awasthi, G. P.; Lee, J.; Park, C. H.; Kim, C. S., Synthesis, characterization, organic compound degradation activity and antimicrobial performance of g-C$_3$N$_4$ sheets customized with metal nanoparticles-decorated TiO$_2$ nanofibers. *RSC Advances* **2016,** *6* (60), 55079-55091.

78. Pant, B.; Park, M.; Lee, J. H.; Kim, H.-Y.; Park, S.-J., Novel magnetically separable silver-iron oxide nanoparticles decorated graphitic carbon nitride nano-sheets: a multifunctional photocatalyst via one-step hydrothermal process. *Journal of Colloid and Interface Science* **2017,** *496*, 343-352.

79. Vidyasagar, D.; Ghugal, S. G.; Kulkarni, A.; Mishra, P.; Shende, A. G.; Umare, S. S.; Sasikala, R., Silver/Silver (II) oxide (Ag/AgO) loaded graphitic carbon nitride microspheres: An effective visible light active photocatalyst for degradation of acidic

dyes and bacterial inactivation. *Applied Catalysis B: Environmental* **2018,** *221*, 339-348.

80. Li, C.; Sun, Z.; Zhang, W.; Yu, C.; Zheng, S., Highly efficient g-C3N4/TiO2/kaolinite composite with novel three-dimensional structure and enhanced visible light responding ability towards ciprofloxacin and S. aureus. *Applied Catalysis B: Environmental* **2018,** *220*, 272-282.

81. Li, G.; Nie, X.; Chen, J.; Jiang, Q.; An, T.; Wong, P. K.; Zhang, H.; Zhao, H.; Yamashita, H., Enhanced visible-light-driven photocatalytic inactivation of Escherichia coli using g-C_3N_4/TiO_2 hybrid photocatalyst synthesized using a hydrothermal-calcination approach. *Water Research* **2015,** *86*, 17-24.

82. Liu, B.; Han, X.; Wang, Y.; Fan, X.; Wang, Z.; Zhang, J.; Shi, H., Synthesis of g-C_3N_4/BiOI/BiOBr heterostructures for efficient visible-light-induced photocatalytic and antibacterial activity. *Journal of Materials Science: Materials in Electronics* **2018,** *29* (16), 14300-14310.

83. Xia, D.; Wang, W.; Yin, R.; Jiang, Z.; An, T.; Li, G.; Zhao, H.; Wong, P. K., Enhanced photocatalytic inactivation of Escherichia coli by a novel Z-scheme g-C_3N_4/m-Bi_2O_4 hybrid photocatalyst under visible light: the role of reactive oxygen species. *Applied Catalysis B: Environmental* **2017,** *214*, 23-33.

84. Tian, Y.; Zhou, F.; Zhan, S.; Zhu, Z.; He, Q., Mechanisms on the enhanced sterilization performance of fluorocarbon resin composite coatings modified by g-C_3N_4/Bi_2MoO_6 under the visible-light. *Journal of Photochemistry and Photobiology A: Chemistry* **2018,** *350*, 10-16.

85. Wang, R.; Kong, X.; Zhang, W.; Zhu, W.; Huang, L.; Wang, J.; Zhang, X.; Liu, X.; Hu, N.; Suo, Y., Mechanism insight into rapid photocatalytic disinfection of Salmonella based on vanadate QDs-interspersed g-C_3N_4 heterostructures. *Applied Catalysis B: Environmental* **2018,** *225*, 228-237.

86. Ouyang, K.; Dai, K.; Chen, H.; Huang, Q.; Gao, C.; Cai, P., Metal-free inactivation of E. coli O157: H7 by fullerene/C_3N_4 hybrid under visible light irradiation. *Ecotoxicology and Environmental Safety* **2017,** *136*, 40-45.

87. Dai, K.; Lu, L.; Liu, Q.; Zhu, G.; Wei, X.; Bai, J.; Xuan, L.; Wang, H., Sonication assisted preparation of graphene oxide/graphitic-C_3N_4 nanosheet hybrid with reinforced photocurrent for photocatalyst applications. *Dalton Transactions* **2014,** *43* (17), 6295-6299.

88. Li, Y.; Zhang, C.; Shuai, D.; Naraginti, S.; Wang, D.; Zhang, W., Visible-light-driven photocatalytic inactivation of MS_2 by metal-free g-C_3N_4: Virucidal performance and mechanism. *Water Research* **2016,** *106*, 249-258.

89. Song, J.; Wang, X.; Ma, J.; Wang, X.; Wang, J.; Xia, S.; Zhao, J., Removal of Microcystis aeruginosa and Microcystin-LR using a graphitic-C_3N_4/TiO_2 floating

photocatalyst under visible light irradiation. *Chemical Engineering Journal* **2018,** *348*, 380-388.

90. Song, J.; Wang, X.; Ma, J.; Wang, X.; Wang, J.; Zhao, J., Visible-light-driven in situ inactivation of Microcystis aeruginosa with the use of floating g-C$_3$N$_4$ heterojunction photocatalyst: performance, mechanisms and implications. *Applied Catalysis B: Environmental* **2018,** *226*, 83-92.

91. Wang, X.; Wang, X.; Zhao, J.; Song, J.; Su, C.; Wang, Z., Adsorption-photocatalysis functional expanded graphite C/C composite for in-situ photocatalytic inactivation of Microcystis aeruginosa. *Chemical Engineering Journal* **2018,** *341*, 516-525.

Chapter 3

3 Synthesis and photocatalytic antibacterial properties of poly [2,11'-thiophene-ethylene -thiophene-alt-2,5-(3-carboxyl)-thiophene]

Conductive polymers have been demonstrated to be able to inactivate microbials under light irradiation due to their broad visible light absorption. Polythiophene (PTh) and its derivatives can generate singlet oxygen to kill microbials due to the presence of sulfur. In this chapter, the recent research progress of PTh based derivatives and composites for antimicrobials is reviewed. A new PTh derivative PTET-T-COOH for effective photocatalytic inactivation of two gram-positive bacteria including *S. aureus* and *S. suis* is presented. In addition, the recycling stability and the antibacterial mechanism of PTET-T-COOH is discussed in detail.

3.1 Abstract

Designing new antimicrobial surfaces which are effective under visible light irradiation without leaching toxic ions is a current challenge for effective disinfection. This work examined the synthesis and characterization of a new polymeric system poly[2,11'-thiophene-ethylene-thiophene-alt-2,5-(3-carboxyl)-thiophene] (PTET-T-COOH) with broad light absorption. Its photocatalytic disinfection performance against *S. aureus* and *S. suis* was evaluated, showing over 99.999 % inactivation for both bacteria under visible light irradiation at a low concentration of PTET-T-COOH (0.1 mg/mL). The active species generated and responsible for the photocatalytic disinfection were confirmed to be singlet oxygen and free electrons by using scavengers and electron spin resonance spectroscopy (ESR). PTET-T-COOH demonstrated excellent chemical stability under visible light irradiation, with the carboxyl group providing possibility for chemical bonding to suitable functionalities for the development of novel antibacterial coatings.

3.2 Introduction

Infectious diseases originating from bacteria have drawn increasing attention due to their causation for both disease and death.[1] With the emergence of antibiotic resistant

microorganisms, antibiotics have gradually lost their activity for inactivating bacteria. New types of antimicrobial materials are required to kill antibiotic-resistant strains. Conventional antimicrobial materials such as metals (e.g. Ag^+) or their ions can kill bacteria by physical and/or chemical interactions.[2] However, they are restricted by their high cost or toxicity due to leaching.[3] In recent years, photocatalytic technology has been of interest for environmental remediation and disinfection. Numerous inorganic photo-catalysts (TiO_2, ZnO, g-C_3N_4)[4] have been examined which form reactive oxygen species (ROSs) when irradiated, to destroy microbes.[4, 5]

Compared to inorganic photo-catalysts, investigation of organic photocatalysts is rather new in spite of their many advantages including chemically tunable electronic structure, excellent biocompatibility, low cost and low toxicity. Additionally, organic photocatalysts on the surfaces of polymer and textiles can be easily realized by chemical bonding. This makes the exploration of novel and efficient organic antimicrobial agents is of significant importance.

Conductive polymers have been extensively explored in numerous applications including organic photovoltaics, sensors, emitting diodes, supercapacitors, transistors and photocatalytic applications.[6, 7] Recent work with several conductive polymers including polyaniline (PANI),[8] polypyrrole (PPy)[9] and polythiophene (PTh)[10] have shown antibacterial or photo sensitizer activity when incorporated with various inorganic photo-active agents. By extending their light absorption spectrum and promoting the separation of photogenerated electrons and holes,[5] the assemblies photocatalytic activity was enhanced.

As one of the most potent conducting polymers, sulfur-containing polythiophene (PTh) and its derivatives can absorb visible and near infrared light for yielding triplet states to excite the triplet oxygen followed by efficient production of singlet oxygen and other ROSs.[11] Functional group modification of PTh and incorporation with other inorganic or organic ingredients were exploited for broadening its application scope. Many efforts have been focused on the applications of PTh and its derivatives in photocatalytic water splitting to produce hydrogen,[12] photodegradation of organic pollutants [13] and photocatalytic

organic synthesis.[14] Several composite photocatalysts based on PTh and its derivatives also have been reported for photo-induced disinfection. For example, Ai et al. utilized PTh/MnO$_2$ composite to kill 99.9 % Escherichia coli (*E. coli*) and staphylococcus aureus (*S. aureus*) cells upon 6 h solar light exposure (1 mg/mL).[15] Synergistic effects in Cu-doped zinc oxide/polythiophene ternary composites were found to provide better antibacterial activities than those from either individual component.[16] Organic semiconductors have many merits including low cost, good stability and biocompatibility, adjustable band gap, and abundant element resources.[17] A complex was formed between water-soluble polythiophene and a cationic porphyrin through electrostatic interactions. Efficient energy transfer from polythiophene to porphyrin occurred in this complex and yielded singlet oxygen and photocatalytic disinfection under exposure to white light.[18] In addition, a flexible, thin and transparent anti-microbial film of polyterthiophene/porphyrin was fabricated on PET sheets and behaved efficient inactivation toward *E. coli.*[19]

Compared to these composite photocatalysts, single PTh-based photocatalysts provide potential for enhanced stability and less leaching problems. Although several pristine PTh derivatives have demonstrated good photocatalytic inactivation ability, the disinfection performance, the stability and recyclability still needs to be enhanced. [11, 20] Herein, a novel conductive polymer PTh derivative, PTET-T-COOH was synthesized in this work and its photocatalytic inactivation effects on *S. aureus* and *S. suis* were investigated comprehensively with the reusability and photocatalytic antimicrobial mechanism being examined in detail.

3.3 Experimental Section

3.3.1 Materials

N-bromosuccinimide (C$_4$H$_4$BrNO$_2$), thiophene-3-carboxylic acid (C$_5$H$_4$O$_2$S), tetrakis (triphenylphosphine) palladium (C$_{72}$H$_{60}$P$_4$Pd), thiophene-2-carbaldehyde, n-butyllithium (n-BuLi, 2.4 M in hexanes), titanium tetrachloride (TiCl$_4$), trimethyltin chloride, 2-(tributylstannyl)thiophene and bromobenzene were purchased from Energy Chemical (Shanghai, China). Tetrahydrofuran (THF), zinc (Zn), sodium carbonate (Na$_2$CO$_3$), magnesium sulfate (MgSO$_4$), petroleum ether, hexane, dichloromethane (CH$_2$Cl$_2$),

chloroform (CHCl$_3$), methanol, acetic acid and toluene was purchased from Sinopharm Chemical Reagent Beijing Co., Ltd. (Beijing, China). Nitrogen gas (N$_2$) was supplied by Siping Hongyuan Gas Co., Ltd. (Siping, China). Tryptic soy broth (TSB) and tryptic soy agar (TSA) were purchased from Qingdao Hope Bio-Technology Co., Ltd (Qingdao, China). Phosphate buffered saline (PBS) (pH = 7.2) was purchased from Beijing Solarbio Science & Technology Co., Ltd. (Beijing, China). SYTO-9 and propidium iodide (PI) were purchased from invitrogen (American). 3, 4-Dihydro-2-methyl-1,1-dimethylethyl ester-2H-pyrrole-2-carboxylic acid-1-oxide (BMPO), 5,5-di-methyl-1-pyrroline N-oxide (DMPO) were purchased from DOJINDO (Japan) and 4-hydroxy-2,2,6,6-tetramethyl-1-piperidine (TEMP) were supplied by Sigma-Aldrich. Ethylenediamine tetraacetic acid disodium salt (EDTA-2Na) was purchased from Changchun Tianjia Biological Techonogy Co., Ltd. (Changchun, China), tertbutyl alcohol (TBA), K$_2$Cr$_2$O$_7$, and NaN$_3$ were purchased from Sinopharm Chemical Reagent Beijing Co., Ltd (Beijing, China). L-Ascorbic acid was purchased from Beijing Bailingwei Technology Co., Ltd. (Beijing, China).

3.3.2   Synthesis of poly[2,11'-thiophene-ethylene-thiophene-alt-(2,5-(3-carboxyl) -thiophene] (PTET-T-COOH)

Synthesis of compound T-E-T [21]: Thiophene-2-carbaldehyde (5 g, 44.6 mmol) was dissolved in dry THF (50 mL) at -18 °C before the addition of titanium tetrachloride (3.4 g, 18 mmol in 18 mL of THF). After being stirred at -18 °C for 0.5 h, the reaction mixture was warmed to room temperature. Subsequently, Zn (21 g, 320 mmol) in batches was added and the mixture was refluxed for 4 h and then cooled to room temperature. Na$_2$CO$_3$ (5 g) was added to quench the reaction and to bring the pH value of the resulting mixture to 6-8. After that, the mixture was extracted with CH$_2$Cl$_2$ (2×30 mL). The organic phase was dried over MgSO$_4$ and concentrated under vacuum at 45 °C. The residue was purified by column chromatography on silica gel using petroleum ether/dichloromethane (1:20) as an eluent followed by rotary evaporation to afford a pale yellow solid (3 g, 70%). ^{1}H NMR (400 MHz, CDCl$_3$), δ (ppm): 7.18 (d, 2H), 7.06 (s, 2H), 7.04 (d, 2H), 6.99 (t, 2H). ^{13}C NMR (100 MHz, CDCl$_3$), δ (ppm): 142.3, 127.6, 126.0, 124.3, 121.4.

Synthesis of compound T-E-T-Tin [22]: n-BuLi (2.4 mL, 2.4 M in hexanes) was added dropwise to a solution of T-E-T (2 g, 10 mmol) in anhydrous THF (50 mL) at -78 °C (low temperature thermostatic bath of EYELA) under nitrogen gas protection. After being stirred at -78 °C for 2 h, the reaction mixture was warmed to room temperature and stirred for 0.5 h. Subsequently, the mixture was cooled to -78 °C again before the addition of trimethyltin chloride (2.3 g, 24 mmol). After being stirred at -78 °C for an additional 2 h, the solution was warmed to room temperature and then quenched with H_2O (30 mL). The reaction mixture was extracted with CH_2Cl_2 (2×30 mL). The organic phase was dried over anhydrous $MgSO_4$. After the solvent had been removed under vacuum at 45 °C, the residue was purified by recrystallization from ethanol to yield a yellow needlelike solid (1.54 g, 28%). ^1H NMR (400 MHz, $CDCl_3$), δ (ppm): 7.12 (d, 2H), 7.09 (s, 2H), 7.07 (d, 2H), 0.37 (t, 18H). ^{13}C NMR (100 MHz, $CDCl_3$), δ (ppm): 148.2, 137.5, 135.7, 127.0, 121.2, -8.3.

Synthesis of compound 2,5-dibromothiophene-3-carboxylic acid [23]: In a dry two-necked round-bottomed flask, thiophene-3-carboxylic acid (5 g, 39 mmol) was dissolved in $CHCl_3$ under nitrogen, with acetic acid (20 mL) added dropwise. After the addition of *N*-bromosuccinimide (14.4 g, 81.9 mmol) in portions at 0 °C, the reaction mixture was stirred for 1 h at 0 °C. The mixture was further stirred overnight after being warmed to room temperature. After that, the mixture was poured into ice-water (30 mL) and extracted with CH_2Cl_2 (2×30 mL). After removal of the dichloromethane using a rotary evaporator at 45 °C, the crude products were purified by column chromatography on silica gel using petroleum ether/dichloromethane (1:1) to give a white solid (6.7 g, 60 %). ^1H NMR (400 MHz, $CDCl_3$), δ (ppm): 7.41 (s, 1H). ^{13}C NMR (100 MHz, $CDCl_3$), δ (ppm): 165.4, 132.0, 130.7, 121.4, 111.7.

Synthesis of polymer PTET-T-COOH: T-E-T-Tin (329 mg, 0.634 mmol) and 2,5-dibromothiophene-3-carboxylic acid (180 mg, 0.634 mmol) were dissolved in anhydrous toluene (40 mL). The mixture solution was purged with nitrogen for 20 min before $Pd(PPh_3)_4$ (70 mg, 0.060 mmol) was added. After being degassed for another 20 min, the mixture was then stirred at 110 °C for 72 h. Then 2-(tributylstannyl) thiophene (100 mg) and bromobenzene (100 mg) as end-cappers were added in sequence and allowed to stir at 110 °C for 12 h, respectively. The mixture was poured into methanol (200 mL) and filtered.

After Soxhlet extraction with hexane, methanol and chloroform for 24 h each, the polymer was reprecipitated from methanol to afford a purple solid (180 mg, 89 %). Solid-state ^{13}C NMR (500 MHz), δ (ppm): 170.5, 142.5, 135.8, 127.4. ^{1}H NMR (600 MHz, DMSO-d$_6$), δ (ppm): 7.48 (Br, protons of carbonyl adjacent thiophene), 7.23-7.06 (protons of di(thiophen-2-yl) ethane).

3.3.3   Measurements

Fourier transform infrared (FT-IR) spectra of samples were investigated by FT-IR spectrometer (PE Frontier, USA) within the wavelength range of 500-4000 cm^{-1} by mixing samples with KBr to form KBr pellets. Field emission scanning electron microscope (FESEM) (JSM-7800F, Japan) and energy-dispersive spectroscopy (EDS) (X-Max80 (OXFORD, Britain) were employed for analyzing the samples. UV-visible absorption spectra were collected on UV-Vis-NIR spectrophotometer (UV-3600, Shimadzu, Japan). X-ray diffraction (XRD) of PTET-T-COOH was obtained using an X-ray diffractometer (Thermo Fisher Scios. America). The X-ray photoelectron spectroscopy (XPS) were conducted by Excalab 250Xi (thermofisher America). ^{1}H NMR spectrum of polymer PTET-T-COOH was collected using a Varian INOVA 600 spectrometer at 25 °C. Sample was dissolved in DMSO-d_6 and the chemical shifts were referenced to tetramethylsilane (TMS; 0.0 ppm). Molecular weight and dispersity (Đ) of the synthesized polymer PTET-T-COOH were measured on a Polymer Laboratories (A Varian, Inc. Co.) Cirrus gel permeation chromatography (GPC) system (PL-GPC 220) using a refractive index detector and 3 × PLgel 10 μm MIXED-B (Varian, Inc.) columns. THF eluent flow rate was 1 mL/min; temperature was 30 °C; the system was calibrated using a series of polystyrene narrow standards with peak molecular weight Mp = 580 - 6,035,000 Da).

3.3.4   Testing of photocatalytic antibacterial properties of PTET-T-COOH

Gram-positive *S. aureus* (USA 300) and *S. suis* were chosen as model bacteria which were cultured in TSB at 37 °C for 12 h and then purified by high-speed freezing centrifuge at 12000 rpm for 2 min and washed twice with 1mL PBS, resulting in a cell count of

approximately $7\sim8\times10^8$ colony forming units (cfu)/mL. Typically, 3 mg of photocatalyst were dispersed in 30 mL of PBS solution (0.1 mg/mL) in a 120 mL self-designed glass jacketed reactor containing 600 μL of bacteria solution ($7\sim8\times10^8$ cfu/mL). The bacteria concentration for photocatalytic antibacterial test was about 10^7 cfu/mL. The reaction was carried out in a GHX-3 photochemical reaction instrument equipped with a 250 W Xenon arc lamp and an optical cutoff filter ($\lambda< 420$ nm). The visible light intensity was fixed at 80 mW/cm^2. The temperature was kept at 30 °C using a cryostatic tank. At given time intervals, 100 μL of tested suspension sample was pipetted out and serially diluted using PBS and spread on nutrient TSA plates. After incubation at 37 °C for 18 h, the cell densities were checked to determine the survival bacterial numbers. Control experiments (*S. aureus* or *S. suis* with PTET-T-COOH in dark and *S. aureus* or *S. suis* without PTET-T-COOH under irradiation) were also carried out. All materials and glassware had been autoclaved at 121 °C at 0.1 MPa for 20 min before use and all the experiments were repeated for three times. The process of photocatalytic antibacterial test is illustrated in Figure 3.1.
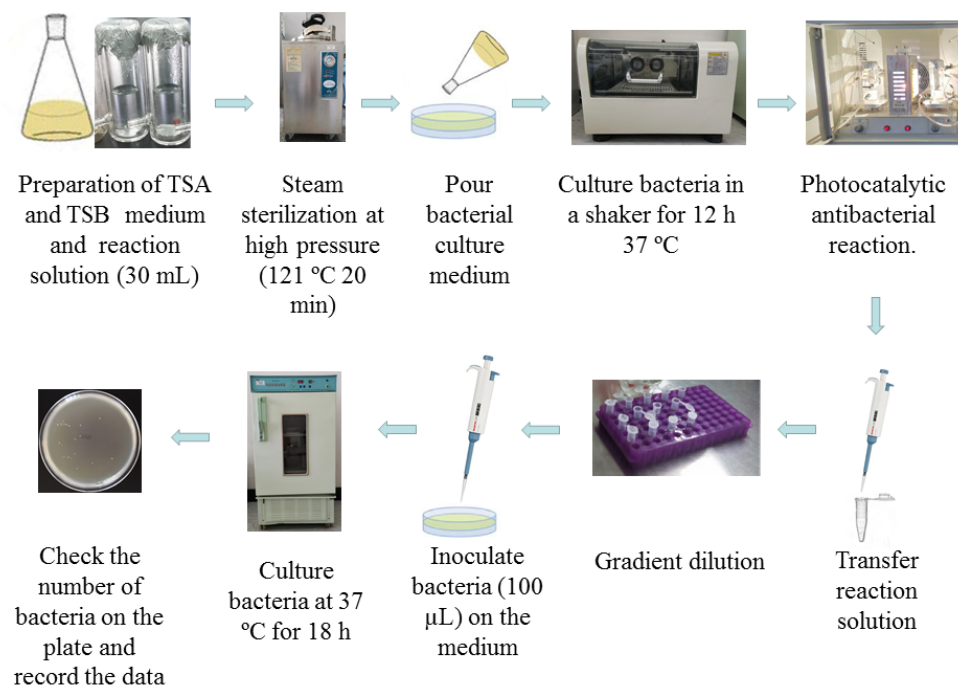
Figure 3.1. The illustration of photocatalytic antibacterial test.

3.3.5   Study of photocatalytic antibacterial mechanism

Rabbit plasma test

Staphylococcal coagulase is an important virulence factor for *S. aureus.* Coagulase converts host prothrombin to staphylothrombin, leading to activation of the protease activity of thrombin. It was predicted that coagulase could protect bacteria from phagocytic and immune defenses by causing localized clotting. The interaction between PTET-T-COOH and bacteria culture was to examine whether the expression of coagulase in *S. aureus* survival. A tube coagulation assay based on freeze-dried rabbit plasma was performed. PTET-T-COOH (3 mg) was added to bacteria culture (30 mL) and allowed to react for 0 min, 30 min, 60 min and 120 min. 300 μL of reaction solution collected at different times were added to 500 μL of PBS solution containing rabbit plasma in small ampoule of glass tubes. The mixture samples were incubated at 37 °C for 6 h, and rabbit plasma coagulation was examined.

Fluorescence microscopy observation of bacteria

Fluorescent-based cell live/dead tests were conducted for investigating the integrity of bacterial cell membranes. In brief, the bacterial liquids before and after 120 min irradiation treatment in the control and experimental groups were collected and centrifuged at 8000 rpm for 2 min with the supernatant discarded. The obtained bacteria were dispersed in 50 μL sterile PBS solution and stained with 25 μL of SYTO-9 (6 mg/mL in sterilized deionized water) and 25 μL of PI (6 mg/mL in sterilized deionized water) solution for 15 min in the dark at room temperature. Lastly, 10 μL of stained bacterial liquid was taken out and dropped on the center of slide and then imaged using a laser scanning confocal microscopy (Nikon Ti-s, Japan).

Active species trapping experiments

In order to study the active species generated in PTET-T-COOH, ethylenediamine tetraacetic acid disodium salt (EDTA-2Na, 0.5 mmol/L), tertbutyl alcohol (TBA, 10 mmol/L), L-Ascorbic acid (2 mmol/L), $K_2Cr_2O_7$ (2 mM) and NaN_3 (2 mmol/L) were used

as the traps of holes (h^+), hydroxyl radicals (•OH), superoxide (•O$_2^-$), electrons (e^-) and $^1O_2$, respectively. Electron spin resonance (ESR) analysis was conducted on using a Bruker EMX-Plus spectrometer and the concentration of spin traps of DMPO, BMPO and TEMP is 0.22 mmol/L in deionized water.

Photoelectrochemical measurements

Photocurrent tests were studied using a CHI 760D electrochemical workstation (Shanghai Chenhua Instrument Co. Ltd., China) in a conventional three-electrode structure with an as-prepared sample as the working electrode. A Pt plate was the counter electrode and an Ag/AgCl electrode was the reference electrode. A 0.5 mol L^{-1} Na$_2$SO$_4$ aqueous solution was the electrolyte. Each working electrode was fabricated as follows: 10 mg photocatalyst was ultrasonically dispersed in 1 mL DMF to achieve homogeneous suspension. Subsequently, the obtained suspension was dropped onto a pre-cleaned ITO sheet (0.25 cm^2). Finally, the electrode was dried at 60 °C for 4 h. 300 W xenon lamp was used as the visible light source ($\lambda > 420$ nm).

3.4   Results and Discussion

3.4.1   Synthesis and characterization of PTET-T-COOH

The conjugated polymer **PTET-T-COOH** was synthesized in three steps as shown in Figure 3.2. Starting from 2-thiophene-carboxaldehyde, the (E)-1,2-di(thiophen-2-yl) ethane (**T-E-T**) was prepared with a McMurry reaction under the catalysis of titanium tetrachloride.
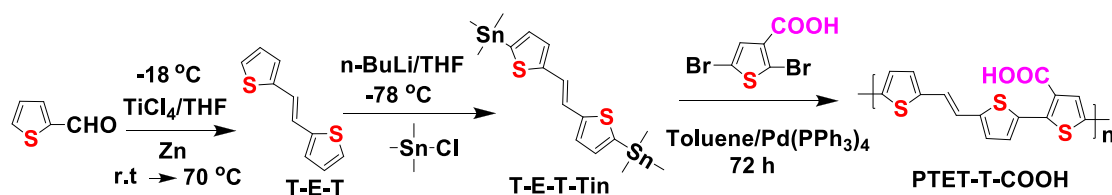
Figure 3.2. Synthetic scheme for PTET-T-COOH.

The T-E-T-Tin was further synthesized with lithiation of n-BuLi and nucleophilic additions of trimethyltin chloride. The targeted conjugated polymer PTET-T-COOH was obtained

through the palladium-catalyzed Stille coupling polymerization between T-E-T-Tin and 2,5-dibromothiophene-3-carboxylic acid. The intermediate compounds and PTET-T-COOH were characterized by FT-IR (Figure 3.3), ^{1}H NMR (Figure 3.4) and ^{13}C NMR (Figure 3.5) spectroscopies. Conventional synthetic strategies for synthesizing PTh and PTh derivatives usually utilize oxidative polymerization, Grignardmeta thesis polymerization, or Kumada catalyst-transfer polycondensation and typically afford homopolymers or block copolymers.[24, 25] In this work, 2,5-di bromothiophene-3-carboxylic acid monomer and T-E-T-Tin monomer with a larger planar structure were copolymerized by adopting palladium-catalyzed Stille polymerization to easily afford alternating PTET-T-COOH.

As seen in Figure 3.3a, there are three major peaks in the spectrum of T-E-T-Tin at 936, 773, and 532 cm^{-1}. These peaks are attributed to =C-H out of plane deformation vibration CH$_3$ rocking, and Sn-C asymmetric stretching modes, respectively. The two peaks in the FT-IR spectrum of the reactant 2,5-dibromothiophene-3-carboxylic acid at 3102 and 1692 cm^{-1} (Figure 3.3b) are ascribed to carboxylic O-H and C=O stretching modes, respectively while the peaks at 1528, 1438, and 1250 cm^{-1} are attributable to the ring vibration mode. When polymerizing the dibromo carboxylic acid with T-E-T-Tin to form the final product, PTET-T-COOH, several major FT-IR peaks are observed at 3098, 3063, 3014, 2915, 1696, 1559, 1426, 1397, 933, and 791 cm^{-1}. In addition to the peaks at 3098 and 1696 cm^{-1} attributed to carboxylic O-H and C=O stretching modes, respectively, the peaks at 3063, 3014, and 2915 cm^{-1} are attributed to C-H stretching modes. The peaks at 1559, 1426 and 1397 cm^{-1} are ascribed to ring vibration. The peaks at 933 and 791 cm^{-1} are assigned to =C-H out of plane deformation and ring C-H deformation vibrations, respectively. These FT-IR results demonstrate successful synthesis of T-E-T-Tin, 2,5-dibromothiophene-3-carboxylic acid and PTET-T-COOH. Moreover, ^{1}H and ^{13}C NMR spectra of the synthesized T-E-T, T-E-T-Tin, and 2,5-dibromothiophene-3-carboxylic acid (Figure 3.4 and 3.5) further confirmed successful syntheses of these intermediates. The targeted conjugated polymer PTET-T-COOH exhibits insolubility in common organic solvents, such as chloroform and toluene, but there is certain solubility in highly polar solvents, such as dimethyl sulfoxide (DMSO) and o-dichlorobenzene.
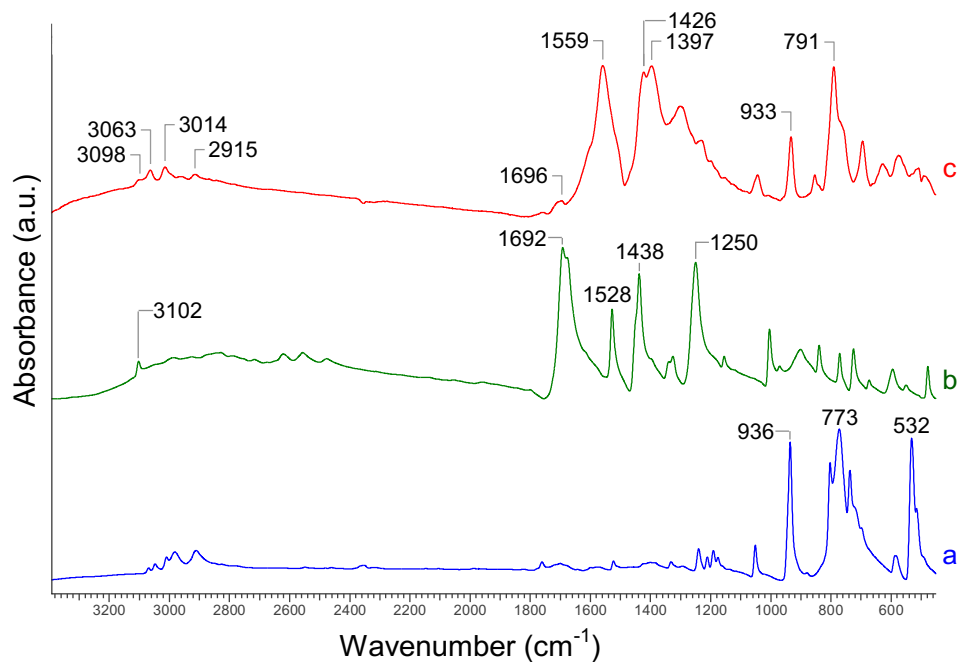
Figure 3.3. FT-IR spectra of (a) T-E-T-Tin, (b) 2,5-dibromothiophene-3-carboxylic acid, and (c) PTET-T-COOH.
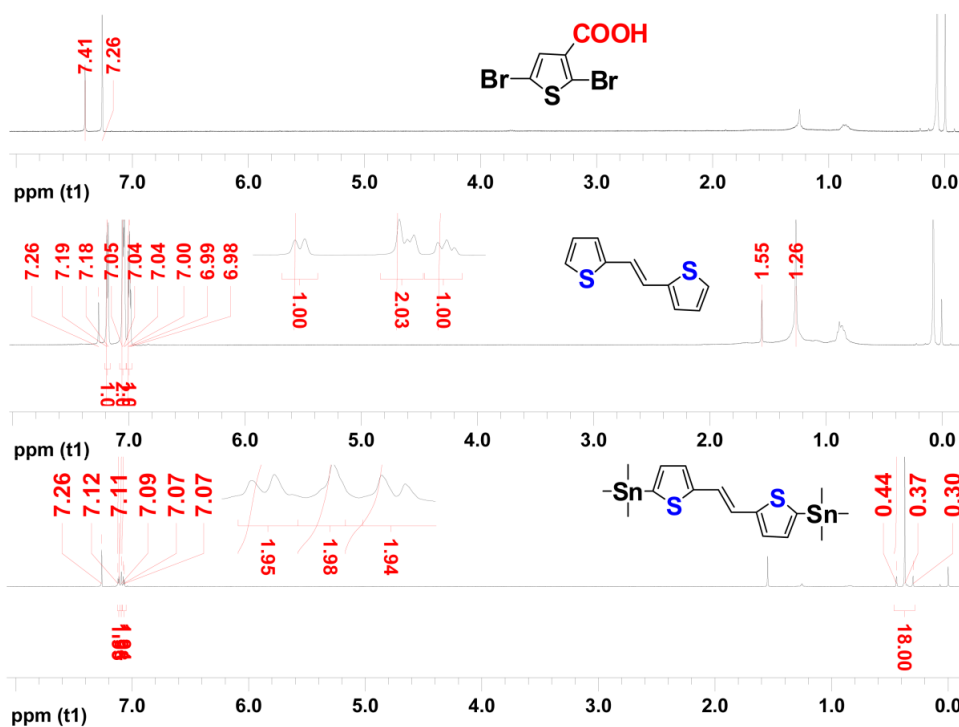
Figure 3.4. ^{1}H NMR spectra of compound 2,5-dibromothiophene-3-carboxylic acid, T-E-T and T-E-T-Tin in CDCl$_3$.
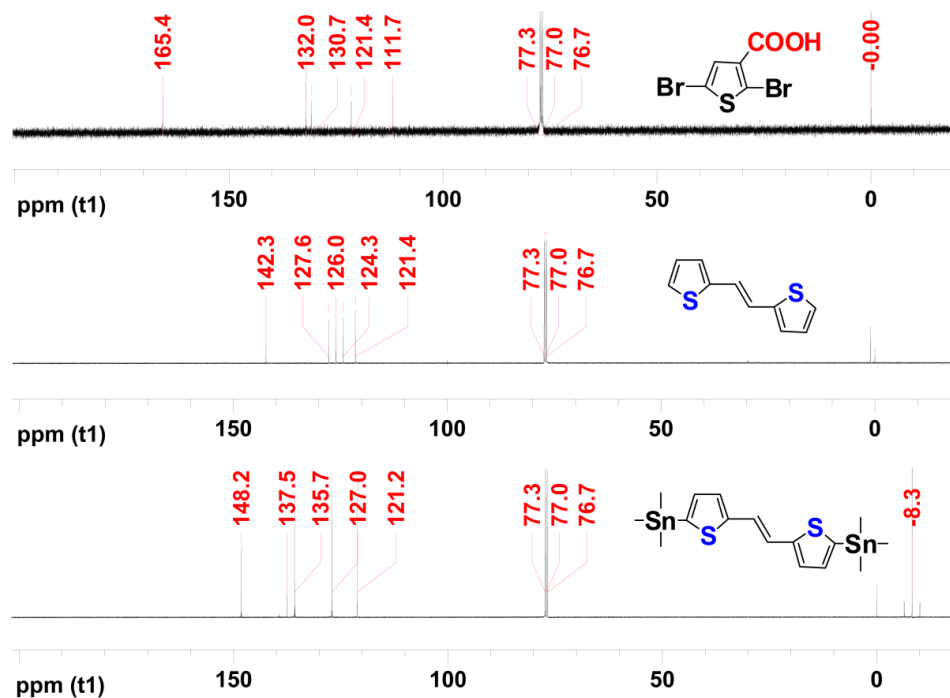
Figure 3.5. ^{13}C NMR spectra of 2,5-dibromothiophene-3-carboxylic acid, T-E-T and T-E-T-Tin in CDCl$_3$.

The polymer PTET-T-COOH was dissolved in DMSO-d$_6$ and characterized by ^{1}H NMR spectrum (Figure 3.6). The proton signals of carbonyl adjacent thiophene at 7.48 ppm were observed for PTET-T-COOH and the signals of down field resonance ranged from 7.23 to 7.06 ppm were assigned to proton signals of T-E-T units, which agreed well with the proton signals of monomers before polymerization, respectively. Besides, the characteristic broad peaks were observed for PTET-T-COOH after polymerization like other conjugated polymers. Solid-state ^{13}C NMR spectrum of the final polymer PTET-T-COOH is provided in Figure 3.7, showing a resonance at 170.5 ppm for the carboxyl carbon (-C=O), confirming the presence of carboxyl group.[26] Signals in the range from 127 to 142 ppm are assigned to sp^2-hybridized carbon atoms within the vinyl spacers and the thiophene moieties.[27]
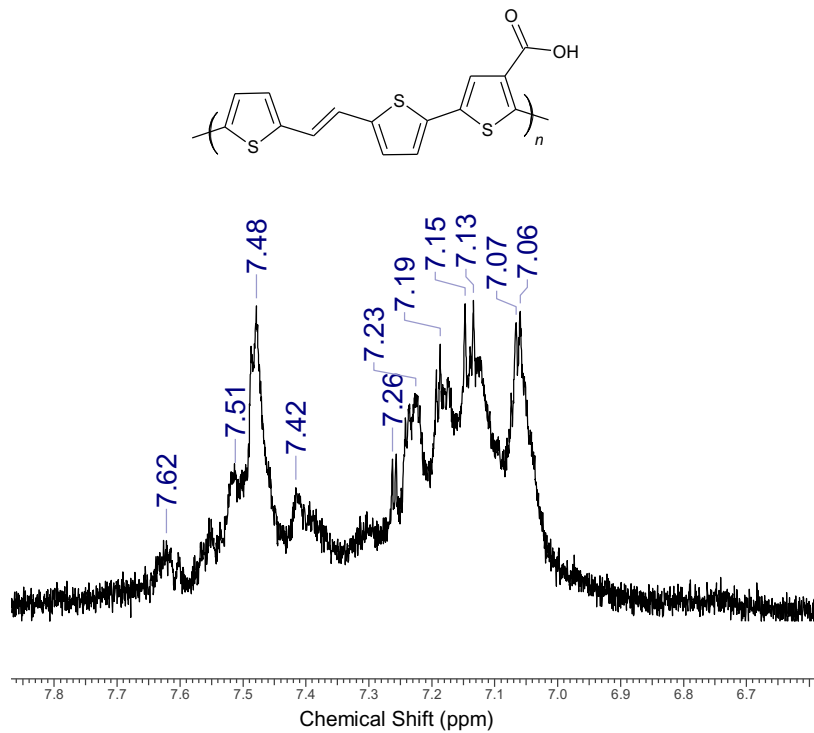
Figure 3.6. ^{1}H NMR spectrum of polymer PTET-T-COOH in DMSO-d_6.
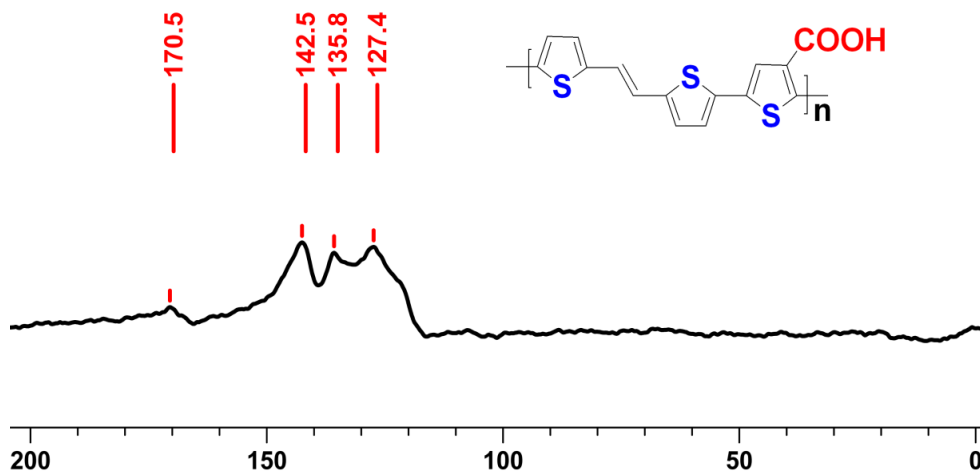
Figure 3.7. Solid-state ^{13}C NMR spectrum of polymer PTET-T-COOH.

The XPS survey spectrum demonstrates that the surface of PTET-T-COOH consists of C, O and S (Figure 3.8 a). The high-resolution spectra of C 1s, O 1s and S 2p are shown in

Figure 3.8 b-d. The high-resolution C 1s spectrum of PTET-T-COOH can be decomposed into five peaks. Two conspicuous peaks centered at 284.2 and 284.8 eV are observed, representing C-C sp^2 and C-C sp^3 in the framework of PTET-T-COOH, respectively.[28] The characteristic peak of C-S bond at 285.1 eV in C 1s spectra reveals the S atom in the thiophene of PTET-T-COOH.[28] The peak centered at 287.1 eV is typical for the C-O bond. Moreover, the weak signal at 288.7 eV can be attributed to the C=O units in the carboxyl groups. [29] The O1s spectra of PTET-T-COOH can be deconvoluted into two peaks which correspond to O-H (531.7 eV) and C=O (532.7 eV), respectively. The sulfur in PTET-T-COOH was also examined in the S 2p XPS spectra. The binding energies of 164.1 and 165.3 eV from the S 2p spectrum of PTET-T-COOH with spin-orbital splitting of 1.2 eV indicates the S 2p3/2 and S 2p1/2 states of sulfur in the thiophene units.[30]
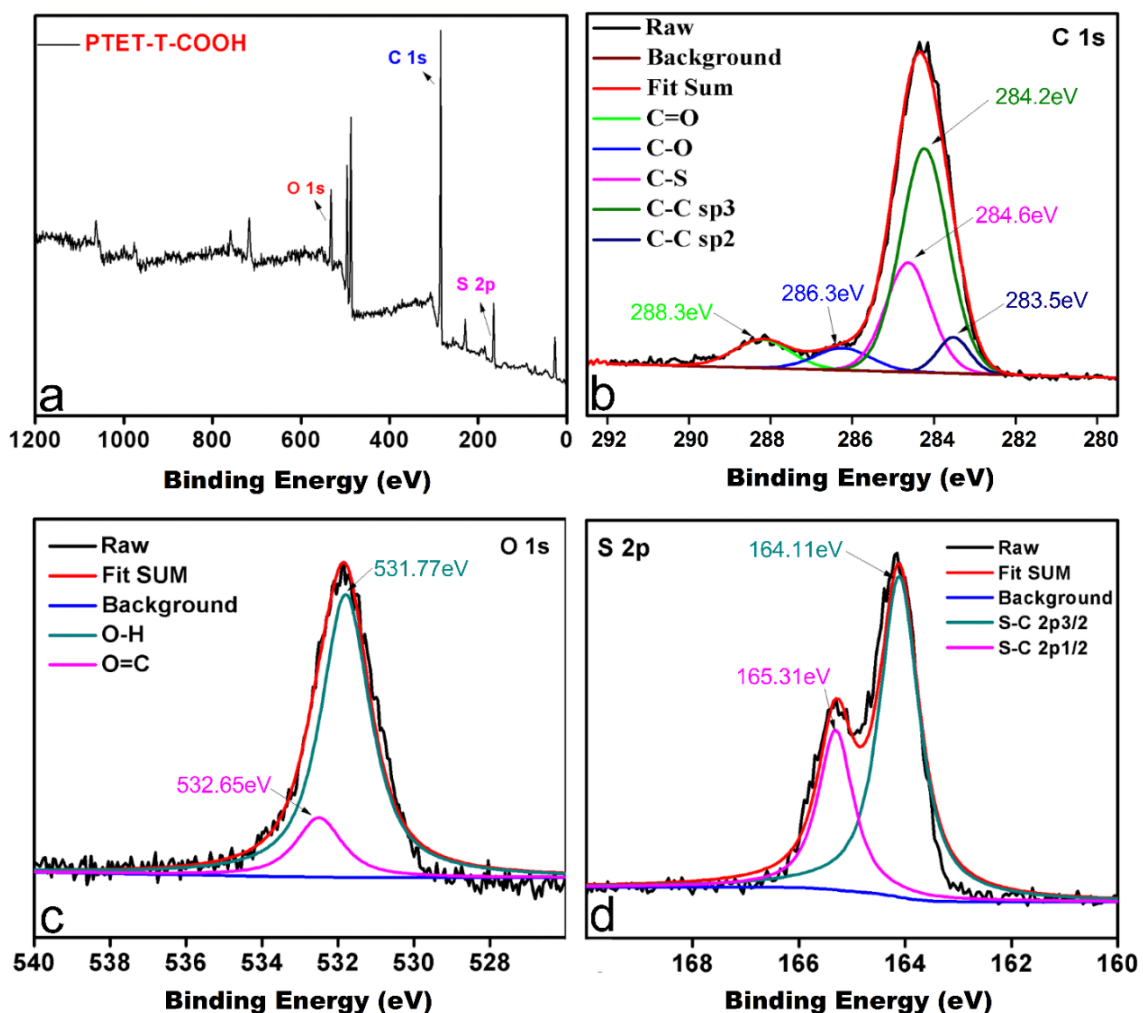
Figure 3.8. (a) XPS spectrum of PTET-T-COOH. (b) High-resolution C1s peak in the XPS spectrum of PTET-T-COOH. (c) High-resolution O 1s peak in the XPS spectrum of PTET-T-COOH. (d) High-resolution S2p peak in the XPS spectrum of PTET-T-COOH.

In addition, the synthesized polymer PTET-T-COOH was also characterized by SEM, EDS and UV-Vis. SEM images show that PTET-T-COOH possesses bulky morphology and the C, O and S elements are observed in the EDS spectrum (Figure 3.9). The optical properties of PTET-T-COOH were analyzed by UV-Vis absorption spectrum (Figure 3.10). The PTET-T-COOH film exhibited a broad absorption band covering UV and almost the entire visible light range, attributed to localized π-$\pi*$ transition between the aryl units.[31] Furthermore, the weak shoulder peak indicates that the majority of the conjugated polymers were self-organized forming aggregates in the solid state.[32] The synthesized PTET-T-COOH exhibited an absorption edge (λ_{onset}) at 650 nm. The optical band gap (E_g^{opt}) was calculated to be 1.90 eV according to the empirical equation $E_g^{opt} = 1240/\lambda_{onset}$. In comparison, poly(3-hexylthiophene) P3HT, a popular semicrystalline polymer, is the dominant light-harvesting absorber of incident sunlight, has a similar E_g^{opt} of 1.9~2.1 eV.[39] In addition, PTET-T-COOH exhibits a much broader absorption spectrum in comparison to that of P3HT, attributed to the increased polarizability in the structure.[38]
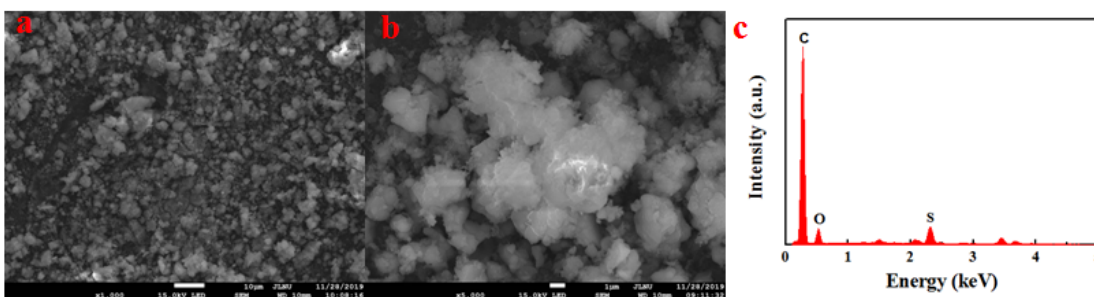
Figure 3.9. SEM images and EDX spectrum of PTET-T-COOH.
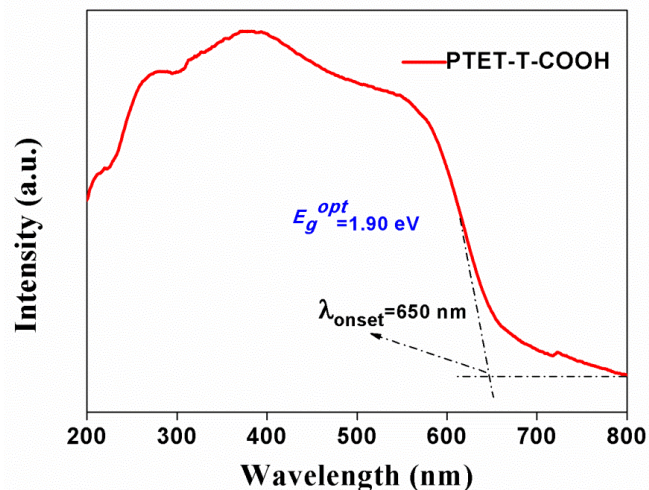
Figure 3.10. UV-Vis absorption spectra of PTET-T-COOH.

3.4.2   Photocatalytic antibacterial properties of PTET-T-COOH

Two gram-positive bacteria, *S. aureus* and streptococci suis, were chosen to investigate the antibacterial activity of PTET-T-COOH. Light control without adding PTET-T-COOH, dark control with adding PTET-T-COOH and photocatalytic disinfection by mixing PTET-T-COOH powder in the bacterial suspension were performed. As displayed in Figure 3.11, negligible disinfection activity on *S. aureus* cells was found for the two control experiments, visible light control without adding PTET-T-COOH and dark control while adding PTET-T-COOH. On the contrary, *S. aureus* was efficiently destroyed in the presence of PTET-T-COOH under visible light with approximately 98 % and 99.9999 % of bacteria being killed in 30 min and 2 h, respectively, with a low concentration of 0.1 mg/mL. The amount of *S. aureus* bacteria decreased with the increase of illumination time up to 2h as demonstrated in the images (Figure 3.11c). For comparison of antibacterial capability and stability, we reviewed the disinfection performances of some photocatalysts based on PTh (its derivatives) and graphic carbon nitride (g-C_3N_4) which is one of the most popular visible light responsive photocatalysts and have been widely studied in various photocatalytic fields.[27, 33] The inactivation efficiency of our PTET-T-COOH on *S. aureus* cells is among the best results (Table 3.1) with a much lower concentration of antibacterial materials than those in g-C_3N_4 based systems.

Figure 3.11. (a) Photocatalytic inactivation efficiency and (b) cell density of PTET-T-COOH against *S. aureus*; (c) Images of *S. aureus* colonies on an agar plate before and under different visible light irradiation time.

Table 3.1. The representative photocatalysts based on PTh derivatives and g-C_3N_4 with their concentration, target microorganisms and photocatalytic disinfection performances.

Photocatalyst	Concentration	Bacteria	Photocatalytic performance
PTP/TPPN [9]	[TPPN] 3.0 μM, [PTP] 12.0 μM	*E. coli.*	killing efficiency 70 % 5 min
polythiophene/ MnO$_2$ [15]	1000 μg/mL	*S. aureus*	6 log 360 min
Polythiophene/Porphyrin[19]	film	*E. coli*	killing efficiency 65% (blue light)

polythiophene/ $Cu_xZn_{1-x}O$ [16]	minimal inhibitory concentration 10 µg/mL	*S. aureus*	inhibition zone 35.4 mm
P3HT-Im [20]	10 µg/mL	*S. aureus*	killing efficiency 99.8%
P3HT-Im P3HT-T [11]	10 µg/mL	*Bacillus atrophaeus*	killing efficiency 99.9%
Ag/g-C$_3$N$_4$ [34]	60 µg/mL	*S. aureus*	killing efficiency ~ 100% 30 min
g-C$_3$N$_4$-AgBr [35]	100 µg/mL	*S. aureus*	6.4 log 150 min
g-C$_3$N$_4$/ZnO/stellerite [36]	100 µg/mL	*S. aureus*	7 log 120 min
g-C$_3$N$_4$-BiFeO$_3$-Cu$_2$O [37]	150 µg/mL	*S. aureus*	inhibition zone 18±0.5 mm
g-C$_3$N$_4$/BiOI [38]	200 µg/mL	*S. aureus*	7 log 60 min
1/0.3-CNS/TNS/CuBA [39]	1000 µg/mL	*S. aureus*	7 log 90 min
g-C$_3$N$_4$-nitride nanosheet [40]	100 µg/mL	*S. aureus*	4.24 log 120 min
CDQs/g-C$_3$N$_4$ [41]	1000 µg/mL	*S. aureus*	7 log 220 min
g-C$_3$N$_4$/α-Fe$_2$O$_3$/CeO$_2$ [42]	200 µg/mL	*S. aureus*	inhibition zone 14 ± 0.5 mm
g-C$_3$N$_4$ quantum dots [43]	100 µg/mL	*S. aureus*	killing efficiency 90 % 180 min

C$_3$N$_4$/PDINH [44]	500 µg/mL	*S. aureus*	killing efficiency 90 %
Bi@Co@CN [45]	200 µg/mL	*S. aureus*	7 log 30 min
PTET-T-COOH (This work)	100 µg/mL	*S. aureus*	6 log 120 min

Streptococci are another kind of gram-positive antibiotic-resistant strain which live in pairs or chains of varying length. Diseases caused from *S. suis* range from strep throat to necrotizing fasciitis.[46] Photocatalytic disinfection activity PTET-T-COOH against *S. suis* is depicted in Figure 3.12. Similar to its activity on *S. aureus* cells, negligible disinfection activity on *S. suis* was found for the two control experiments, visible light control without adding PTET-T-COOH and dark control with adding PTET-T-COOH. Under visible light irradiation, PTET-T-COOH killed approximately 98 % and over 99.999 % of *S. suis* cells in 30 min and 2 h, respectively, with a low concentration of 0.1 mg/mL. The number of *S. suis* bacteria decreased continuously with increasing illumination time up to 2 h, as demonstrated in the images (Figure 3.12c).
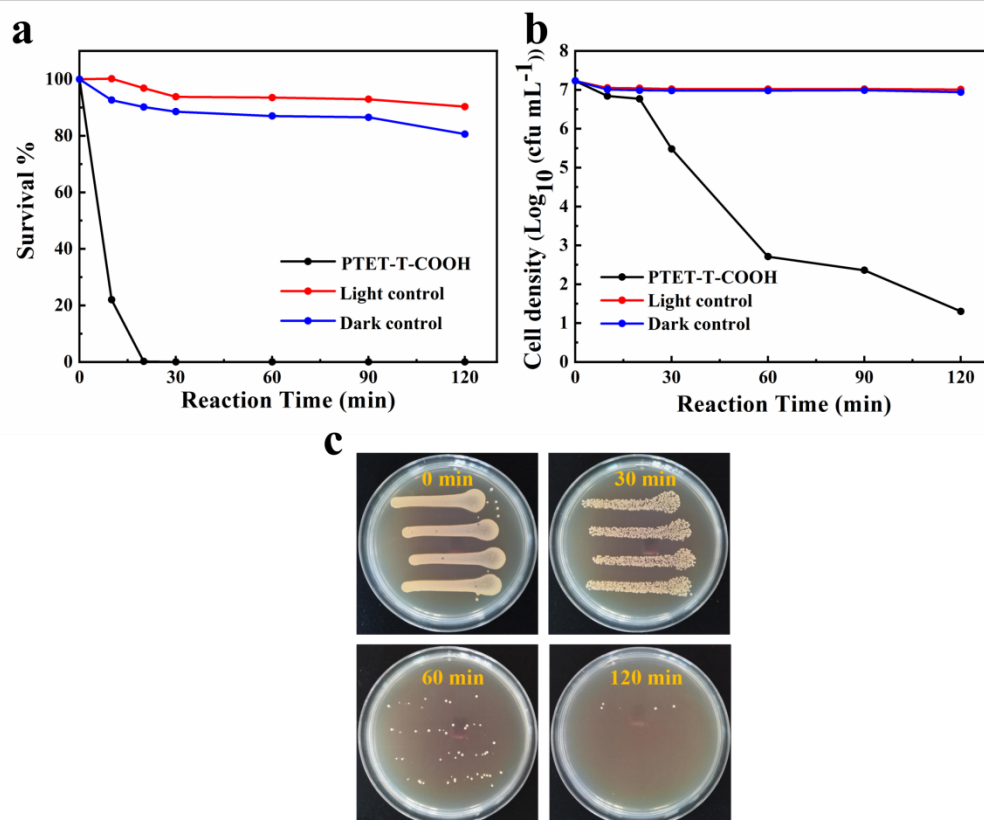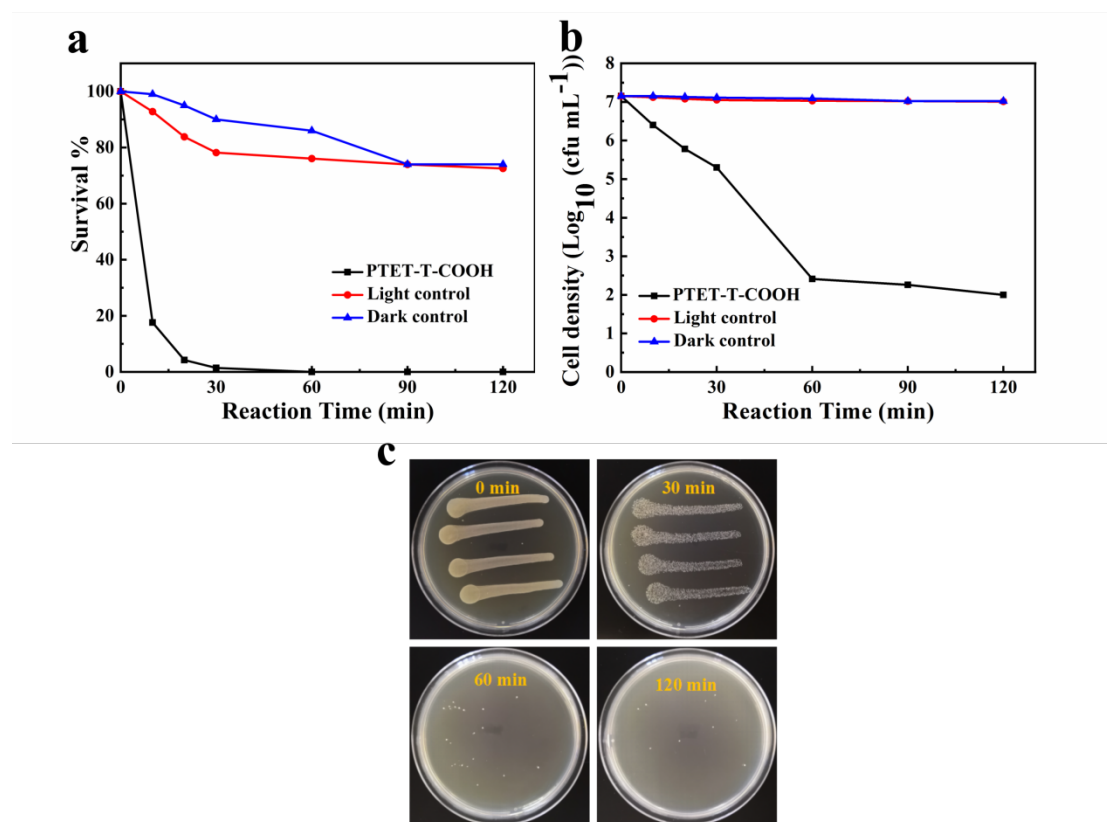
Figure 3.12. (a) Photocatalytic inactivation efficiency and (b) cell density of PTET-T-COOH against *S. suis*; (c) Images of *S. suis* colonies on an agar plate before and under different visible light irradiation time.

In our study, cycling runs of PTET-T-COOH were carried out to study its photocatalytic stability against *S. aureus*. PTET-T-COOH was collected from the photocatalytic disinfection and sterilized by high temperature for repeating use. After five cycles, PTET-T-COOH still exhibited excellent inactivation efficiency as demonstrated in Figure 3.13. Cell densities of *S. aureus* were decreased from 7-log to 1.3-log for the first three cycles, to around 2.5-log for the fourth and fifth runs. Slight decrease of photocatalytic activity of PTET-T-COOH is probably due to the loss of PTET-T-COOH during recycling treatment.
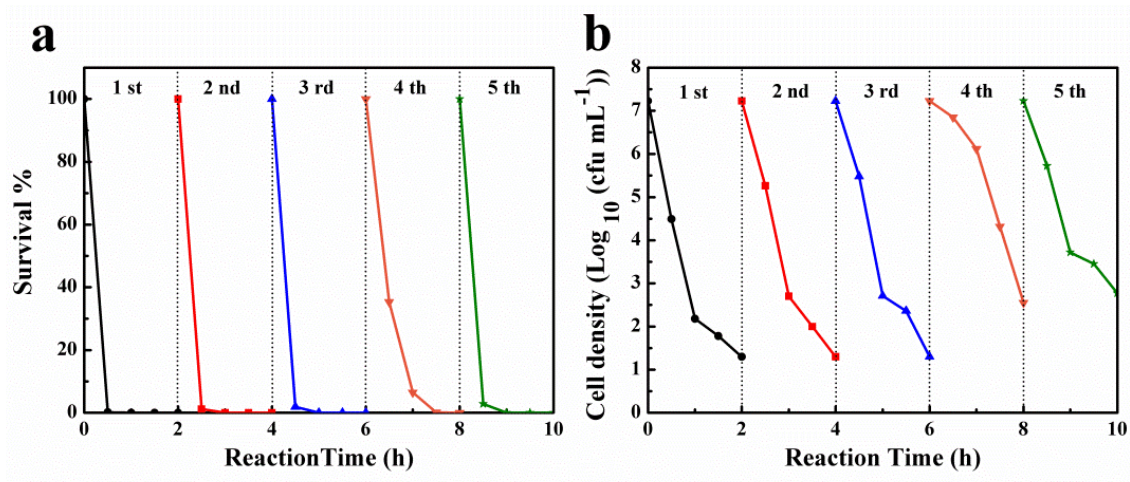
Figure 3.13. Stability test of PTET-T-COOH on *S. aureus* (10^7 cfu mL^{-1}, 30 mL) under visible light for five successive applications.

The chemical stability of PTET-T-COOH before and after the five cycle antibacterial reactions against *S. aureus* was evaluated by FT-IR and powder X-ray diffraction (XRD). As seen in Figure 3.14, the FT-IR spectra of PTET-T-COOH before and after the five cycles are almost identical, indicating that the chemical structure did not change substantially during the 5 runs of visible light photocatalytic disinfection experiments. XRD showed that PTET-T-COOH samples before and after the five cycles were

predominantly amorphous with some degree of preferred ordering in the low-angle region. The presence of the weak and broad reflection peaks with 2θ values of around 23.5 for PTET-T-COOH before and after the five cycles can be assigned to the π-π stacked interlayer form.[47] The similar XRD patterns of PTET-T-COOH samples before and after the five cycles also confirmed the chemical stability of PTET-T-COOH in 5 runs of visible light photocatalytic disinfection experiments.
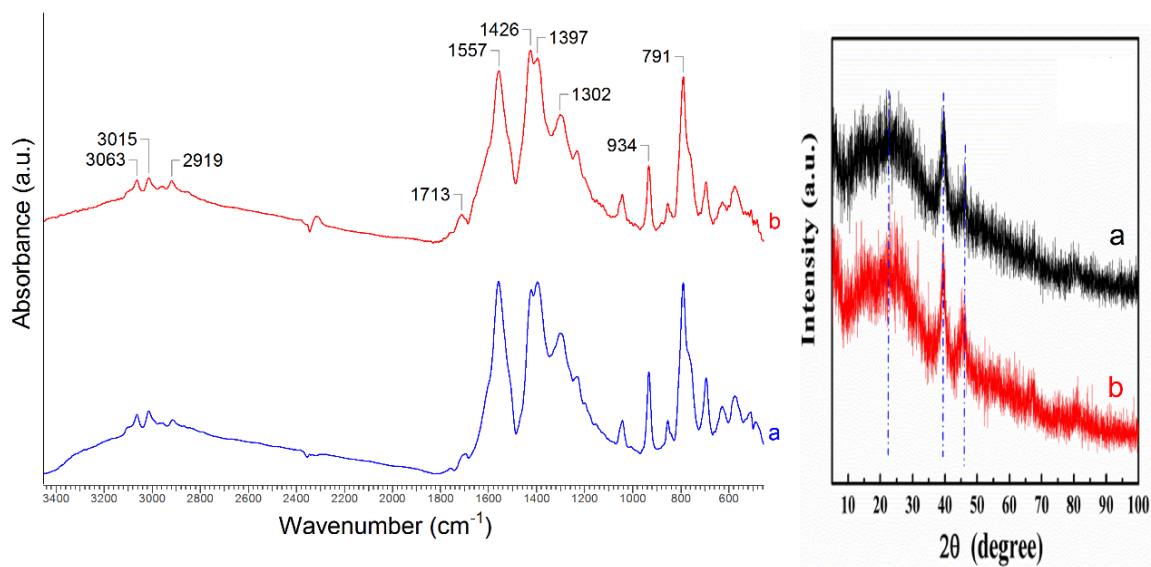
Figure 3.14. (left) FT-IR spectra and (right) XRD patterns of PTET-T-COOH (a) before and (b) after five runs.

Apart from *S. aureus* and *S. suis*, the photocatalytic disinfection efficiency of PTET-T-COOH against gram-negative strain *E. coli* was also examined in our study. Unfortunately, almost no inactivation effect was observed (Figure 3.15). This phenomenon always occurs in various photosensitizers which are generators of singlet oxygen. Compared to Gram-positive bacteria, Gram-negative bacteria such as *E. coli* have an additional outer membrane which can hinder the interaction between photocatalyst and bacteria and the interception of singlet oxygen.
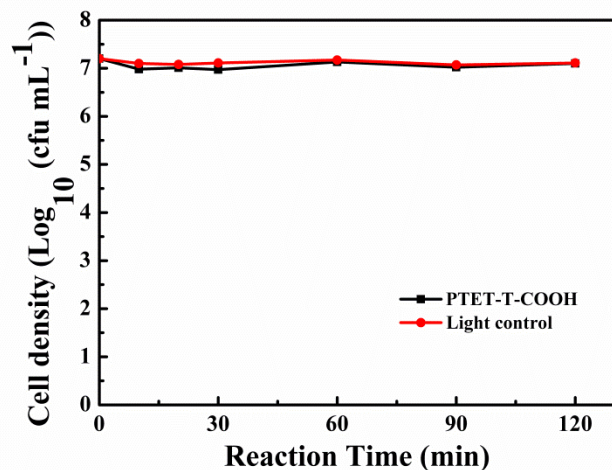
Figure 3.15. Photocatalytic inactivation efficiency of PTET-T-COOH against *E. coli.*

3.4.3 Photocatalytic antibacterial mechanism of PTET-T-COOH

For studying the mechanism underlying the inactivation performance of PTET-T-COOH toward *S. aureus*, rabbit plasma coagulation was carried out. Live *S. aureus* can produce plasma coagulase which can be released into the rabbit plasma which leads to the coagulation of rabbit plasma. Figure 3.16 exhibits the effect of *S. aureus* exposed to different times of irradiation at 0, 30, 60 and 120 min on freeze-dried rabbit plasma. After 60 min, due to the increase of dead bacterial cells, the amount of plasma coagulase decreased, and the rabbit plasma began to flow. After 120 min of irradiation treatment with PTET-T-COOH photocatalyst, rabbit plasma became liquid from solid state completely owing to the lack of plasma coagulase implying *S. aureus* cells were killed efficiently.
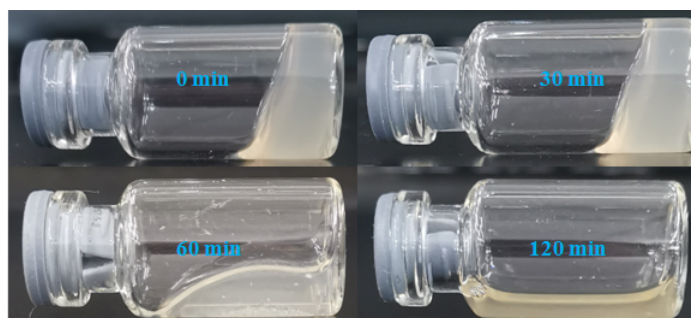
Figure 3.16. Images of flowability of Rabbit Plasma in the presence of *S. aureus* and PTET-T-COOH upon increasing irradiation times.

Additionally, for studying the integrity of *S. aureus* cell membranes, fluorescence-based live/dead experiments of bacterial cells were performed. SYTO-9 and PI fluorescent nucleic acid dyes were used to stain the cells. SYTO-9 is a live bacterial cell stain which can permeate through an unbroken membrane and show green fluorescence, while PI is a cell-impermeable stain with red fluorescence which labels only dead cells. As depicted in Figure 3.17, few dead cells were observed in the control experiment after 2 h of visible light irradiation. However, a stronger red fluorescence was observed in the bacterial cells with PTET-T-COOH photocatalysts in comparison with the control. This implied that the cell membranes of *S. aureus* were seriously destroyed during the disinfection process.
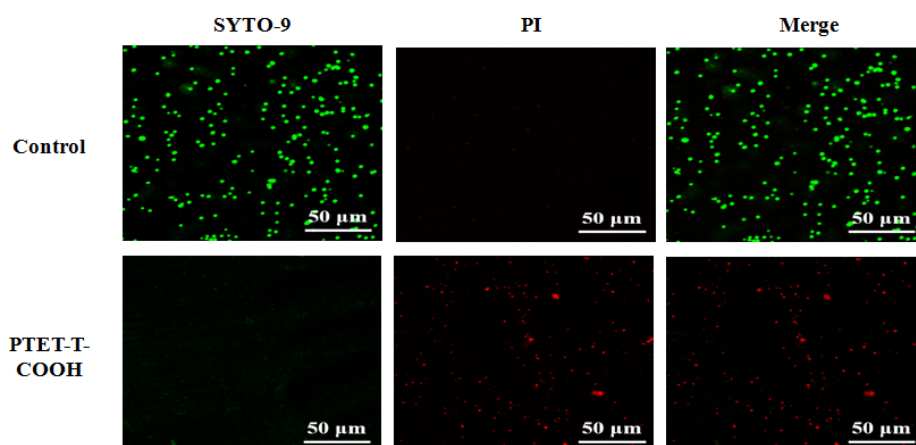
Figure 3.17. Fluorescent staining of control and PTET-T-COOH.

Reactive oxygen species (ROSs) including hole (h^+), electron (e^-), hydroxyl radical (•OH), superoxide radical (•O_2^-) and $^1O_2$ were reactive species reported in the photocatalytic disinfection. For interpreting the mechanism of the polymer-induced disinfection, EDTA-2Na, TBA, L-Ascorbic acid, $K_2Cr_2O_7$, and NaN_3, were applied as the scavengers of holes (h^+), hydroxyl radicals (•OH), superoxide (•O_2^-), electrons (e^-) and $^1O_2$, respectively.[27] As displayed in Figure 10a, scavengers have no effect of bacterial inactivation alone under illumination. Different levels of bacterial inactivation were observed after adding PTET-T-COOH (Figure 3.18). The addition of $K_2Cr_2O_7$ and NaN_3 decreased the bacterial

inactivation significantly in comparison to the addition of other scavengers. This proved that e^- and $^1O_2$ species played vital roles in the reaction process. Additionally, electron spin response (ESR) was employed for further exploring the active ROSs. BMPO is a cyclic nitrone spin trap that can also be used for the detection and characterization of superoxide anions in vitro or in vivo. DMPO is a nitric oxide trap which can be used to detect hydroxyl radicals.[48] TEMP is a piperidinol molecule which is used to detect singlet oxygen of PTh derivative (P3HT) because TEMO can react with $^1O_2$ to produce 2,2,6,6-tetramethyl-4-piperidone-N-oxyl (TEMPO). [49] For DMPO-•OH and BMPO-•O_2^- under visible light irradiation and TEMP-$^1O_2$ in the dark, no obvious signals were detected (Figure 3.19). However, the characteristic 1:1:1 triplet signal of the TEMP-$^1O_2$ adduct provided direct evidence of singlet oxygen generation in the photocatalytic system under illumination which is characteristic of photosensitizers including polythiophene and its derivatives.[11] The sulfur in the repeat unit of PTET-T-COOH can result in spin-orbit coupling and efficient singlet-triplet intersystem crossing. This can yield triplet excited state and sensitize the triplet oxygen (ground state of oxygen) to produce singlet oxygen and destroy *S. aureus* and *S. suis* cells.[50] It has been reported that P3HT, as an important PTh derivative and a p-type semiconductor, can be degraded by •O_2^-.[51] This poses a disadvantage to decrease the stability of organic solar cells using P3HT.[52] In addition, it was previously demonstrated that $^1O_2$ was unreactive to P3HT.[49, 53] According to the trapping experiments and the ESR results, $^1O_2$ is the responsible ROSs rather than •O_2^-. This can help explain the excellent chemical stability of PTET-T-COOH even after 5 cycling runs.
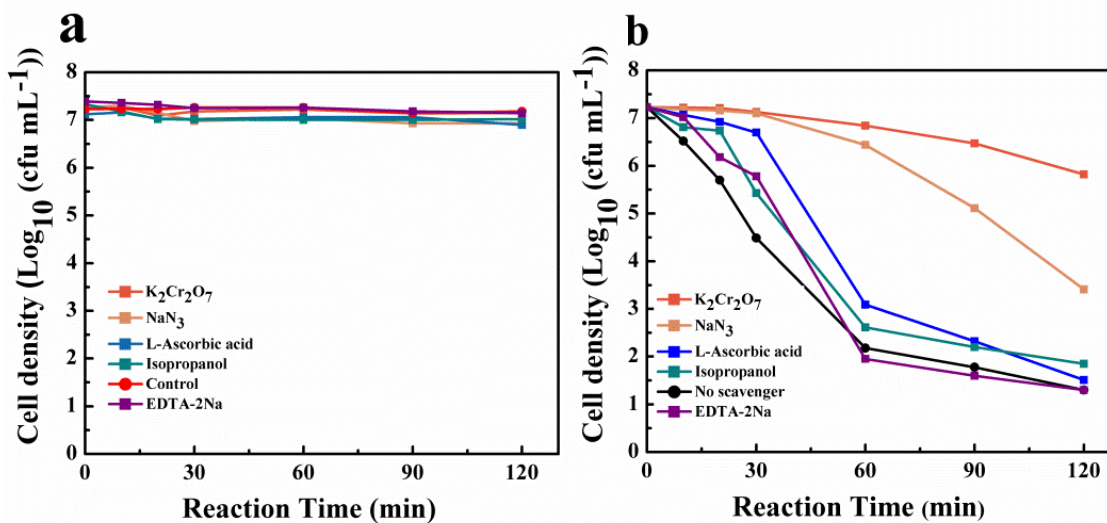
Figure 3.18. Photocatalytic inactivation efficiency against *S. arueus* (a) before and (b) after adding PTET-T-COOH using different scavengers under visible light irradiation.
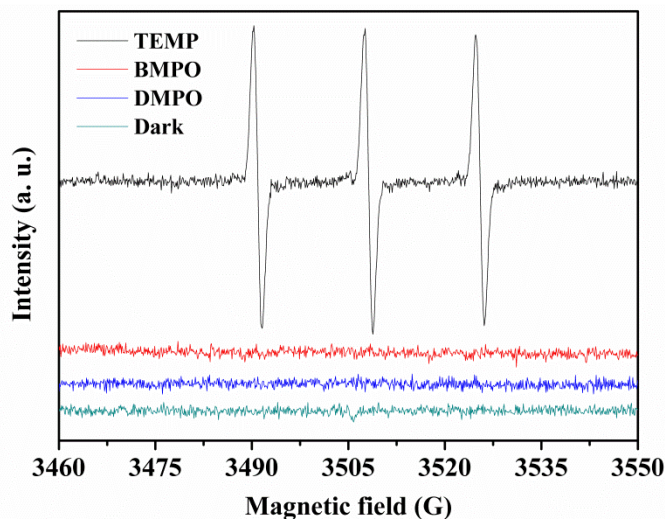
Figure 3.19. Spin trapping-ESR spectra of PTET-T-COOH solution after visible light irradiation.

In order to evaluate the separation efficiency of photogenerated electron-hole pairs, photocurrent responses of PTET-T-COOH and g-C_3N_4 which was used as a reference sample were measured. As depicted in Figure 3.20, PTET-T-COOH demonstrated stronger photocurrent signals than that of g-C_3N_4, indiacting efficient dissociation and transportation of charege carriers occurred in PTET-T-COOH conjugated system.
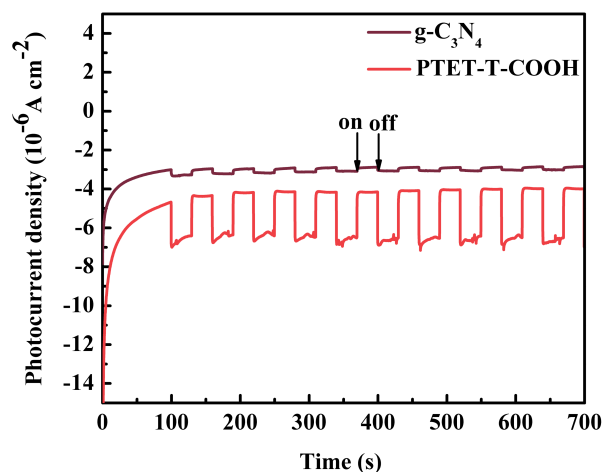
Figure 3.20. Transient photocurrent responses and EIS changes of bulk g-C$_3$N$_4$ and PTET-T-COOH.

3.5 Conclusions

A conductive polymer PTET-T-COOH was successfully synthesized and characterized by detailed NMR, FT-IR and XPS characterization. The photocatalytic antibacterial properties of PTET-T-COOH against two Gram-positive bacteria *S. aureus* and *S. suis* under visible light irradiation were investigated. Both *S. aureus* and *S. suis* were efficiently destroyed in the presence of PTET-T-COOH under visible light with approximately 98 % and over 99.999 % of bacteria being killed in 30 min and 2 h, respectively, with a low PTET-T-COOH concentration of 0.1 mg/mL. The photocatalytic antibacterial mechanism of PTET-T-COOH was studied in detail by using ROSs scavengers and ESR, revealing that the generated singlet oxygen and free electrons were responsible for the disinfection process. In addition, the synthesized PTET-T-COOH demonstrated excellent chemical stability and reusability.

3.6 References

1. Jones, K. E.; Patel, N. G.; Levy, M. A.; Storeygard, A.; Balk, D.; Gittleman, J. L.; Daszak, P., Global trends in emerging infectious diseases. *Nature* **2008,** *451* (7181), 990.

2. Rice, K. M.; Ginjupalli, G. K.; Manne, N. D. P. K.; Jones, C. B.; Blough, E. R., A review of the antimicrobial potential of precious metal derived nanoparticle constructs. *Nanotechnology* **2019,** *30* (37), 372001.

3. Lee, Y.-J.; Lee, D.-J., Impact of adding metal nanoparticles on anaerobic digestion performance – A review. *Bioresource Technology* **2019,** *292*, 121926.

4. Sun, G.; Hong, K. H., Photo-induced antimicrobial and decontaminating agents: recent progresses in polymer and textile applications. *Textile Research Journal* **2013,** *83* (5), 532-542.

5. Lee, S. L.; Chang, C.-J., Recent developments about conductive polymer based composite photocatalysts. *Polymers* **2019,** *11* (2), 206.

6. Wang, C.; Dong, H.; Jiang, L.; Hu, W., Organic semiconductor crystals. *Chemical Society Reviews* **2018,** *47* (2), 422-500.

7. Kamyshny, A.; Magdassi, S., Conductive nanomaterials for 2D and 3D printed flexible electronics. *Chemical Society Reviews* **2019,** *48* (6), 1712-1740.

8. Liu, L.; Ding, L.; Liu, Y.; An, W.; Lin, S.; Liang, Y.; Cui, W., A stable Ag_3PO_4@PANI core@shell hybrid: Enrichment photocatalytic degradation with π-π conjugation. *Applied Catalysis B: Environmental* **2017,** *201*, 92-104.

9. Yuan, X.; Floresyona, D.; Aubert, P.-H.; Bui, T.-T.; Remita, S.; Ghosh, S.; Brisset, F.; Goubard, F.; Remita, H., Photocatalytic degradation of organic pollutant with polypyrrole nanostructures under UV and visible light. *Applied Catalysis B: Environmental* **2019,** *242*, 284-292.

10. Gao, B.; Iftekhar, S.; Srivastava, V.; Doshi, B.; Sillanpää, M., Insights into the generation of reactive oxygen species (ROS) over polythiophene/$ZnIn_2S_4$ based on different modification processing. *Catalysis Science & Technology* **2018,** *8* (8), 2186-2194.

11. Brown, D. M.; Yang, J.; Strach, E. W.; Khalil, M. I.; Whitten, D. G., Size and substitution effect on antimicrobial activity of polythiophene polyelectrolyte derivatives under photolysis and dark conditions. *Photochemistry and Photobiology* **2018,** *94* (6), 1116-1123.

12. Truc, N. T. T.; Hanh, N. T.; Nguyen, D. T.; Trang, H. T.; Nguyen, V. N.; Ha, M. N.; Nguyen, T. D. C.; Pham, T.-D., Novel overall photocatalytic water splitting of tantalum nitride sensitized/protected by conducting polymers. *Journal of Solid State Chemistry* **2019,** *269*, 361-366.

13. Kharazi, P.; Rahimi, R.; Rabbani, M., Study on porphyrin/$ZnFe_2O_4$@ polythiophene nanocomposite as a novel adsorbent and visible light driven photocatalyst for the removal of methylene blue and methyl orange. *Materials Research Bulletin* **2018,** *103*, 133-141.

14. Kaur, M.; Pramanik, S.; Kumar, M.; Bhalla, V., Polythiophene-encapsulated bimetallic au-Fe$_3$O$_4$ Nano-hybrid materials: a potential tandem photocatalytic system for nondirected C (sp^2)–H activation for the synthesis of Quinoline carboxylates. *ACS Catalysis* **2017,** *7* (3), 2007-2021.

15. Shang, K.; Ai, S.; Ma, Q.; Tang, T.; Yin, H.; Han, H., Effective photocatalytic disinfection of E. coli and S. aureus using polythiophene/MnO$_2$ nanocomposite photocatalyst under solar light irradiation. *Desalination* **2011,** *278* (1-3), 173-178.

16. Ma, G.; Liang, X.; Li, L.; Qiao, R.; Jiang, D.; Ding, Y.; Chen, H., Cu-doped zinc oxide and its polythiophene composites: Preparation and antibacterial properties. *Chemosphere* **2014,** *100*, 146-151.

17. Zhang, Z.; Zhu, Y.; Chen, X.; Zhang, H.; Wang, J., A full‐spectrum metal‐free porphyrin supramolecular photocatalyst for dual functions of highly efficient hydrogen and oxygen evolution. *Advanced Materials* **2019,** *31* (7), 1806626.

18. Xing, C.; Xu, Q.; Tang, H.; Liu, L.; Wang, S., Conjugated polymer/porphyrin complexes for efficient energy transfer and improving light-activated antibacterial activity. *Journal of the American Chemical Society* **2009,** *131* (36), 13117-13124.

19. Liu, L.; Chen, J.; Wang, S., Flexible antibacterial film deposited with polythiophene–porphyrin composite. *Advanced Healthcare Materials* **2013,** *2* (12), 1582-1585.

20. Huang, Y.; Pappas, H. C.; Zhang, L.; Wang, S.; Cai, R.; Tan, W.; Wang, S.; Whitten, D. G.; Schanze, K. S., Selective imaging and inactivation of bacteria over mammalian cells by imidazolium-substituted polythiophene. *Chemistry of Materials* **2017,** *29* (15), 6389-6395.

21. Starčević, K.; Boykin, D. W.; Karminski‐Zamola, G., New amidino‐benzimidazolyl thiophenes: Synthesis and photochemical synthesis. *Heteroatom Chemistry: An International Journal of Main Group Elements* **2003,** *14* (3), 218-222.

22. Linshoeft, J.; Heinrich, A. C.; Segler, S. A.; Gates, P. J.; Staubitz, A., Chemoselective cross-coupling reactions with differentiation between two nucleophilic sites on a single aromatic substrate. *Organic Letters* **2012,** *14* (22), 5644-5647.

23. Li, Y.; Liu, M.; Chen, L., Polyoxometalate built-in conjugated microporous polymers for visible-light heterogeneous photocatalysis. *Journal of Materials Chemistry A* **2017,** *5* (26), 13757-13762.

24. Kim, J.-S.; Kim, J.-H.; Lee, W.; Yu, H.; Kim, H. J.; Song, I.; Shin, M.; Oh, J. H.; Jeong, U.; Kim, T.-S., Tuning mechanical and optoelectrical properties of poly (3-hexylthiophene) through systematic regioregularity control. *Macromolecules* **2015,** *48* (13), 4339-4346.

25. Bhardwaj, D.; Gupta, S.; Yadav, P.; Bhargav, R.; Patra, A., All conjugated poly (3‑hexylthiophene)‑block‑poly (hexyl‑3, 4‑ethylenedioxythiophene) copolymers. *ChemistrySelect* **2017,** *2* (29), 9557-9562.

26. Khan, I. A.; Mirza, Z. M.; Kumar, A.; Verma, V.; Qazi, G. N., Piperine, a phytochemical potentiator of ciprofloxacin against Staphylococcus aureus. *Antimicrobial Agents and Chemotherapy* **2006,** *50* (2), 810-812.

27. Fu, J.; Yu, J.; Jiang, C.; Cheng, B., g‑C_3N_4‑Based heterostructured photocatalysts. *Advanced Energy Materials* **2018,** *8* (3), 1701503.

28. Prasad, K. P.; Chen, Y.; Sk, M. A.; Than, A.; Wang, Y.; Sun, H.; Lim, K.-H.; Dong, X.; Chen, P., Fluorescent quantum dots derived from PEDOT and their applications in optical imaging and sensing. *Materials Horizons* **2014,** *1* (5), 529-534.

29. Huang, W.; Ma, B. C.; Lu, H.; Li, R.; Wang, L.; Landfester, K.; Zhang, K. A., Visible-light-promoted selective oxidation of alcohols using a covalent triazine framework. *ACS Catalysis* **2017,** *7* (8), 5438-5442.

30. Huang, W.; Byun, J.; Rörich, I.; Ramanan, C.; Blom, P. W.; Lu, H.; Wang, D.; Caire da Silva, L.; Li, R.; Wang, L., Asymmetric covalent triazine framework for enhanced visible‑light photoredox catalysis via energy transfer cascade. *Angewandte Chemie International Edition* **2018,** *57* (27), 8316-8320.

31. Zhu, E.; Hai, J.; Wang, Z.; Ni, B.; Jiang, Y.; Bian, L.; Zhang, F.; Tang, W., Two-dimensional polyfluorenes bearing thienylenevinylene π-bridge-acceptor side chains for photovoltaic solar cells. *The Journal of Physical Chemistry C* **2013,** *117* (47), 24700-24709.

32. Alley, N. J.; Liao, K.-S.; Andreoli, E.; Dias, S.; Dillon, E. P.; Orbaek, A. W.; Barron, A. R.; Byrne, H. J.; Curran, S. A., Effect of carbon nanotube-fullerene hybrid additive on P3HT: PCBM bulk-heterojunction organic photovoltaics. *Synthetic Metals* **2012,** *162* (1-2), 95-101.

33. Zhang, C.; Li, Y.; Shuai, D.; Shen, Y.; Xiong, W.; Wang, L., Graphitic carbon nitride (g-C_3N_4)-based photocatalysts for water disinfection and microbial control: A review. *Chemosphere* **2019,** *214*, 462-479.

34. 34.   Bing, W.; Chen, Z.; Sun, H.; Shi, P.; Gao, N.; Ren, J.; Qu, X., Visible-light-driven enhanced antibacterial and biofilm elimination activity of graphitic carbon nitride by embedded Ag nanoparticles. *Nano Research* **2015,** *8* (5), 1648-1658.

35. Deng, J.; Liang, J.; Li, M.; Tong, M., Enhanced visible-light-driven photocatalytic bacteria disinfection by g-C_3N_4-AgBr. *Colloids and Surfaces B: Biointerfaces* **2017,** *152*, 49-57.

36. Zhang, W.; Yu, C.; Sun, Z.; Zheng, S., Visible-light-driven catalytic disinfection of staphylococcus aureus using sandwich structure g-C$_3$N$_4$/ZnO/stellerite hybrid photocatalyst. *Journal of Microbiology and Biotechnology* **2018,** *28* (6), 957-967.

37. Vignesh, S.; Muppudathi, A. L.; Sundar, J. K., Multifunctional performance of g-C$_3$N$_4$-BiFeO$_3$-Cu$_2$O hybrid nanocomposites for magnetic separable photocatalytic and antibacterial activity. *Journal of Materials Science: Materials in Electronics* **2018,** *29* (13), 10784-10801.

38. Li, Y.; Wang, Q.; Huang, L.; Xu, X.; Xie, M.; Wang, H.; Huang, S.; Zhang, F.; Zhao, Z.; Yang, J., Enhanced LED-light-driven photocatalytic antibacterial by g-C$_3$N$_4$/BiOI composites. *Journal of Materials Science: Materials in Electronics* **2019,** *30* (3), 2783-2794.

39. Khan, M. A.; Mutahir, S.; Wang, F.; Zhou, J.-W.; Lei, W.; Xia, M., Facile synthesis of CNS/TNS sensitized with Cu biphenylamine frameworks for remarkable photocatalytic activity for organic pollutants degradation and bacterial inactivation. *Solar Energy* **2019,** *186*, 204-214.

40. Liu, H.; Ma, S.; Shao, L.; Liu, H.; Gao, Q.; Li, B.; Fu, H.; Fu, S.; Ye, H.; Zhao, F.; Zhou, J., Defective engineering in graphitic carbon nitride nanosheet for efficient photocatalytic pathogenic bacteria disinfection. *Applied Catalysis B: Environmental* **2020,** *261*, 118201.

41. Tang, C.; Liu, C.; Han, Y.; Guo, Q.; Ouyang, W.; Feng, H.; Wang, M.; Xu, F., Nontoxic carbon quantum dots/g‑C$_3$N$_4$ for efficient photocatalytic inactivation of staphylococcus aureus under visible light. *Advanced Healthcare Materials* **2019,** 1801534.

42. Vignesh, S.; Suganthi, S.; Sundar, J. K.; Raj, V., Construction of α-Fe$_2$O$_3$/CeO$_2$ decorated g-C$_3$N$_4$ nanosheets for magnetically separable efficient photocatalytic performance under visible light exposure and bacterial disinfection. *Applied Surface Science* **2019,** *488*, 763-777.

43. Yadav, P.; Nishanthi, S. T.; Purohit, B.; Shanavas, A.; Kailasam, K., Metal-free visible light photocatalytic carbon nitride quantum dots as efficient antibacterial agents: An insight study. *Carbon* **2019,** *152*, 587-597.

44. Wang, L.; Zhang, X.; Yu, X.; Gao, F.; Shen, Z.; Zhang, X.; Ge, S.; Liu, J.; Gu, Z.; Chen, C., An all‑organic semiconductor C$_3$N$_4$/PDINH heterostructure with advanced antibacterial photocatalytic therapy activity. *Advanced Materials* **2019,** 1901965.

45. Wang, R.; Zhang, B.; Liang, Z.; He, Y.; Wang, Z.; Ma, X.; Yao, X.; Sun, J.; Wang, J., Insights into rapid photodynamic inactivation mechanism of Staphylococcus aureus via rational design of multifunctional nitrogen-rich carbon-coated bismuth/cobalt nanoparticles. *Applied Catalysis B: Environmental* **2019,** *241*, 167-177.

46. Segura, M., Streptococcus suis: an emerging human threat. *The Journal of Infectious Diseases* **2009,** *199* (1), 4-6.

47. Pachfule, P.; Acharjya, A.; Roeser, J. r. m.; Langenhahn, T.; Schwarze, M.; Schomäcker, R.; Thomas, A.; Schmidt, J., Diacetylene functionalized covalent organic framework (COF) for photocatalytic hydrogen generation. *Journal of the American Chemical Society* **2018,** *140* (4), 1423-1427.

48. Wang, F.; Feng, Y.; Chen, P.; Wang, Y.; Su, Y.; Zhang, Q.; Zeng, Y.; Xie, Z.; Liu, H.; Liu, Y., Photocatalytic degradation of fluoroquinolone antibiotics using ordered mesoporous g-C_3N_4 under simulated sunlight irradiation: kinetics, mechanism, and antibacterial activity elimination. *Applied Catalysis B: Environmental* **2018,** *227*, 114-122.

49. Chen, L.; Yamane, S.; Mizukado, J.; Suzuki, Y.; Kutsuna, S.; Uchimaru, T.; Suda, H., ESR study of singlet oxygen generation and its behavior during the photo-oxidation of P3HT in solution. *Chemical Physics Letters* **2015,** *624*, 87-92.

50. Burrows, H. D.; Seixas de Melo, J.; Serpa, C.; Arnaut, L. G.; Miguel, M. d. G.; Monkman, A. P.; Hamblett, I.; Navaratnam, S., Triplet state dynamics on isolated conjugated polymer chains. *Chemical Physics* **2002,** *285* (1), 3-11.

51. Manceau, M.; Bundgaard, E.; Carlé, J. E.; Hagemann, O.; Helgesen, M.; Søndergaard, R.; Jørgensen, M.; Krebs, F. C., Photochemical stability of π-conjugated polymers for polymer solar cells: a rule of thumb. *Journal of Materials Chemistry* **2011,** *21* (12), 4132-4141.

52. Reese, M. O.; Nardes, A. M.; Rupert, B. L.; Larsen, R. E.; Olson, D. C.; Lloyd, M. T.; Shaheen, S. E.; Ginley, D. S.; Rumbles, G.; Kopidakis, N., Photoinduced degradation of polymer and polymer–fullerene active layers: experiment and theory. *Advanced Functional Materials* **2010,** *20* (20), 3476-3483.

53. Manceau, M.; Rivaton, A.; Gardette, J. L., Involvement of singlet oxygen in the solid‐state photochemistry of P3HT. *Macromolecular Rapid Communications* **2008,** *29* (22), 1823-1827.

Chapter 4

4   Fabrication and photocatalytic antibacterial properties of PTET-T-COOH/PU coating

Polyurethanes (PUs) are among the most popular polymers due to their wide variety of industrial applications. Various antibacterial materials were incorporated with PUs' to prevent the colonization of bacteria and fungi on the surface of PUs products. Photocatalytic disinfection of materials consisting of PU and photocatalysts has been shown to be an efficient way to kill bacteria during the past decade due to its low cost, efficiency and non-toxicity. Up to now, most reports are focused on TiO_2/PU composites which have shown antibacterial properties under UV light. Thus, exploring visible light responsive photocatalytic antibacterial coating based on PUs is of great importance.

4.1   Abstract

Exploring of novel visible region responsive antimicrobial coating is of great significance for antibacterial activity applications owing to widespread multidrug-resistant infections. Herein, the photocatalytic disinfection performance of a poly [2,11'-thiophene-ethylene-thiophene-alt -(2,5-(3-carboxyl)-thiophene] (PTET-T-COOH)/polyurethane (PU) coating was evaluated. The coating showed excellent photocatalytic bactericidal effect on *S. aureus* (7-log inactivation) in 4 h under visible-light exposure. PTET-T-COOH/PU coating demonstrated plausible stability and their antibacterial activity underwent over five runs. The chemical interaction between PTET-T-COOH and NCO-terminated pre-PU was confirmed by ATR-FTIR analyses.

4.2   Introduction

Inorganic photocatalytic ingredients were incorporated into polymers for antibacterial and/or self-cleaning coatings by physical blending processes which led to limited surface antibacterial capacity.[54] In addition, strong agglomeration and leaching of inorganic photocatalysts are hindrances for their practical applications. Therefore, it is urgent to achieve efficient and stable antibacterial coating. Self-cleaning polymers for paints and coatings possess tremendous potential for both industrial and household settings. The merit

of conductive polymers coating is their process ability, compared with other conductive materials such as organic small molecules or inorganic photocatalysts.[55] Herein, a PTET-T-COOH/PU coating was fabricated successfully and their photocatalytic inactivation effects on *S. aureus* were explored. PTET-T-COOH/PU coating was found to exhibit excellent antimicrobial activity and stability on *S. aureus* under visible light. PTET-T-COOH/PU active layer was uniformly grown on a polyurethane substrate by spin coating and the polyurethane substrate provided an ideal support for convenient recycling. In addition, chemical bonding between carboxyl groups of PTET-T-COOH and isocyanate groups of pre-polyurethane was formed and confirmed by a series of ATR-FTIR measurements.

4.3 Experimental Section

4.3.1 Materials

N, N-Dimethylformamide (DMF, chromatographically pure) was purchased from Energy Chemical (Shanghai, China). Tryptic Soy Broth (TSB), Tryptic Soy Agar (TSA) were purchased from Qingdao Hope Bio-Technology Co., Ltd (Qingdao, China). Phosphate Buffered Saline (PBS) was purchased from Beijing Solarbio Science & Technology Co., Ltd. (Beijing, China). 1, 4-butanediol ($C_4H_{10}O_2$), poly (ethylene glycol) ($HO(CH_2CH_2O)_nH$, PEG2000 (average molecular weight 2000 g/mol) and isophorone diisocyanate ($C_{12}H_{18}N_2O_2$, IPDI) were purchased from Saen Chemical Technology Co., Ltd. (Shanghai, China). IPDI and PEG600 (average molecular weight 600 g/mol) used in preparation of samples for ATR-FTIR determination were purchased from SigmaAldrich. The water used in all experiments was deionized (DI).

4.3.2 Fabrication of PTET-T-COOH/PU coating

A bilayer PTET-T-COOH/PU coating was prepared by coating a bottom layer of PU onto a glass slide followed by linking a top layer of PTET-T-COOH/PU to the bottom layer of PU as shown in Figure 4.1. In a typical experiment, to a solution of 15.07 g (0.0075 mol) of poly (ethylene glycol) (PEG2000) in 30 mL anhydrous DMF in a three-neck round-bottom flask, 4.45 g (0.02 mol) of isophorone diisocyanate (IPDI) was slowly added with mechanical stirring under nitrogen protection. After the solution was stirred at 70 °C for

2.5 h, a viscous transparent pale yellowish pre-polyurethane was obtained. A part of the pre-polyurethane was reacted with 3 drops of 1, 4-butanediol as chain extender at 95 °C for 30 min under stirring to achieve polyurethane (PU) as the materials for the bottom layer coating. 10 mL of polyurethane were spin-coated onto a glass slide (2 cm × 3 cm) and dried in a vacuum oven at 60 °C for 12 h to make the bottom layer of PU coating. Afterwards, 3 mg of PTET-T-COOH and 1 mL of the pre-polyurethane were dissolved in 1 mL of 1,2-dichlorobenzene by sonication for 4 h followed by filtration using a syringe filter to get a transparent solution. The solution was then spin-coated onto the bottom layer of PU coating. The sample was heated at 60 °C for 12 h to obtain a bilayer PTET-T-COOH/PU coating. The detailed scheme of chemical reactions is displayed in Figure 4.1.
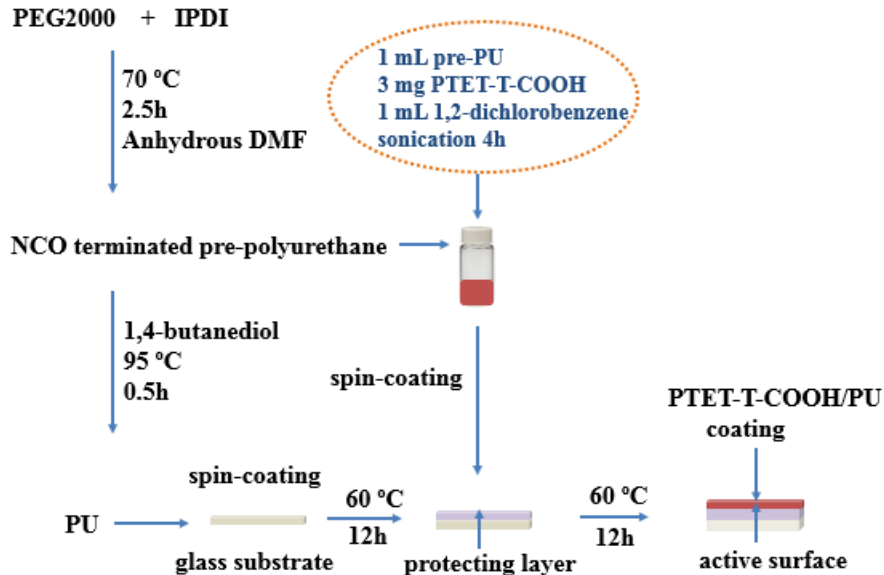
Figure 4.1. Illustration of fabrication process of PTET-T-COOH/PU coating.
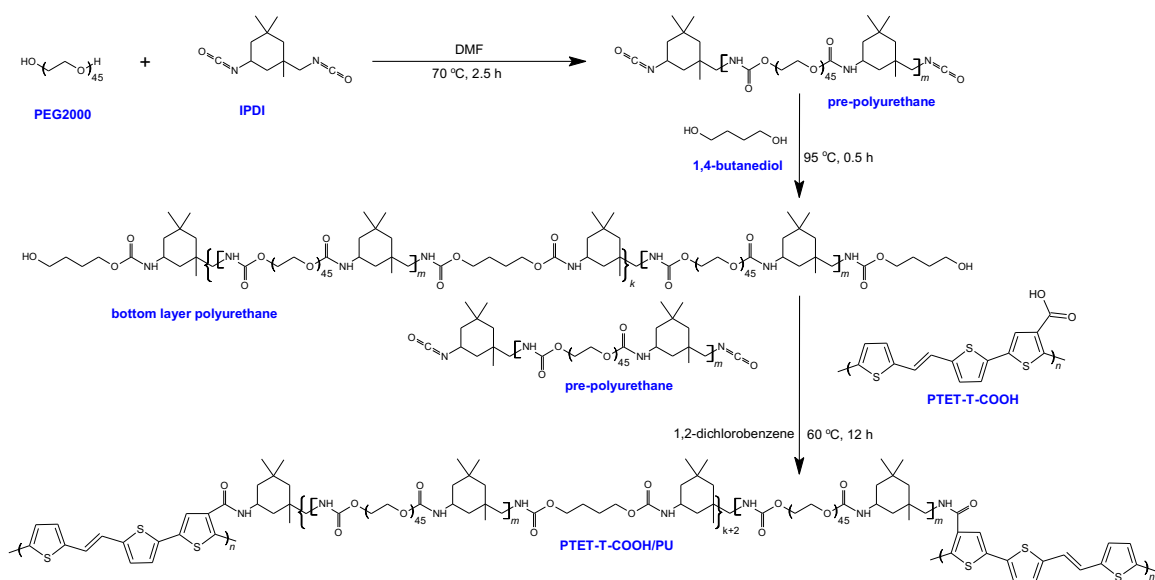
Figure 4.2. Reaction scheme for the synthesis of bilayer coating of PTET-T-COOH/PU.

4.3.3 Preparation of samples for ATR-FTIR determination

In order to confirm the reaction between PTET-T-COOH and NCO groups of IPDI using FTIR technique, a series of experiments were designed carried out. As the content of PTET-T-COOH in PTET-T-COOH/PU coating is low, this leads to the challenges for the detection of new peaks. Firstly, to verify the successful synthesis of pre-polyurethane, 1g of IPDI (4.5 mmol) and 1g of PEG600 (1.7 mmol) were added into a vial and then the mixture was heated at 60 °C for 5 h to form NCO terminated pre-polyurethane (pre-PU). Then, to confirm the chemical reaction between PTET-T-COOH and IPDI, 15 mg of PTET-T-COOH powder and 12 mg of IPDI liquid were mixed thoroughly and then the mixture was heated at 60 °C for 12 h in a vial to obtain hard and crisp polyamide product. Finally, for verifying formation of chemical bonding between carboxyl groups of PTET-T-COOH and isocyanate group of IPDI, 14.6 mg of PTET-T-COOH and 32 mg of pre-PU was mixed and heated at 60 °C for 12 h to obtain PTET-T-COOH/PU powder. Simultaneously, 14.6 mg of PTET-T-COOH was ultrasonically dispersed in 1 mL CHCl$_3$ to achieve homogeneous suspension and dropped onto a surface of pre-PU in a vial. Then the mixture was also heated at 60 °C for 12 h to obtain PTET-T-COOH/PU coating.

71

4.3.4 Measurements

In order to determine the chemical composition of PTET-T-COOH/PU coating, FTIR spectra of samples were measured using attenuated total reflectance (ATR) technique on a Nicolet 6700 spectrometer at ambient temperature within the wavenumber range of 600-4000 cm^{-1} for 64 scans at 4 cm^{-1} resolution for each sample. X-ray photoelectron spectroscopy (XPS) was conducted by Excalab 250Xi (thermofisher America) to analyze the surface chemical composition of the coatings. Field emission scanning electron microscope (FESEM) (JSM-7800F, Japan) was employed for analyzing the morphology of the coatings. UV-visible absorption spectra were collected on a UV-Vis-NIR spectrophotometer (UV-3600, Shimadzu, Japan).

4.3.5 Testing of photocatalytic antibacterial property of PTET-T-COOH/PU coating

Gram-positive *S. aureus* (USA 300) was chosen as model bacteria which were cultured in TSB at 37 °C for 12 h and then purified by high-speed freezing centrifuge at 12000 rpm for 2 min and washed twice with 1 mL PBS, resulting in a cell count of approximately 7~8×10^8 colony forming units (cfu)/mL. Briefly, A glass plate covered by PTET-T-COOH/PU with 2×3 cm was immersed in 30 mL of PBS solution (0.1 mg/mL) in a 120 mL self-designed glass jacketed reactor containing 600 μL of bacteria solution. The bacteria concentration for photocatalytic antibacterial test was about 10^7 cfu/mL. The reaction was carried out in a GHX-3 photochemical reaction instrument equipped with a 250 W Xenon arc lamp and an optical cutoff filter (λ< 420 nm). The visible light intensity was fixed at 80 mW/cm^2. The temperature was kept at 30 °C using a cryostatic tank. At given time intervals, 100 μL of tested suspension sample was pipetted out and serially diluted using PBS and spread on nutrient TSA plates. After incubation at 37 °C for 18 h, the cell densities were checked to determine the survival bacterial numbers. Control experiments including *S. aureus* with PTET-T-COOH/PU in dark, *S. aureus* without PTET-T-COOH and with PU under irradiation) were also carried out. All materials and glassware were firstly autoclaved at 121 °C at 0.1 MPa for 20 min before use and all the experiments were repeated for three times.

4.4 Results and Discussion

4.4.1 Characterization of PTET-T-COOH/PU composite and coating

The pre-polyurethane was successfully synthesized and confirmed by FTIR technique. Figure 4.3 provides the FTIR spectra of IPDI, PEG600, mixture of IPDI and PEG600 before reaction and the pre-polyurethane formed between IPDI and PEG600. In the spectrum of pre-polyurethane, the new peak at 1716 cm^{-1} is assigned to C=O from urethane and band at 1531 cm^{-1} stems from amide II mode which was ascribed to a mixed contribution of N-H in-plane bending and the C-N stretching vibrations. In addition, the peak at 3328 cm^{-1} is attributed to NH stretching vibrations.[3, 4] Hydroxyl association peak of PEG600 (Figure 4.3a and c) appears at 3454 cm^{-1}. Peaks at 2951 and 2867 cm^{-1} are attributed to CH stretching vibrations of IPDI and PEG600, respectively. Characteristic peaks from isocyanate of IPDI are located at 2245 cm^{-1}. C-O absorption peaking at 1102 cm^{-1} is observed in PEG600 (a), mixture of PEG600 and IPDI (c), and pre-polyurethane (d).

The generation of chemical bonding between the carboxyl group and isocyanate of IPDI was verified by FTIR technique. Figure 4.4 shows the infrared spectra of IPDI, PTET-T-COOH and the synthesized polyamide from these two ingredients. Compared to IPDI and PTET-T-COOH, new bands at 3307 cm^{-1} belonged to NH stretching vibrations and the peak at 1627 cm^{-1} is attributed to C=O stretching vibrations in polyamide. Peaks at 1553 and 1430 cm^{-1} are ascribed to ring vibration of PTET-T-COOH in polyamide. Simultaneously, the bands at 929 and 787 cm^{-1} are ascribed to =C-H out of plane deformation and ring C-H deformation vibrations from PTET-T-COOH, which are clearly evident. In addition, peaks at 1462 and 1363 cm^{-1} originated from IPDI. These results indicated the successful chemical interaction was formed between NCO from IPDI and carboxyl groups from PTET-T-COOH.
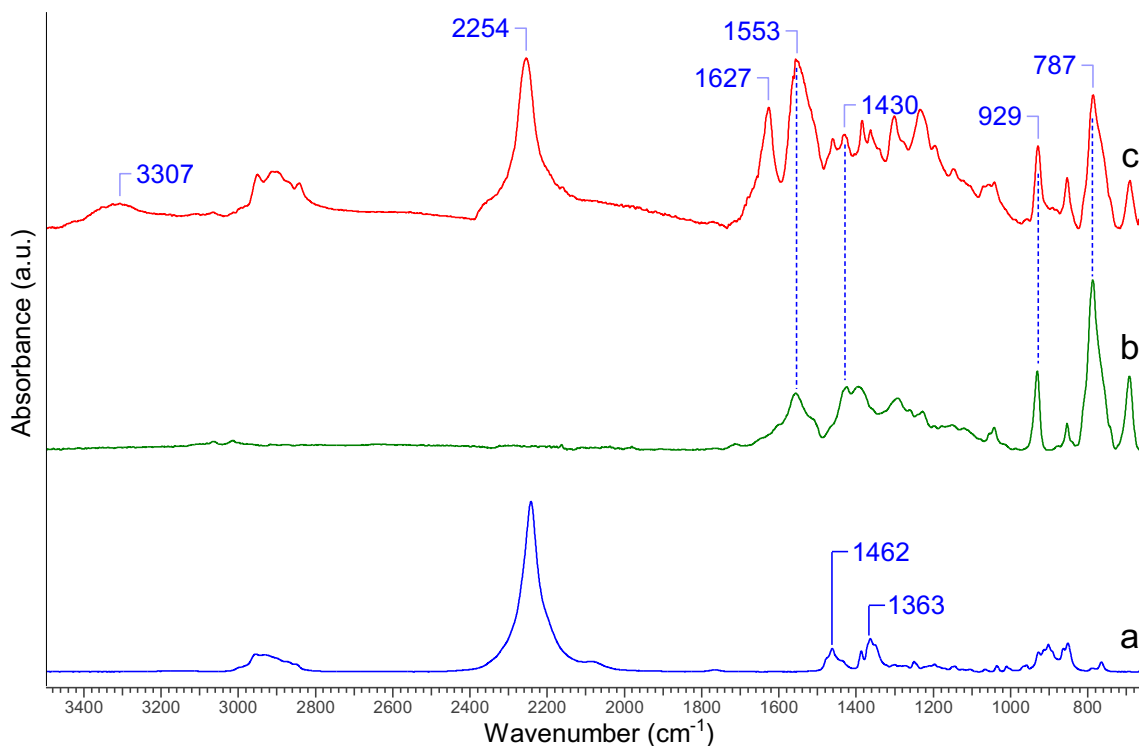
Figure 4.4. FTIR spectra of (a) IPDI, (b) PTET-T-COOH and (c) the synthesized polyamide.

The successful linkage of PTET-T-COOH and PU by chemical bonding was also confirmed by FTIR. The characteristic bands of NH stretching vibrations at 3180-3450 cm^{-1} can be observed in pre-polyurethane, PTET-T-COOH/PU powder, PTET-T-COOH/PU coating and polyamide from IPDI and PTET-T-COOH, as shown in Figure 4.5. Pre-polyurethane, PTET-T-COOH/PU powder and PTET-T-COOH/PU coating all possessed C=O from urethane at 1715 cm^{-1} and amide II mode at 1530 cm^{-1} as well as peak at 1100 cm^{-1} from material PEG600. C=O stretching vibrations peaks can be seen in PTET-T-COOH/PU powder (1634 cm^{-1}), PTET-T-COOH/PU coating (1632 cm^{-1}) and polyamide (1626 cm^{-1}). In addition, the peak at 932 cm^{-1} existed in these three samples is attributed to =C-H out of plane deformation and vibrations from PTET-T-COOH. The peak at 1362 cm^{-1} in the four samples come from material IPDI. These results suggested the chemical bonding between IPDI and PTET-T-COOH in PTET-T-COOH/PU composite was formed successfully.
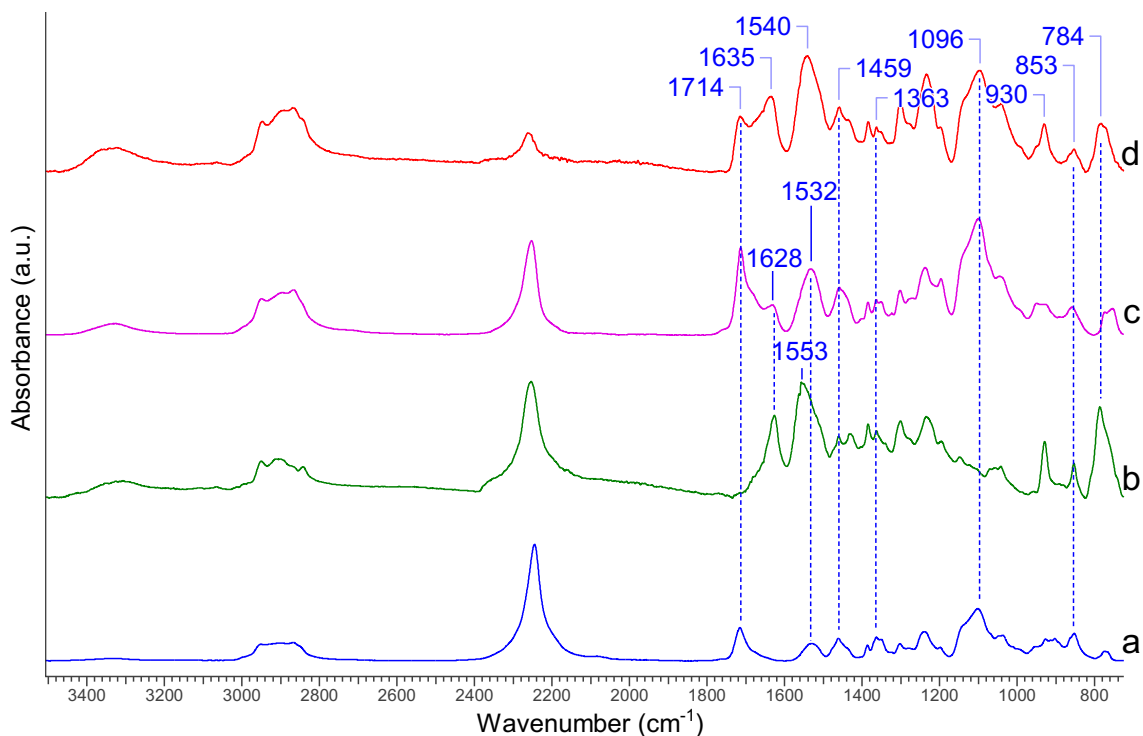
Figure 4.5. FTIR spectra of (a) pre-polyurethane, (b) polyamide, (c) PTET-T-COOH/PU coating, and (d) PTET-T-COOH/PU powder.

The surface composition of PTET-T-COOH, PU and PTET-T-COOH/PU was also investigated by the XPS technique. The XPS survey spectra show the presence of carbon, nitrogen, oxygen, and sulfur elements and all the peaks found in the heterostructure belonged to the PU and PTET-T-COOH, as shown in Figure 4.6.
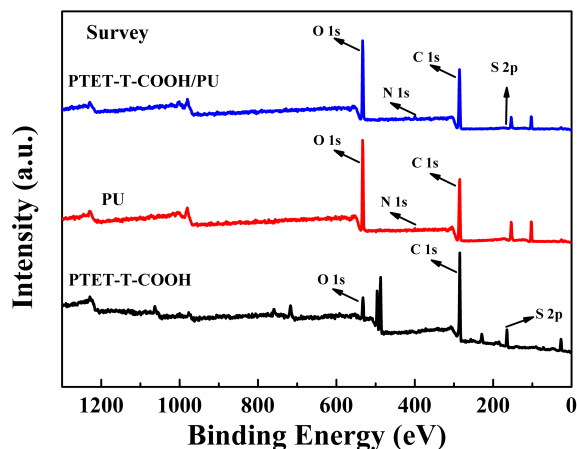
Figure 4.6. XPS survey spectra of PTET-T-COOH/PU, PU and PTET-T-COOH.

High resolution XPS spectra of C1s in PTET-T-COOH/PU, PU and PTET-T-COOH are given in Figure 4.7. The C1s spectrum in PTET-T-COOH peaking at 289.59, 286.79, 286.32, 285.09 and 284.61 eV are attributed to carboxy $\underline{C}$(=O)-O, alkoxy $\underline{C}$-O-H, $\underline{C}$-S, C=C (sp^3 bonded carbons) and C=C (sp^2 bonded carbons), respectively. These values and their assignments are in agreement with those reported in literature and are summarized in Table 4.1.[56, 57] The characteristic peaks of C1s spectrum in PTET-T-COOH/PU coating changed to lower energy level due to the formation of chemical bonding between the carboxyl groups in PTET-T-COOH and isocyanate groups in pre-polyurethane. The characteristic peaks of N-C(=O) appeared at 399.77 eV and 399.86 eV in PU and PTET-T-COOH/PU coating, as demonstrated in Figure 4.8.
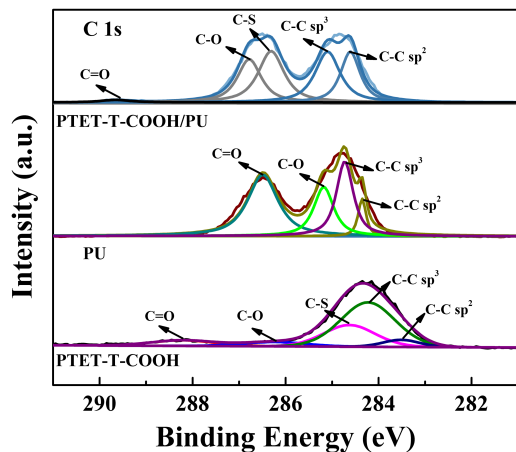
Figure 4.7. High resolution XPS spectra of C1s in PTET-T-COOH/PU, PU and PTET-T-COOH.
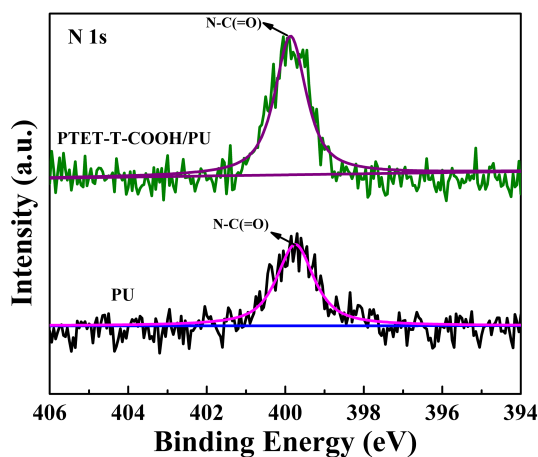
Figure 4.8. High resolution XPS spectra of N1s in PTET-T-COOH/PU and PU.

High resolution XPS spectra of O1s in PTET-T-COOH/PU, PU and PTET-T-COOH are given in Figure 4.9 and are summarized in Table 4.1. These values are in accordance with other publications. In PTET-T-COOH/PU, peaks at 532.97 eV and 532.36 eV could be ascribed to O=C and O-C, respectively. In PU, apart from O=C and O-C peaks, obvious OH peak at 531.95 eV can be found.
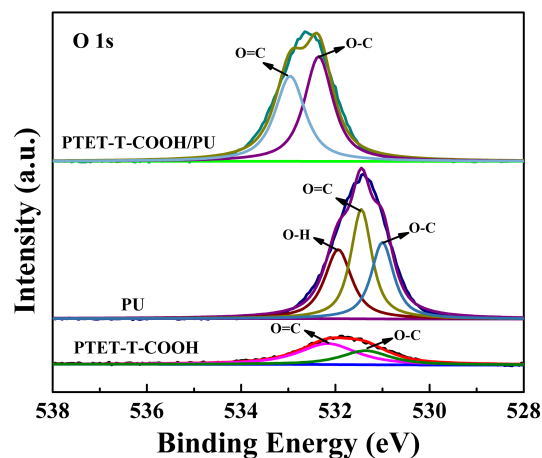
Figure 4.9. High resolution XPS spectra of O1s in PTET-T-COOH/PU, PU and PTET-T-COOH.

High resolution XPS spectra of S2p in PTET-T-COOH/PU and PTET-T-COOH are depicted in Figure 4.10 and are summarized in Table 4.1. The peaks at 165.32 and 164.16 arising from $S2p^{3/2}$ and $S2p^{1/2}$ in PTET-T-COOH became weak in PTET-T-COOH/PU, attributed to the incorporation of the large PU moiety.
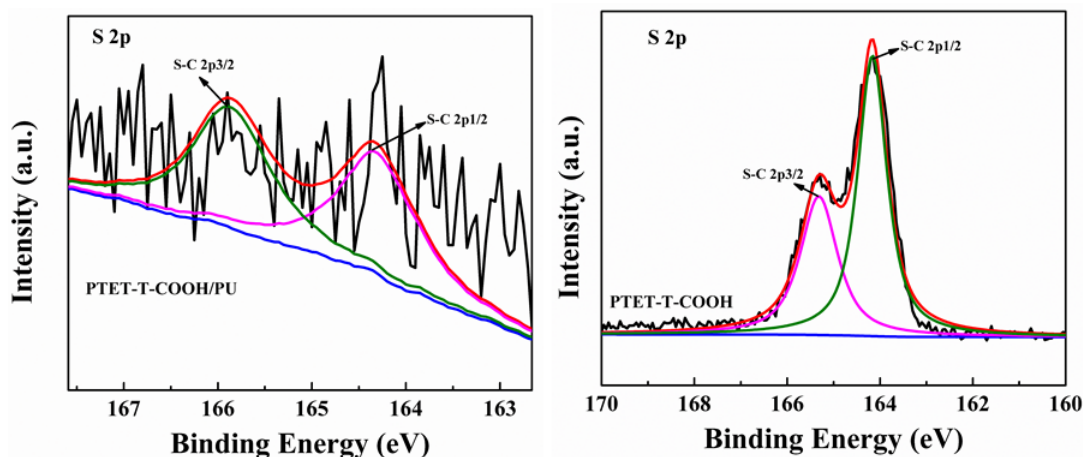
Figure 4.10. High resolution XPS spectra of S2p in PTET-T-COOH/PU and PTET-T-COOH.

Table 4.1. High-resolution C 1s, O 1s, S2p and N 1s spectra of PTET-T-COOH, PU and PTET-T-COOH/PU.

		PTET-T-COOH	PU	PTET-T-COOH/PU
C 1s	C=O	288.23	286.51	289.59
	C-O	286.31	285.19	286.79
	C-S	284.58	\	286.32
	C-C sp^3	284.22	284.73	285.09
	C-C sp^2	283.51	284.35	284.61
O 1s	O-H	\	531.95	\
	O=C	532.16	531.45	532.97
	O-C	531.32	530.99	532.36
S 2p	S-C 2p$^{3/2}$	165.32	\	165.09
	S-C 2p$^{1/2}$	164.16	\	164.36
N 1s	N-C(=O)-O	\	399.77	399.86

SEM images of PTET-T-COOH powder (a), PU (b) and PTET-T-COOH/PU coatings before and after reactions are demonstrated in Figure 4.11. PTET-T-COOH shows a bulky morphology. After integration into PU coating, a smooth surface is evident and the PTET-T-COOH particles are distributed evenly throughout the PU substrate.
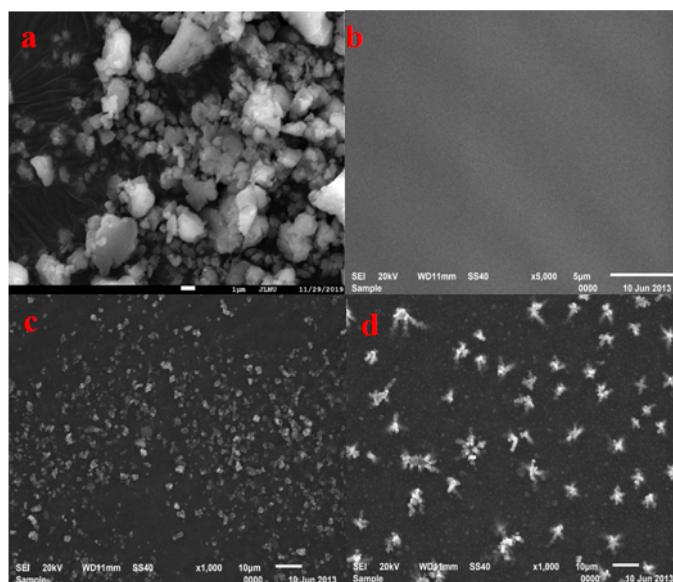
Figure 4.11. SEM images of (a) PTET-T-COOH powder, (b) PU coating and PTET-T-COOH/PU coatings (c) before and (d) after reaction.

The optical properties of PU, PTET-T-COOH and PU/PTET-T-COOH in solid films were analyzed by UV-Vis absorption spectra. The broad band of PU edged at 250 nm is assigned to the n-π* transition of the carbonyl groups.[58] The PTET-T-COOH membrane exhibited broad absorption band centered at 450 nm attributed to localized π-π∗ transition between the aryl units, indicating the enhanced interchain interactions due to the increased polarizability in the film.[31] The characteristic absorption peaks all appeared in the UV-Vis absorption spectra of PU/PTET-T-COOH membrane when PTET-T-COOH was incorporated with PU. PTET-T-COOH and PU/PTET-T-COOH membrane exhibited an absorption edge (λ_{onset}) at 564 and 580 nm, respectively. The PTET-T-COOH/PU membrane showed blue-shifted UV-visible absorption spectra in comparison to those in the PTET-T-COOH membrane. This indicates that weaker solid-state π-π stacking occurred and the coplanarity between conjugated polymer backbones became more torsional in the composites due to strong interfacial interactions of PU and PTET-T-COOH. Furthermore, a significant absorption peak ranged from 360 to 390 nm was observed, indicating that the heterostructures were linked together by chemical bondings between functionalized groups.[44]
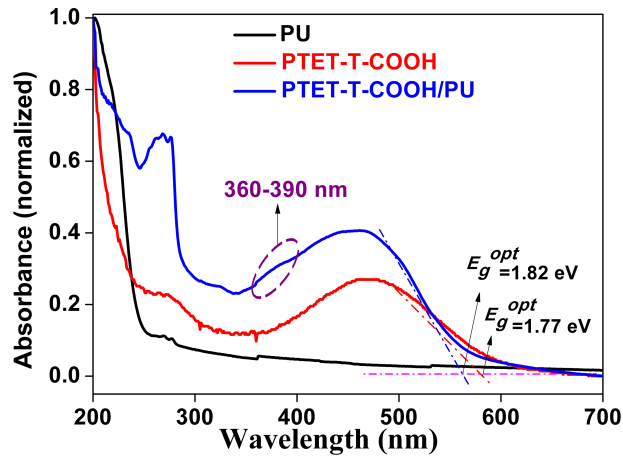
Figure 4.12. UV-vis absorption spectra of PTET-T-COOH, PU and PTET-T-COOH/PU coatings.

The contact angles of pristine PU and PTET-T-COOH/PU coatings were measured to investigate their hydrophobicity, as shown in Figure. 4.13. The average contact angles of pure PU and PTET-T-COOH/PU are 76.7° and 89.5°, respectively. This indicates the incorporation of PTET-T-COOH into PU structure contributed to hydrophobicity.
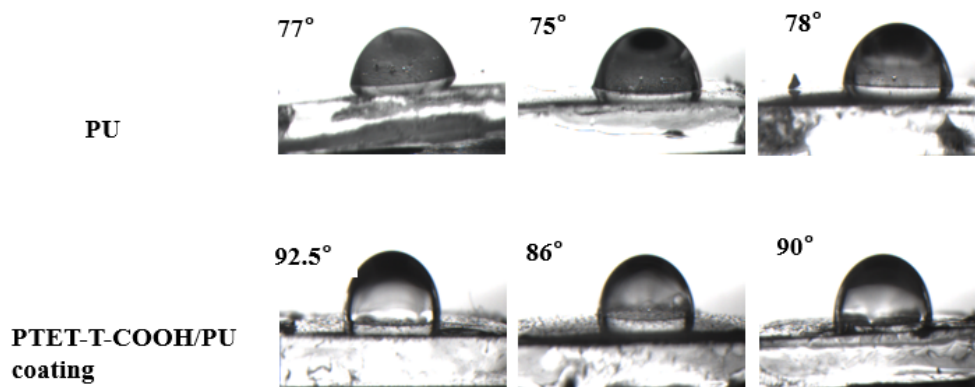
Figure 4.13. Contact angles of PU and PTET-T-COOH/PU coatings.

4.4.2 Photocatalytic antibacterial properties of PTET-T-COOH/PU

Photocatalytic activity of PTET-T-COOH/PU toward *S. aureus* was evaluated, as shown in Figure. 4.14. Here (a) compares the cell density of sample against *S. aureus* under different conditions. PTET-T-COOH/PU in the dark and under illumination as well as PU coating under irradiation had almost no effect on *S. aureus*. However, *S. aureus* can be efficiently killed in the presence of PTET-T-COOH/PU coating under visible light. Over a period of 4 h of visible light irradiation, PTET-T-COOH/PU demonstrated 7-log inactivation of *S. aureus* concentration (100 %) inactivation efficiency. The images (Figure. 4.15) showed that adding the catalysts caused an obvious decrease of *S. aureus* cells with increasing illumination time. In addition, the disinfection cycle test results demonstrated that PTET-T-COOH/PU coating possesses satisfactory disinfection activity on *S. aureus*. After three cycles, PTET-T-COOH/PU still exhibited high inactivation efficiency of 100 %. Cell densities of *S. aureu*s decreased 7-log for the first three cycles and the inactivation were 4-log and 2-log for the fourth and fifth runs, respectively. The decrease of photocatalytic activity of PTET-T-COOH was mainly due to the leaching of excessive PTET-T-COOH from polyurethane surface. Hence, it is necessary to optimize the ratio of

PTET-T-COOH to pre-polyurethane and make sure strong interaction between these two ingredients through chemical bonding and avoid any aggregation. In order to compare the disinfection effects of PTET-T-COOH/PU, the representative PU based photoactive agents were surveyed, as summarized in Table 4.2.
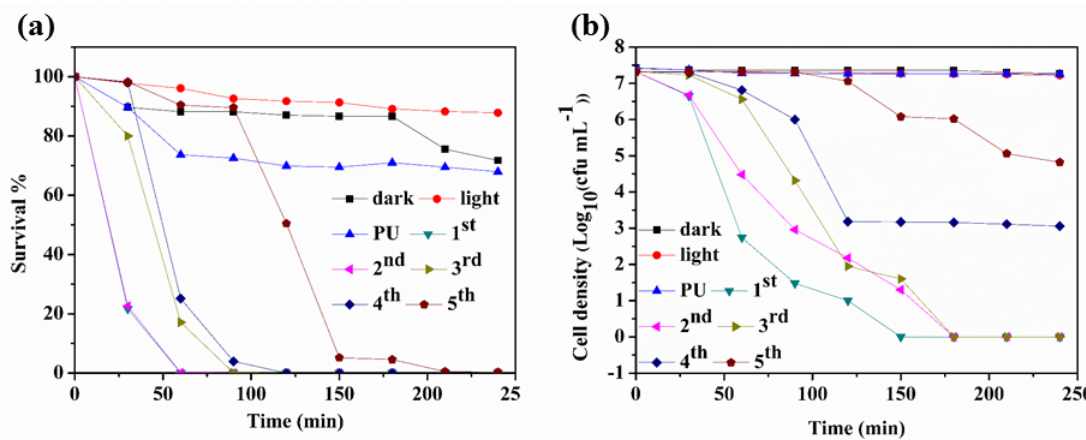
Figure 4.14. (a) Photocatalytic inactivation efficiency and (b) cell density of PTET-T-COOH/PU against *S. aureus* (10^7 cfu mL^{-1}, 30 mL).
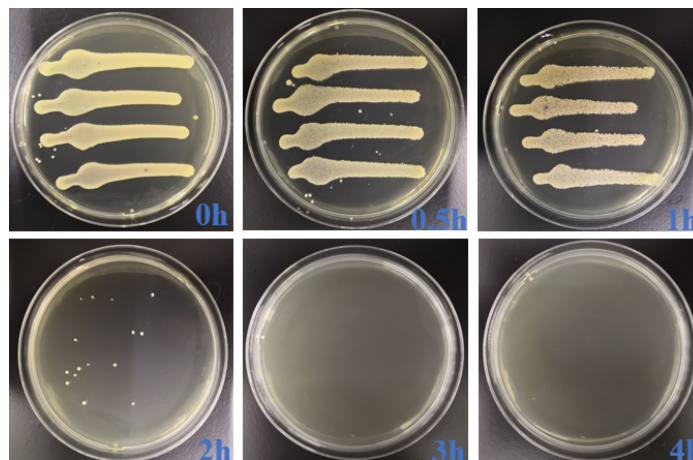
Figure 4.15. Images of *S. aureus* colonies on an agar plate before and after visible light irradiation for 4 h using PTET-T-COOH/PU coating for the first run.

Table 4.2. The representative photocatalysts based on PU with their target microorganisms and photocatalytic disinfection performances.

Photocatalyst	Bacteria	Photocatalytic performance	Journal	Year

TiO$_2$/PU reactor[59]	*L. pneumophila*		J. Hazard. Mater.	2010
TiO$_2$/PU[60]	*E. coli*	killing efficiency 99% 60 min (UV-Vis)	Nanotechnology	2012
Ag/TiO$_2$/PU[61]	*E. coli*	killing efficiency 99.9% 60 min (UV light)	Int. J. Nanotechnol.	2013
FA/TiO$_2$/PU[62]	*E. coli*	3.5 log 180 min (UV light)	Ceram. Int.	2014
TiO$_2$/WPU[63]	*Aspergillus niger*	antifungal capacity (UV light)	Colloid Surface A	2015
TiO$_2$/PU[64]	*E. coli*	3.5 log 120 min (UV light)	J. Food. Sci	2015
TiO$_2$/PU[65]	*E. coli*	killing efficiency 92% 10 min (UV)	LWT-Food. Sci. Technol.	2016
R-TiO$_2$/styrene acrylic PU/ [66]	*E. coli*	6 log 90 min (UV)	Adv. Nat. Sci.: Nanosci. Nanotechnol.	2016
TiO$_2$/PU[67]	*C. albicans*	killing efficiency 85% (UV)	Appl. Surf. Sci.	2017
PU acrylate-Ag/TiO$_2$[68]	*E. coli.*	killing efficiency 97% 150 min (UV)	Int. J. Polym. Mater.	2017
ZnO/PU[69]	*E. coli*	3.5 log 180 min (UV)	J. Colloid. Interf. Sci.	2018
hCQDs/PU[70]	*S. aureus*	5 log 60 min (visible)	ACS Biomater. Sci. Eng.	2018
Ag-TiO$_2$/WPU[71]	*Bacillus atrophaeus*	killing efficiency over 99 % (UV)	Photochem. Photobiol.	2018
Ag@AgCl-PU/SF[72]	*E. coli.*	Inhibition zone diameter 12.93 mm (UV-Vis)	Eur. Polym. J.	2019
Polyurethane acrylate PUA/rGO/TiO$_2$[73]	*S. aureus*	killing efficiency 86% 150 min (UV-Vis)	Int. J. Polym. Mater.	2019
FeOx /PU[74]	*E. coli*	5 log 30 min (UV-Vis)	Appl. Catal. B-Environ.	2019
PTET-T-COOH/PU	*S. aureus*	100 % 120 min 6 log 120 min (visible)	This work	

The results summarized above demonstrate that antibacterial materials incorporated in the PUs' polymeric matrices are mainly TiO$_2$ and their photocatalytic disinfection can only be conducted under UV light. Only limited systems such as Ag/TiO$_2$, FeOx/PU, Ag@AgCl-

PU/SF and hCQDs/PU can work under UV-Vis light irradiation. In our case, PTET-T-COOH/PU coating shows 100 % disinfection (6-log inactivation) against *S. aureus* in 2 h under visible light irradiation. These values are amongst the best results reported on PU based photocatalytic antibacterial coatings.

The appearance variation of PTET-T-COOH/PU during the photocatalytic reaction for various cycles was investigated. Figure 4.16 presents optical photos of PTET-T-COOH/PU coating on glass substrate before reaction and after five recycling runs. The as-prepared PTET-T-COOH/PU coating is dark red and opaque. After the first reaction run, the PTET-T-COOH/PU coating was also opaque, but the color turned to orange from red, indicating that excess PTET-T-COOH was removed from the surface of the coating. After the second run, PTET-T-COOH/PU coating became transparent and the color changed to yellow. There was almost no obvious difference in appearance between the coatings after the third, fourth and fifth cycles, suggesting PTET-T-COOH was tightly bonded with PU.
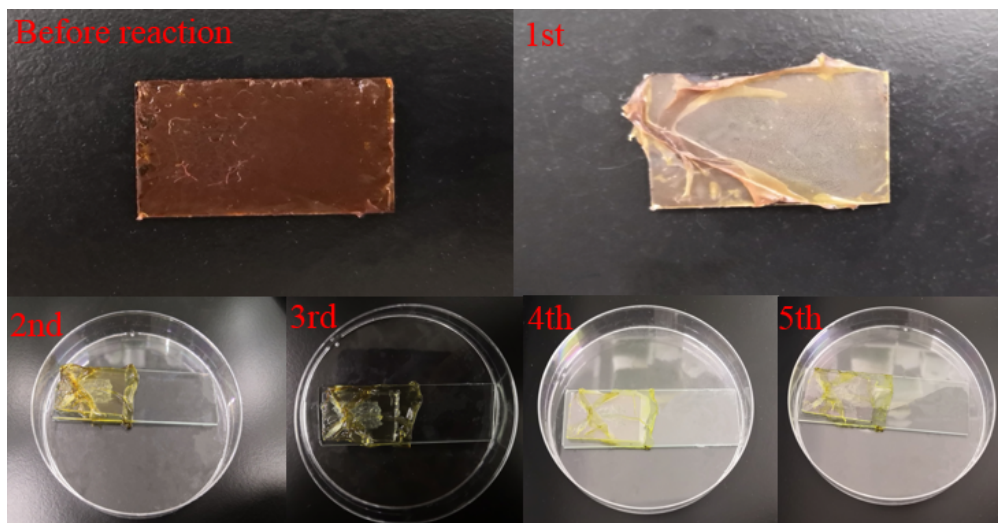
Figure 4.16. Photos of PTET-T-COOH/PU coating before reaction and after each cycle.

In order to obtain stable and transparent PTET-T-COOH/PU coating and avoid any leaching problems, the fabrication process of PTET-T-COOH/PU coating was optimized. Briefly, the dosage of PTET-T-COOH in 1 mL 1,2-dichlorobenzene was decreased to 1 mg from 3 mg. In addition, the solution treated by sonication was further filtered by using a syringe filter to achieve transparent solution. As demonstrated in Figure 4.17, transparent

PTET-T-COOH/PU was obtained and there was no obvious change in color and transparency after the photocatalytic reaction. However, obvious swelling of coating was also observed, and the fabrication process of PU should be further optimized.
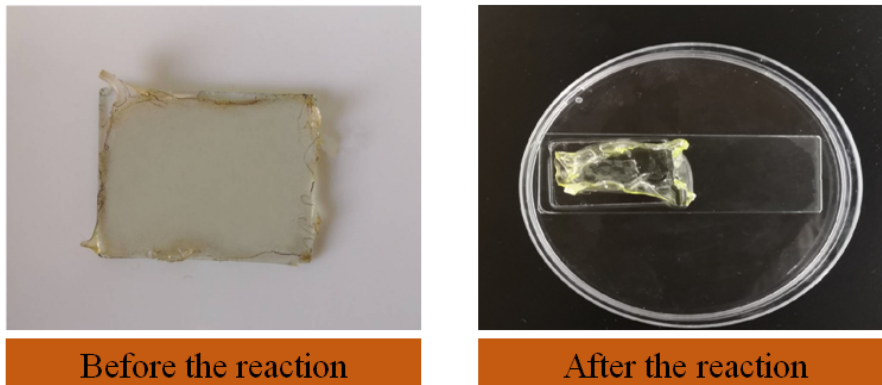
Figure 4.17. Photos of optimized coating before and after reaction.

The survival rate and cell density of *S. aureus* under different conditions were estimated and provided in Figure 4.18. In the dark control (with PTET-T-COOH/PU coating), light control (*S. aureus* under illumination alone) as well as PU coating under irradiation, more than 67 % of *S. aureus* cells survived after 4 h. However, *S. aureus* can be efficiently killed in the presence of PTET-T-COOH/PU coating under visible light. Over a period of 4 h of visible-light irradiation, PTET-T-COOH/PU demonstrated 5-log inactivation of *S. aureus* (100% inactivation efficiency). Further repeating experiments can be followed to test the recycling stability of PTET-T-COOH/PU coating.
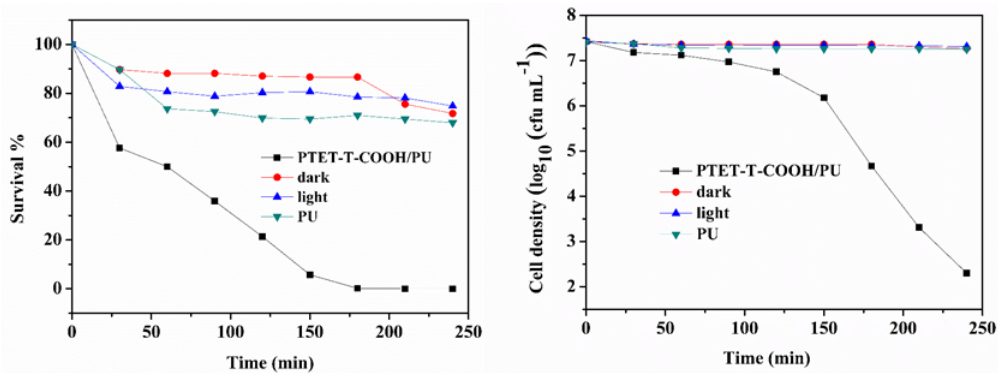
Figure 4.18. (left) Photocatalytic inactivation efficiency and (right) cell density of optimized PTET-T-COOH/PU against *S. aureus* (10^7 cfu mL^{-1}, 30 mL).

4.5 Conclusions

Efficient photocatalytic antimicrobial PTET-T-COOH/PU coatings by using PU as protective layer and PTET-T-COOH/PU composite as photoactive layer were fabricated. ATR-FTIR and XPS techniques were used to confirm the successful formation of chemical bonding between carboxyl groups of PTET-T-COOH and NCO-terminated pre-polyurethane. PTET-T-COOH/PU coating can kill *S. aureus* completely in 4 h and behaved moderate recycling stability. By optimizing fabrication process of PTET-T-COOH/PU coating, transparent and efficient coating was obtained. This work offered a promising platform for exploration environmentally friendly, low cost and sustainable antimicrobial surface.

4.6 References

1. Jones, K. E.; Patel, N. G.; Levy, M. A.; Storeygard, A.; Balk, D.; Gittleman, J. L.; Daszak, P., Global trends in emerging infectious diseases. *Nature* **2008,** *451* (7181), 990.

2. Rice, K. M.; Ginjupalli, G. K.; Manne, N. D. P. K.; Jones, C. B.; Blough, E. R., A review of the antimicrobial potential of precious metal derived nanoparticle constructs. *Nanotechnology* **2019,** *30* (37), 372001.

3. Lee, Y.-J.; Lee, D.-J., Impact of adding metal nanoparticles on anaerobic digestion performance – A review. *Bioresource Technology* **2019,** *292*, 121926.

4. 4. Sun, G.; Hong, K. H., Photo-induced antimicrobial and decontaminating agents: recent progresses in polymer and textile applications. *Textile Research Journal* **2013,** *83* (5), 532-542.

5. Lee, S. L.; Chang, C.-J., Recent developments about conductive polymer based composite photocatalysts. *Polymers* **2019,** *11* (2), 206.

6. Wang, C.; Dong, H.; Jiang, L.; Hu, W., Organic semiconductor crystals. *Chemical Society Reviews* **2018,** *47* (2), 422-500.

7. Kamyshny, A.; Magdassi, S., Conductive nanomaterials for 2D and 3D printed flexible electronics. *Chemical Society Reviews* **2019,** *48* (6), 1712-1740.

8. Liu, L.; Ding, L.; Liu, Y.; An, W.; Lin, S.; Liang, Y.; Cui, W., A stable Ag$_3$PO$_4$@PANI core@shell hybrid: Enrichment photocatalytic degradation with π-π conjugation. *Applied Catalysis B: Environmental* **2017,** *201*, 92-104.

9. Yuan, X.; Floresyona, D.; Aubert, P.-H.; Bui, T.-T.; Remita, S.; Ghosh, S.; Brisset, F.; Goubard, F.; Remita, H., Photocatalytic degradation of organic pollutant with polypyrrole nanostructures under UV and visible light. *Applied Catalysis B: Environmental* **2019,** *242*, 284-292.

10. Gao, B.; Iftekhar, S.; Srivastava, V.; Doshi, B.; Sillanpää, M., Insights into the generation of reactive oxygen species (ROS) over polythiophene/ZnIn$_2$S$_4$ based on different modification processing. *Catalysis Science & Technology* **2018,** *8* (8), 2186-2194.

11. Brown, D. M.; Yang, J.; Strach, E. W.; Khalil, M. I.; Whitten, D. G., Size and substitution effect on antimicrobial activity of polythiophene polyelectrolyte derivatives under photolysis and dark conditions. *Photochemistry and Photobiology* **2018,** *94* (6), 1116-1123.

12. Truc, N. T. T.; Hanh, N. T.; Nguyen, D. T.; Trang, H. T.; Nguyen, V. N.; Ha, M. N.; Nguyen, T. D. C.; Pham, T.-D., Novel overall photocatalytic water splitting of tantalum nitride sensitized/protected by conducting polymers. *Journal of Solid State Chemistry* **2019,** *269*, 361-366.

13. Kharazi, P.; Rahimi, R.; Rabbani, M., Study on porphyrin/ZnFe$_2$O$_4$@ polythiophene nanocomposite as a novel adsorbent and visible light driven photocatalyst for the removal of methylene blue and methyl orange. *Materials Research Bulletin* **2018,** *103*, 133-141.

14. Kaur, M.; Pramanik, S.; Kumar, M.; Bhalla, V., Polythiophene-encapsulated bimetallic au-Fe$_3$O$_4$ Nano-hybrid materials: a potential tandem photocatalytic system for nondirected C (sp^2)–H activation for the synthesis of Quinoline carboxylates. *ACS Catalysis* **2017,** *7* (3), 2007-2021.

15. Shang, K.; Ai, S.; Ma, Q.; Tang, T.; Yin, H.; Han, H., Effective photocatalytic disinfection of E. coli and S. aureus using polythiophene/MnO$_2$ nanocomposite photocatalyst under solar light irradiation. *Desalination* **2011,** *278* (1-3), 173-178.

16. Ma, G.; Liang, X.; Li, L.; Qiao, R.; Jiang, D.; Ding, Y.; Chen, H., Cu-doped zinc oxide and its polythiophene composites: Preparation and antibacterial properties. *Chemosphere* **2014,** *100*, 146-151.

17. Zhang, Z.; Zhu, Y.; Chen, X.; Zhang, H.; Wang, J., A full‐spectrum metal‐free porphyrin supramolecular photocatalyst for dual functions of highly efficient hydrogen and oxygen evolution. *Advanced Materials* **2019,** *31* (7), 1806626.

18. Xing, C.; Xu, Q.; Tang, H.; Liu, L.; Wang, S., Conjugated polymer/porphyrin complexes for efficient energy transfer and improving light-activated antibacterial activity. *Journal of the American Chemical Society* **2009,** *131* (36), 13117-13124.

19. Liu, L.; Chen, J.; Wang, S., Flexible antibacterial film deposited with polythiophene–porphyrin composite. *Advanced Healthcare Materials* **2013,** *2* (12), 1582-1585.

20. Huang, Y.; Pappas, H. C.; Zhang, L.; Wang, S.; Cai, R.; Tan, W.; Wang, S.; Whitten, D. G.; Schanze, K. S., Selective imaging and inactivation of bacteria over mammalian cells by imidazolium-substituted polythiophene. *Chemistry of Materials* **2017,** *29* (15), 6389-6395.

21. Starčević, K.; Boykin, D. W.; Karminski‐Zamola, G., New amidino‐benzimidazolyl thiophenes: Synthesis and photochemical synthesis. *Heteroatom Chemistry: An International Journal of Main Group Elements* **2003,** *14* (3), 218-222.

22. Linshoeft, J.; Heinrich, A. C.; Segler, S. A.; Gates, P. J.; Staubitz, A., Chemoselective cross-coupling reactions with differentiation between two nucleophilic sites on a single aromatic substrate. *Organic Letters* **2012,** *14* (22), 5644-5647.

23. Li, Y.; Liu, M.; Chen, L., Polyoxometalate built-in conjugated microporous polymers for visible-light heterogeneous photocatalysis. *Journal of Materials Chemistry A* **2017,** *5* (26), 13757-13762.

24. Kim, J.-S.; Kim, J.-H.; Lee, W.; Yu, H.; Kim, H. J.; Song, I.; Shin, M.; Oh, J. H.; Jeong, U.; Kim, T.-S., Tuning mechanical and optoelectrical properties of poly (3-hexylthiophene) through systematic regioregularity control. *Macromolecules* **2015,** *48* (13), 4339-4346.

25. Bhardwaj, D.; Gupta, S.; Yadav, P.; Bhargav, R.; Patra, A., All conjugated poly (3‐hexylthiophene)‐block‐poly (hexyl‐3, 4‐ethylenedioxythiophene) copolymers. *ChemistrySelect* **2017,** *2* (29), 9557-9562.

26. Khan, I. A.; Mirza, Z. M.; Kumar, A.; Verma, V.; Qazi, G. N., Piperine, a phytochemical potentiator of ciprofloxacin against Staphylococcus aureus. *Antimicrobial Agents and Chemotherapy* **2006,** *50* (2), 810-812.

27. Fu, J.; Yu, J.; Jiang, C.; Cheng, B., g‐C_3N_4‐Based heterostructured photocatalysts. *Advanced Energy Materials* **2018,** *8* (3), 1701503.

28. Prasad, K. P.; Chen, Y.; Sk, M. A.; Than, A.; Wang, Y.; Sun, H.; Lim, K.-H.; Dong, X.; Chen, P., Fluorescent quantum dots derived from PEDOT and their applications in optical imaging and sensing. *Materials Horizons* **2014,** *1* (5), 529-534.

29. Huang, W.; Ma, B. C.; Lu, H.; Li, R.; Wang, L.; Landfester, K.; Zhang, K. A., Visible-light-promoted selective oxidation of alcohols using a covalent triazine framework. *ACS Catalysis* **2017,** *7* (8), 5438-5442.

30. Huang, W.; Byun, J.; Rörich, I.; Ramanan, C.; Blom, P. W.; Lu, H.; Wang, D.; Caire da Silva, L.; Li, R.; Wang, L., Asymmetric covalent triazine framework for enhanced visible‐light photoredox catalysis via energy transfer cascade. *Angewandte Chemie International Edition* **2018,** *57* (27), 8316-8320.

31. Zhu, E.; Hai, J.; Wang, Z.; Ni, B.; Jiang, Y.; Bian, L.; Zhang, F.; Tang, W., Two-dimensional polyfluorenes bearing thienylenevinylene π-bridge-acceptor side chains for photovoltaic solar cells. *The Journal of Physical Chemistry C* **2013,** *117* (47), 24700-24709.

32. Alley, N. J.; Liao, K.-S.; Andreoli, E.; Dias, S.; Dillon, E. P.; Orbaek, A. W.; Barron, A. R.; Byrne, H. J.; Curran, S. A., Effect of carbon nanotube-fullerene hybrid additive on P3HT: PCBM bulk-heterojunction organic photovoltaics. *Synthetic Metals* **2012,** *162* (1-2), 95-101.

33. Zhang, C.; Li, Y.; Shuai, D.; Shen, Y.; Xiong, W.; Wang, L., Graphitic carbon nitride (g-C$_3$N$_4$)-based photocatalysts for water disinfection and microbial control: A review. *Chemosphere* **2019,** *214*, 462-479.

34. Bing, W.; Chen, Z.; Sun, H.; Shi, P.; Gao, N.; Ren, J.; Qu, X., Visible-light-driven enhanced antibacterial and biofilm elimination activity of graphitic carbon nitride by embedded Ag nanoparticles. *Nano Research* **2015,** *8* (5), 1648-1658.

35. Deng, J.; Liang, J.; Li, M.; Tong, M., Enhanced visible-light-driven photocatalytic bacteria disinfection by g-C$_3$N$_4$-AgBr. *Colloids and Surfaces B: Biointerfaces* **2017,** *152*, 49-57.

36. Zhang, W.; Yu, C.; Sun, Z.; Zheng, S., Visible-light-driven catalytic disinfection of staphylococcus aureus using sandwich structure g-C$_3$N$_4$/ZnO/stellerite hybrid photocatalyst. *Journal of Microbiology and Biotechnology* **2018,** *28* (6), 957-967.

37. Vignesh, S.; Muppudathi, A. L.; Sundar, J. K., Multifunctional performance of g-C$_3$N$_4$-BiFeO$_3$-Cu$_2$O hybrid nanocomposites for magnetic separable photocatalytic and antibacterial activity. *Journal of Materials Science: Materials in Electronics* **2018,** *29* (13), 10784-10801.

38. Li, Y.; Wang, Q.; Huang, L.; Xu, X.; Xie, M.; Wang, H.; Huang, S.; Zhang, F.; Zhao, Z.; Yang, J., Enhanced LED-light-driven photocatalytic antibacterial by g-C$_3$N$_4$/BiOI composites. *Journal of Materials Science: Materials in Electronics* **2019,** *30* (3), 2783-2794.

39. Khan, M. A.; Mutahir, S.; Wang, F.; Zhou, J.-W.; Lei, W.; Xia, M., Facile synthesis of CNS/TNS sensitized with Cu biphenylamine frameworks for remarkable photocatalytic activity for organic pollutants degradation and bacterial inactivation. *Solar Energy* **2019,** *186*, 204-214.

40. Liu, H.; Ma, S.; Shao, L.; Liu, H.; Gao, Q.; Li, B.; Fu, H.; Fu, S.; Ye, H.; Zhao, F.; Zhou, J., Defective engineering in graphitic carbon nitride nanosheet for efficient photocatalytic pathogenic bacteria disinfection. *Applied Catalysis B: Environmental* **2020,** *261*, 118201.

41. Tang, C.; Liu, C.; Han, Y.; Guo, Q.; Ouyang, W.; Feng, H.; Wang, M.; Xu, F., Nontoxic carbon quantum dots/g‑C_3N_4 for efficient photocatalytic inactivation of staphylococcus aureus under visible light. *Advanced Healthcare Materials* **2019,** 1801534.

42. Vignesh, S.; Suganthi, S.; Sundar, J. K.; Raj, V., Construction of α-Fe_2O_3/CeO_2 decorated g-C_3N_4 nanosheets for magnetically separable efficient photocatalytic performance under visible light exposure and bacterial disinfection. *Applied Surface Science* **2019,** *488*, 763-777.

43. Yadav, P.; Nishanthi, S. T.; Purohit, B.; Shanavas, A.; Kailasam, K., Metal-free visible light photocatalytic carbon nitride quantum dots as efficient antibacterial agents: An insight study. *Carbon* **2019,** *152*, 587-597.

44. Wang, L.; Zhang, X.; Yu, X.; Gao, F.; Shen, Z.; Zhang, X.; Ge, S.; Liu, J.; Gu, Z.; Chen, C., An all‑organic semiconductor C_3N_4/PDINH heterostructure with advanced antibacterial photocatalytic therapy activity. *Advanced Materials* **2019,** 1901965.

45. Wang, R.; Zhang, B.; Liang, Z.; He, Y.; Wang, Z.; Ma, X.; Yao, X.; Sun, J.; Wang, J., Insights into rapid photodynamic inactivation mechanism of Staphylococcus aureus via rational design of multifunctional nitrogen-rich carbon-coated bismuth/cobalt nanoparticles. *Applied Catalysis B: Environmental* **2019,** *241*, 167-177.

46. Segura, M., Streptococcus suis: an emerging human threat. *The Journal of Infectious Diseases* **2009,** *199* (1), 4-6.

47. Pachfule, P.; Acharjya, A.; Roeser, J. r. m.; Langenhahn, T.; Schwarze, M.; Schomäcker, R.; Thomas, A.; Schmidt, J., Diacetylene functionalized covalent organic framework (COF) for photocatalytic hydrogen generation. *Journal of the American Chemical Society* **2018,** *140* (4), 1423-1427.

48. Wang, F.; Feng, Y.; Chen, P.; Wang, Y.; Su, Y.; Zhang, Q.; Zeng, Y.; Xie, Z.; Liu, H.; Liu, Y., Photocatalytic degradation of fluoroquinolone antibiotics using ordered mesoporous g-C_3N_4 under simulated sunlight irradiation: kinetics, mechanism, and antibacterial activity elimination. *Applied Catalysis B: Environmental* **2018,** *227*, 114-122.

49. Chen, L.; Yamane, S.; Mizukado, J.; Suzuki, Y.; Kutsuna, S.; Uchimaru, T.; Suda, H., ESR study of singlet oxygen generation and its behavior during the photo-oxidation of P3HT in solution. *Chemical Physics Letters* **2015,** *624*, 87-92.

50. Burrows, H. D.; Seixas de Melo, J.; Serpa, C.; Arnaut, L. G.; Miguel, M. d. G.; Monkman, A. P.; Hamblett, I.; Navaratnam, S., Triplet state dynamics on isolated conjugated polymer chains. *Chemical Physics* **2002,** *285* (1), 3-11.

51. Manceau, M.; Bundgaard, E.; Carlé, J. E.; Hagemann, O.; Helgesen, M.; Søndergaard, R.; Jørgensen, M.; Krebs, F. C., Photochemical stability of π-conjugated polymers for polymer solar cells: a rule of thumb. *Journal of Materials Chemistry* **2011,** *21* (12), 4132-4141.

52. Reese, M. O.; Nardes, A. M.; Rupert, B. L.; Larsen, R. E.; Olson, D. C.; Lloyd, M. T.; Shaheen, S. E.; Ginley, D. S.; Rumbles, G.; Kopidakis, N., Photoinduced degradation of polymer and polymer–fullerene active layers: experiment and theory. *Advanced Functional Materials* **2010,** *20* (20), 3476-3483.

53. Manceau, M.; Rivaton, A.; Gardette, J. L., Involvement of singlet oxygen in the solid‐state photochemistry of P3HT. *Macromolecular Rapid Communications* **2008,** *29* (22), 1823-1827.

54. Chai, Y. H.;   Zhou, F.; Zhu, Z. Y., High-efficiency and environment-friendly sterilization PEVE coatings modified with Bi_2WO_6/TiO_2 composites. *Chemical Physics Letters* **2019,** *715*, 173-180.

55. Farag, A. A., Applications of nanomaterials in corrosion protection coatings and inhibitors. *Corrosion Reviews* **2020,** *38* (1), 67-86.

56. Mishra, A. K.; Chattopadhyay, D.; Sreedhar, B.; Raju, K., FT-IR and XPS studies of polyurethane-urea-imide coatings. *Progress in Organic Coatings* **2006,** *55* (3), 231-243.

57. Ederer, J.; Janoš, P.; Ecorchard, P.; Tolasz, J.; Štengl, V.; Beneš, H.; Perchacz, M.; Pop-Georgievski, O., Determination of amino groups on functionalized graphene oxide for polyurethane nanomaterials: XPS quantitation vs. functional speciation. *RSC Advances* **2017,** *7* (21), 12464-12473.

58. Yang, Y.; Sun, C.; Zhou, Y.; Wang, T.; Zhang, Y., Optically active polyurethane based on tyrosine: synthesis, characterization and study of hydrogen bonding. *Polymer Journal* **2016,** *48* (7), 807-812.

59. Josset, S.; Hajiesmaili, S.; Begin, D.; Edouard, D.; Pham-Huu, C.; Lett, M.-C.; Keller, N.; Keller, V., UV-A photocatalytic treatment of Legionella pneumophila bacteria contaminated airflows through three-dimensional solid foam structured photocatalytic reactors. *Journal of hazardous materials* **2010,** *175* (1-3), 372-381.

60. Charpentier, P.; Burgess, K.; Wang, L.; Chowdhury, R.; Lotus, A.; Moula, G., Nano-TiO_2/polyurethane composites for antibacterial and self-cleaning coatings. *Nanotechnology* **2012,** *23* (42), 425606.

61. Ryu, S.-Y.; Park, M.-K.; Kwak, S.-Y., Silver-titania-polyurethane composite nanofibre mat for chemical and biological warfare protection. *International Journal of Nanotechnology* **2013,** *10* (8-9), 771-788.

62. Kim, H. J.; Pant, H. R.; Kim, J. H.; Choi, N. J.; Kim, C. S., Fabrication of multifunctional TiO_2–fly ash/polyurethane nanocomposite membrane via electrospinning. *Ceramics International* **2014,** *40* (2), 3023-3029.

63. Li, K.; Peng, J.; Zhang, M.; Heng, J.; Li, D.; Mu, C., Comparative study of the effects of anatase and rutile titanium dioxide nanoparticles on the structure and properties of waterborne polyurethane. *Colloids and Surfaces A: Physicochemical and Engineering Aspects* **2015,** *470*, 92-99.

64. Yemmireddy, V. K.; Farrell, G. D.; Hung, Y. C., Development of titanium dioxide (TiO_2) nanocoatings on food contact surfaces and method to evaluate their durability and photocatalytic bactericidal property. *Journal of Food Science* **2015,** *80* (8), N1903-N1911.

65. Weng, X.; van Niekerk, J.; Neethirajan, S.; Warriner, K., Characterization of antimicrobial efficacy of photocatalytic polymers against food-borne biofilms. *LWT-Food Science and Technology* **2016,** *68*, 1-7.

66. Nguyen, T. V.; Nguyen, T. A.; Dao, P. H.; Nguyen, A. H.; Do, M. T., Effect of rutile titania dioxide nanoparticles on the mechanical property, thermal stability, weathering resistance and antibacterial property of styrene acrylic polyurethane coating. *Advances in Natural Sciences: Nanoscience and Nanotechnology* **2016,** *7* (4), 045015.

67. Pessoa, R.; dos Santos, V.; Cardoso, S.; Doria, A.; Figueira, F.; Rodrigues, B.; Testoni, G.; Fraga, M.; Marciano, F.; Lobo, A., TiO_2 coatings via atomic layer deposition on polyurethane and polydimethylsiloxane substrates: Properties and effects on C. albicans growth and inactivation process. *Applied Surface Science* **2017,** *422*, 73-84.

68. Li, X.; Xie, J.; Liao, L.; Jiang, X.; Fu, H., UV-curable polyurethane acrylate–Ag/TiO_2 nanocomposites with superior UV light antibacterial activity. *International Journal of Polymeric Materials and Polymeric Biomaterials* **2017,** *66* (16), 835-843.

69. 69.   Kim, J. H.; Joshi, M. K.; Lee, J.; Park, C. H.; Kim, C. S., Polydopamine-assisted immobilization of hierarchical zinc oxide nanostructures on electrospun nanofibrous membrane for photocatalysis and antimicrobial activity. *Journal of Colloid and Interface Science* **2018,** *513*, 566-574.

70. Kováčová, M. r.; Marković, Z. M.; Humpolíček, P.; Mičušík, M.; Švajdlenková, H.; Kleinová, A.; Danko, M.; Kubát, P.; Vajďák, J.; Capakova, Z., Carbon quantum dots modified polyurethane nanocomposite as effective photocatalytic and antibacterial agents. *ACS Biomaterials Science & Engineering* **2018,** *4* (12), 3983-3993.

71. Chitichotpanya, P.; Inprasit, T.; Chitichotpanya, C., In vitro assessment of antibacterial potential and mechanical properties of Ag-TiO$_2$/WPU on medical cotton optimized with response surface methodology. *Journal of Natural Fibers* **2019,** *16* (1), 88-99.

72. Zhou, H.; Wang, X.; Wang, T.; Zeng, J.; Yuan, Z.; Jian, J.; Zhou, Z.; Zeng, L.; Yang, H., In situ decoration of Ag@ AgCl nanoparticles on polyurethane/silk fibroin composite porous films for photocatalytic and antibacterial applications. *European Polymer Journal* **2019,** *118*, 153-162.

73. Li, X.; Wang, S.; Xie, J.; Hu, J.; Fu, H., Polyurethane acrylate-supported rGO/TiO$_2$ electrical conductive and antibacterial nanocomposites. *International Journal of Polymeric Materials and Polymeric Biomaterials* **2019,** *68* (6), 319-327.

74. Suárez Murillo, L. V.; Schärer, A.; Giannakis, S.; Rtimi, S.; Pulgarín, C., Iron-coated polymer films with high antibacterial activity under indoor and outdoor light, prepared by different facile pre-treatment and deposition methods. *Applied Catalysis B: Environmental* **2019,** *243*, 161-174.

Chapter 5

5 Synthesis and photocatalytic antibacterial properties of g-C$_3$N$_4$-NH$_2$ nanosheets

Metal-free polymer graphitic carbon nitride (g-C$_3$N$_4$) material has witnessed a surge of interest during the past decade in various photocatalytic fields including water splitting,[1] CO$_2$ reduction,[2,3] N$_2$ fixation,[4] pollutants removal[5] and so on due to its low cost, no toxicity, and high activity.[6] From 2013, g-C$_3$N$_4$ has become active in photocatalytic disinfection.[7] A range of g-C$_3$N$_4$ with different morphologies including porosity and ultrathin sheets,[8] doping g-C$_3$N$_4$ and g-C$_3$N$_4$ based composites have been reported in succession for inactivation bacteria, viruses and algae.

In order to overcome small surface area and high recombination rate of electrons and holes in bulk g-C$_3$N$_4$, thin g-C$_3$N$_4$ nanosheets with rich amino groups (g-C$_3$N$_4$-NH$_2$) and a reference sample bulk g-C$_3$N$_4$ were prepared in this study. The photocatalytic antibacterial activities of these two samples toward *S. aureus* were compared and reasons for better disinfection performance of g-C$_3$N$_4$-NH$_2$ were also discussed.

5.1 Abstract

G-C$_3$N$_4$ and g-C$_3$N$_4$-NH$_2$ nanosheets were synthesized via thermal polymerization from urea. g-C$_3$N$_4$-NH$_2$ nanosheets possess efficient electron-holes separation, which was confirmed by photoluminescence intensity, photocurrent density and EIS. Thus, g-C$_3$N$_4$-NH$_2$ nanosheets have superior photocatalytic antibacterial property against *S. aureus* to bulk g-C$_3$N$_4$.

5.2 Introduction

Graphitic carbon nitride (g-C$_3$N$_4$) is a popular material in photocatalytic fields such as water splitting to produce hydrogen, carbon dioxide reduction, nitrogen fixation and organic synthesis owing to its suitable bandgap (≈ 2.7 eV), low cost and non-toxicity. In 2013, g-C$_3$N$_4$ based antimicrobials was firstly reported.[7] From then on, the number of publications of g-C$_3$N$_4$ based photocatalysts for photocatalytic disinfection applications

has increased rapidly every year.[9] Various g-C$_3$N$_4$ with different morphologies and compositions were reviewed by several groups.[9-11] At present, high surface area g-C$_3$N$_4$ with porosity and ultrathin sheet structures were reported in photocatalytic disinfection applications.[12-14] The secondary semiconductors incorporation with g-C$_3$N$_4$-based mainly focused on sliver metal and salts (Ag nanoparticles, AgBr, AgCl, Ag$_2$WO$_4$),[15-17] bismuth oxide or salts (Bi$_2$O$_4$, Bi$_2$MoO$_6$, BiVO$_4$ BiOBr, BiOI)[18-20] and carbon materials (C60, graphene).[21, 22] However, compared to study of g-C$_3$N$_4$ in other photocatalytic fields special water splitting, the research of g-C$_3$N$_4$ based antimicrobials is not sufficient and needs to be carried out in detail for their future practical applications. In this thesis, we fabricated g-C$_3$N$_4$ nanosheets with rich NH$_2$ groups (g-C$_3$N$_4$-NH$_2$) by NH$_3$ exfoliation and using urea as raw material. G-C$_3$N$_4$-NH$_2$ showed better photocatalytic inactivation toward *S. aureus* than bulk g-C$_3$N$_4$. The main reasons were investigated by comparing the photoluminescence intensity, photocurrent density and Electron spin resonance (ESR).

5.3 Experimental Section

5.3.1 Materials

Urea and nitric acid were purchased from Aladdin (Shanghai, China) and anhydrous ammonia was obtained from Zhongpu (Zhenjiang, China).

5.3.2 Synthesis of g-C$_3$N$_4$-NH$_2$ nanosheets

Figure 5.1 illustrated the synthesis process of g-C$_3$N$_4$ and g-C$_3$N$_4$-NH$_2$. In detail, 5 g of urea was added to a porcelain boat with a cover for drying 24 h in an oven. Then, bulk g-C$_3$N$_4$ was obtained under static air at 550 °C for 4 h with a heating rate of 2.5 °C/ min (4 g, 80 %) in a muffle furnace. After that, bulk g-C$_3$N$_4$ was added into 200 mL HNO$_3$ solution (1 mol L^{-1}) for etching 24 h to obtain thin g-C$_3$N$_4$ nanosheets. An additional oxidization and etching under air at 500 °C for 4h to form porous oxygen-rich g-C$_3$N$_4$ nanosheets. Lastly, calcination under an NH$_3$ atmosphere at 520 °C for 1 h with a heating rate of 2.0 °C/ min was carried out to exfoliate and to form -NH$_2$ groups on the resulting g-C$_3$N$_4$-NH$_2$ nanosheets (0.8 g, 16 %).
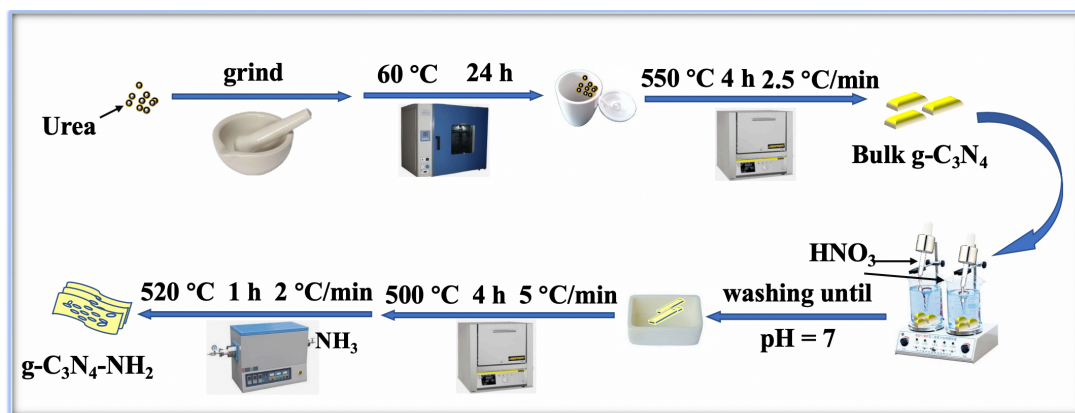
Figure 5.1. Syntheses of g-C$_3$N$_4$ and g-C$_3$N$_4$-NH$_2$.

5.3.3 Measurements

The crystallinity of g-C$_3$N$_4$ and g-C$_3$N$_4$-NH$_2$ was obtained by X-ray diffractometer (XRD, Rigaku, D/MAX-2500) with Cu Kα radiation. Scanning electron microscopy (SEM) was performed using a Hitachi S-4500 field emission SEM. All samples were taken at 10 kV at varying magnifications for different views. The UV-vis diffuse reflectance spectra (DRS) were performed on UV-vis spectrophotometer (Shimadzu UV-2450) with BaSO$_4$ as the reference.

5.3.4 Testing of photocatalytic antibacterial properties of g-C$_3$N$_4$-NH$_2$ nanosheets

Gram-positive *S. aureus* (USA 300) were chosen as model bacteria which were cultured in TSB at 37 °C for 12 h and then purified by high-speed freezing centrifuge at 12000 rpm for 2 min and washed twice with 1mL PBS, resulting in a cell count of approximately 7~8×10^8 colony forming units (cfu)/mL. Typically, 3 mg of photocatalyst was dispersed in 30 mL of PBS solution (0.1 mg/mL) in a 120 mL self-designed glass jacketed reactor containing 600 μL of bacteria solution (7~8×10^8 cfu/mL). The bacteria concentration for photocatalytic antibacterial test was about 10^7 cfu/mL. The reaction was carried out in a GHX-3 photochemical reaction instrument equipped with a 250 W Xenon arc lamp and an optical cutoff filter (λ< 420 nm). The visible light intensity was fixed at 80 mW/cm^2. The temperature was kept at 30 °C using a cryostatic tank. At given time intervals, 100 μL of tested suspension sample was pipetted out and serially diluted using PBS and spread on

nutrient TSA plates. After incubation at 37 °C for 18 h, the cell densities were checked to determine the survival bacterial numbers. Control experiments including *S. aureus* with g-C_3N_4 or g-C_3N_4-NH_2 in dark and *S. aureus* without photocatalyst under irradiation were carried out. All materials and glassware had been autoclaved at 121 °C at 0.1 MPa for 20 min before use and all the experiments were repeated three times.

5.3.5 Study of photocatalytic antibacterial mechanism of g-C_3N_4-NH_2 nanosheets

The separation efficiency of electron-holes is mainly analyzed by photoluminescence (PL) spectra using PerkinElmer LS 55 spectrophotometer. Photocurrent density and electrochemical impedance spectra (EIS) were carried out on VersaSTAT3 and CHI 760E electrochemical workstations.

5.4 Results and Discussion

5.4.1 Characterization of g-C_3N_4-NH_2 nanosheets

The microstructures of samples were examined by SEM determination. Figure 5.2 showed the differences of morphology between g-C_3N_4 and g-C_3N_4-NH_2. Apparently, the size of g-C_3N_4 particles g-C_3N_4-NH_2 nanosheets is similar (about 500 nm). However, the g-C_3N_4-NH_2 sheet structure could be more efficient in photocatalytic process because it can provide a large surface area, more reactive sites and short exciton diffusion length.
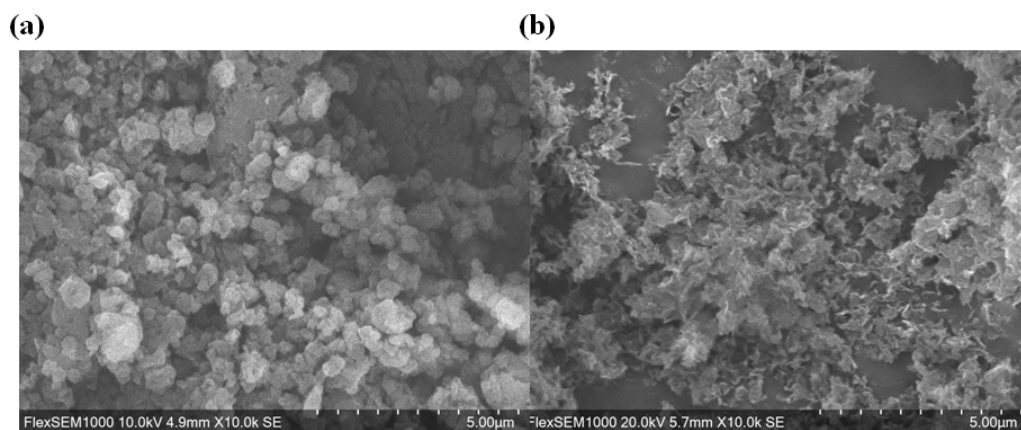

Figure 5.2. SEM images of g-C_3N_4 and g-C_3N_4-NH_2 nanosheets.

XRD spectra were measured to study the chemical structure of samples. As depicted in Figure 5.3, two characteristic peaks exist in g-C_3N_4 and g-C_3N_4-NH_2. The high-angle peak at 27.5° (002) was attributed to the interlayer stacking of the conjugated polymer and the diffraction peak at 13.1° (100) belonged to the in-plane tri-s-triazine units, indicating the successful syntheses of samples.[23] In addition, the characteristic peak (002) intensity of g-C_3N_4-NH_2 was much stronger than that of g-C_3N_4. This suggested that crystallinity of g-C_3N_4-NH_2 was enhanced and the transfer of electrons in the plane can be efficient, thus improvement of photocatalytic performance.[24]

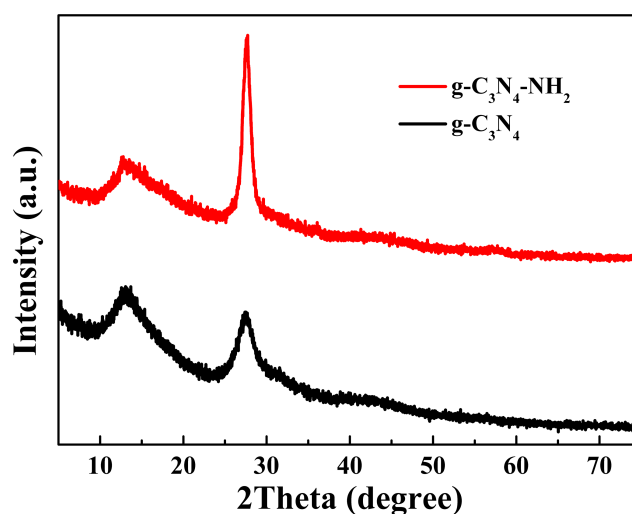**Figure 5.3.** XRD spectra of g-C_3N_4 and g-C_3N_4-NH_2 nanosheets.

UV-Visible light absorption ability of a photocatalyst plays an important role in its photocatalytic process. Figure 5.4 depicted the UV-Visible absorption spectra of g-C_3N_4 and g-C_3N_4-NH_2. G-C_3N_4-NH_2 showed a small redshift compared to g-C_3N_4, corresponding to the band gaps of 2.71 eV and 2.64 eV for g-C_3N_4 and g-C_3N_4-NH_2, respectively (Figure. 5.4b).
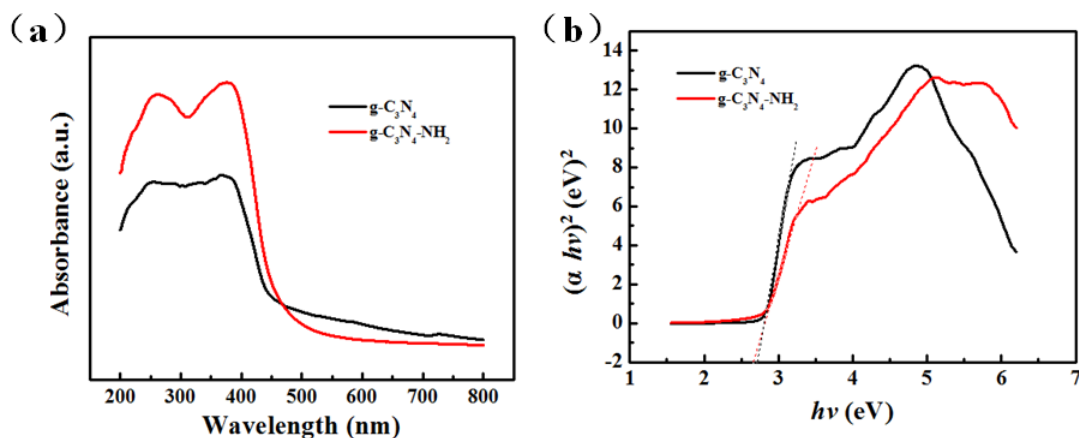
Figure 5.4. UV–vis DRS spectra and plots of $(ahv)^{1/2}$ versus (hv) of as-prepared samples of g-C$_3$N$_4$ and g-C$_3$N$_4$-NH$_2$ nanosheets.

Contact angles were determined for studying the hydrophilicity of samples. Figure 5.5 demonstrated the water contact angles of g-C$_3$N$_4$ and g-C$_3$N$_4$-NH$_2$ were 49.2 º and 31.5 º, implying the rich -NH$_2$ groups increased the hydrophilicity of g-C$_3$N$_4$. In addition, this could also provide efficient chemical interaction between g-C$_3$N$_4$ nanosheets with polyurethane and form stable antibacterial coating based on g-C$_3$N$_4$/polyurethane.
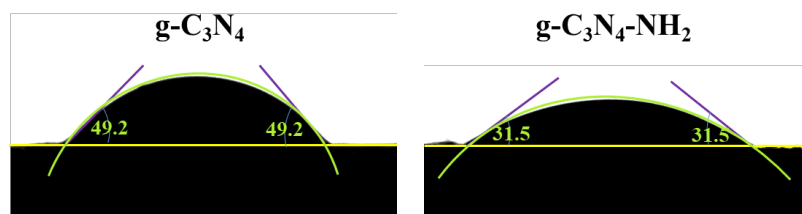
Figure 5.5. Water contact angles of g-C$_3$N$_4$ and g-C$_3$N$_4$-NH$_2$ nanosheets.

5.4.2 Photocatalytic antibacterial properties of g-C$_3$N$_4$-NH$_2$ nanosheets

The photocatalytic disinfection inactivation of g-C$_3$N$_4$ and g-C$_3$N$_4$-NH$_2$ against *S. aureus* were evaluated, as demonstrated in Figure 5.6. In the dark and light control experiments, antibacterial effects can be ignored (less than 20%), indicating that both g-C$_3$N$_4$ and g-C$_3$N$_4$-NH$_2$ themselves had almost no cytotoxicity to *S. aureus*. As expected, g-C$_3$N$_4$-NH$_2$ has superior photocatalytic antibacterial property to g-C$_3$N$_4$. The number of *S. aureus* cells

decreased upon visible light irradiation and more than 80 % of *S. aureus* was killed 2 h later. However, the survival rate was 54.5 % for g-C$_3$N$_4$ against *S. aureus* and less than half of *S. aureus* cells was killed at this time.
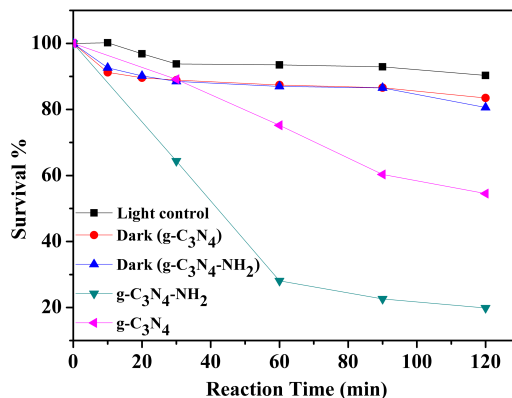
Figure 5.6. Photocatalytic inactivation efficiency of g-C$_3$N$_4$ and g-C$_3$N$_4$-NH$_2$ against *S. aureus*.

5.4.3 Photocatalytic antibacterial mechanism of g-C$_3$N$_4$-NH$_2$ nanosheets

The intensity of photoluminescence (PL) was always used to study the charge carriers' separation efficiency for studying the mechanisms of photocatalyst. Figure 5.7 displayed the PL spectra of g-C$_3$N$_4$ and g-C$_3$N$_4$-NH$_2$. G-C$_3$N$_4$-NH$_2$ exhibited weaker fluorescence intensity than g-C$_3$N$_4$, indicating more efficient dissociation of photogenerated electrons and holes and transportation happened in the g-C$_3$N$_4$-NH$_2$, and more active species can be generated to take part in the photocatalytic reaction.
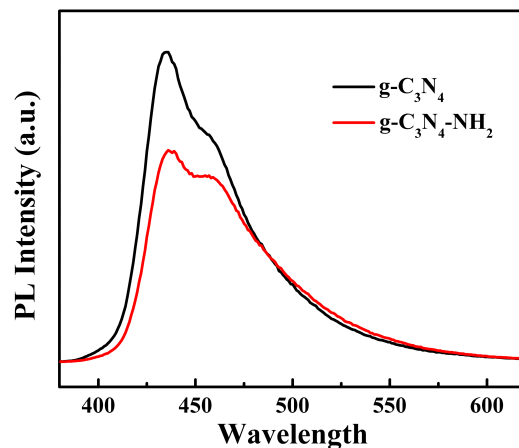
Figure 5.7. PL spectra of g-C$_3$N$_4$ and g-C$_3$N$_4$-NH$_2$ nanosheets.

In addition, photocurrent and electrochemical impedance spectroscopy (EIS) are effective tools for investigating the separation and transport efficiency of charge carriers in photocatalyst. Figure 5.8 suggested g-C$_3$N$_4$-NH$_2$ had higher separation and transport efficiency of electrons and holes than g-C$_3$N$_4$. As we can see, the photocurrent density (0.17 mA cm^{-2}) of g-C$_3$N$_4$-NH$_2$ is much higher than that (0.1 mA cm^{-2}) of g-C$_3$N$_4$. In addition, g-C$_3$N$_4$-NH$_2$ possesses smaller semicircle EIS than g-C$_3$N$_4$, suggesting that the rapid transfer of photogenerated of charge carriers (Figure 5.8b) occurred in g-C$_3$N$_4$-NH$_2$. This was the main reason why g-C$_3$N$_4$-NH$_2$ behaved superior photocatalytic inactivation ability compared to g-C$_3$N$_4$.
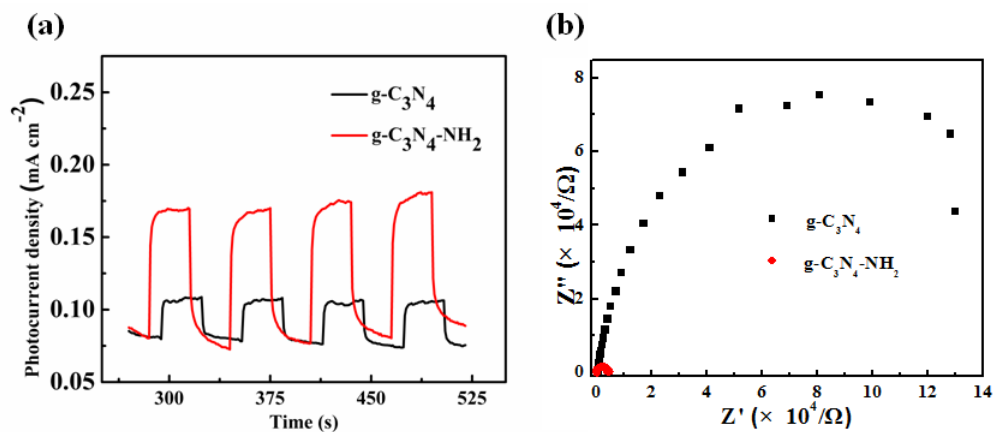
Figure 5.8. Transient photocurrent responses and EIS changes of bulk g-C$_3$N$_4$ and g-C$_3$N$_4$-NH$_2$ nanosheets.

5.5 Conclusions

G-C$_3$N$_4$ and g-C$_3$N$_4$-NH$_2$ were synthesized by thermal polymerization using urea as raw material. G-C$_3$N$_4$-NH$_2$ demonstrated more efficient photocatalytic inactivation against *S. aureus* than bulk g-C$_3$N$_4$ thanks to its high crystallinity and efficient separation and transportation of charge carriers. Importantly, this work would provide a reasonable way to combine g-C$_3$N$_4$ with NOC-terminated pre-polyurethane to fabricate stable photocatalytic antibacterial coating because rich amino groups of g-C$_3$N$_4$ can react with isocyanate groups of pre-polyurethane to form urea easily.

5.6 References

1. Yi, J.; El-Alami, W.; Song, Y.; Li, H.; Ajayan, P. M.; Xu, H., Emerging surface strategies on graphitic carbon nitride for solar driven water splitting. *Chemical Engineering Journal* **2019**, 122812.

2. Ismael, M.; Wu, Y., A mini-review on the synthesis and structural modification of g-C$_3$N$_4$-based materials, and their applications in solar energy conversion and environmental remediation. *Sustainable Energy & Fuels* **2019,** *3* (11), 2907-2925.

3. Xia, Y.; Xiao, K.; Cheng, B.; Yu, J.; Jiang, L.; Antonietti, M.; Cao, S., Improving artificial photosynthesis in carbon nitride by gas‐liquid‐solid Interface management for full light‐induced CO$_2$ reduction to C1‐C2 fuels and O$_2$. *ChemSusChem* **2020,** *13*, 1-6.

4. Liras, M.; Barawi, M.; Víctor, A., Hybrid materials based on conjugated polymers and inorganic semiconductors as photocatalysts: from environmental to energy applications. *Chemical Society Reviews* **2019,** *48* (22), 5454-5487.

5. Zhang, S.; Gu, P.; Ma, R.; Luo, C.; Wen, T.; Zhao, G.; Cheng, W.; Wang, X., Recent developments in fabrication and structure regulation of visible-light-driven g-C$_3$N$_4$-based photocatalysts towards water purification: a critical review. *Catalysis Today* **2019,** *335*, 65-77.

6. Dong, G.; Zhang, Y.; Pan, Q.; Qiu, J., A fantastic graphitic carbon nitride (g-C$_3$N$_4$) material: electronic structure, photocatalytic and photoelectronic properties. *Journal of Photochemistry and Photobiology C: Photochemistry Reviews* **2014,** *20*, 33-50.

7. Wang, W.; Yu, J. C.; Xia, D.; Wong, P. K.; Li, Y., Graphene and g-C$_3$N$_4$ nanosheets cowrapped elemental α-sulfur as a novel metal-free heterojunction photocatalyst for bacterial inactivation under visible-light. *Environmental science & technology* **2013,** *47* (15), 8724-8732.

8. Kang, S.; Zhang, L.; He, M.; Zheng, Y.; Cui, L.; Sun, D.; Hu, B., " Alternated cooling and heating" strategy enables rapid fabrication of highly-crystalline g-C$_3$N$_4$ nanosheets for efficient photocatalytic water purification under visible light irradiation. *Carbon* **2018,** *137*, 19-30.

9. Zhang, C.; Li, Y.; Shuai, D.; Shen, Y.; Xiong, W.; Wang, L., Graphitic carbon nitride (g-C$_3$N$_4$)-based photocatalysts for water disinfection and microbial control: A review. *Chemosphere* **2019,** *214*, 462-479.

10. Murugesan, P.; Moses, J. A.; Anandharamakrishnan, C., Photocatalytic disinfection efficiency of 2D structure graphitic carbon nitride-based nanocomposites: a review. *Journal of Materials Science* **2019,** *54* (19), 12206-12235.

11. Mei, L.; Zhu, S.; Yin, W.; Chen, C.; Nie, G.; Gu, Z.; Zhao, Y., Two-dimensional nanomaterials beyond graphene for antibacterial applications: current progress and future perspectives. *Theranostics* **2020,** *10* (2), 757.

12. Liu, H.; Ma, S.; Shao, L.; Liu, H.; Gao, Q.; Li, B.; Fu, H.; Fu, S.; Ye, H.; Zhao, F.; Zhou, J., Defective engineering in graphitic carbon nitride nanosheet for efficient photocatalytic pathogenic bacteria disinfection. *Applied Catalysis B: Environmental* **2020,** *261*, 118201.

13. Li, R.; Ren, Y.; Zhao, P.; Wang, J.; Liu, J.; Zhang, Y., Graphitic carbon nitride (g-C$_3$N$_4$) nanosheets functionalized composite membrane with self-cleaning and antibacterial performance. *Journal of hazardous materials* **2019,** *365*, 606-614.

14. Chen, Y.; Wang, P.; Liang, Y.; Zhao, M.; Jiang, Y.; Wang, G.; Zou, P.; Zeng, J.; Zhang, Y.; Wang, Y., Fabrication of a three-dimensional porous Z-scheme silver/silver bromide/graphitic carbon nitride@ nitrogen-doped graphene aerogel with enhanced visible-light photocatalytic and antibacterial activities. *Journal of colloid and interface science* **2019,** *536*, 389-398.

15. Adhikari, S. P.; Pant, H. R.; Kim, J. H.; Kim, H. J.; Park, C. H.; Kim, C. S., One pot synthesis and characterization of Ag-ZnO/g-C$_3$N$_4$ photocatalyst with improved photoactivity and antibacterial properties. *Colloids and Surfaces A: Physicochemical and Engineering Aspects* **2015,** *482*, 477-484.

16. Adhikari, S. P.; Awasthi, G. P.; Lee, J.; Park, C. H.; Kim, C. S., Synthesis, characterization, organic compound degradation activity and antimicrobial performance of g-C$_3$N$_4$ sheets customized with metal nanoparticles-decorated TiO$_2$ nanofibers. *RSC Advances* **2016,** *6* (60), 55079-55091.

17. Liu, C.; Tang, Y.-b.; Huo, P.-w.; Chen, F.-y., Novel AgCl/CNTs/g-C$_3$N$_4$ nanocomposite with high photocatalytic and antibacterial activity. *Materials Letters* **2019,** *257*, 126708.

18. Liu, B.; Han, X.; Wang, Y.; Fan, X.; Wang, Z.; Zhang, J.; Shi, H., Synthesis of g-C$_3$N$_4$/BiOI/BiOBr heterostructures for efficient visible-light-induced photocatalytic and antibacterial activity. *Journal of Materials Science: Materials in Electronics* **2018,** *29* (16), 14300-14310.

19. Xia, D.; Wang, W.; Yin, R.; Jiang, Z.; An, T.; Li, G.; Zhao, H.; Wong, P. K., Enhanced photocatalytic inactivation of Escherichia coli by a novel Z-scheme g-C$_3$N$_4$/m-Bi$_2$O$_4$ hybrid photocatalyst under visible light: the role of reactive oxygen species. *Applied Catalysis B: Environmental* **2017,** *214*, 23-33.

20. Tian, Y.; Zhou, F.; Zhan, S.; Zhu, Z.; He, Q., Mechanisms on the enhanced sterilization performance of fluorocarbon resin composite coatings modified by g-C$_3$N$_4$/Bi$_2$MoO$_6$ under the visible-light. *Journal of Photochemistry and Photobiology A: Chemistry* **2018,** *350*, 10-16.

21. Ouyang, K.; Dai, K.; Chen, H.; Huang, Q.; Gao, C.; Cai, P., Metal-free inactivation of E. coli O157: H7 by fullerene/C$_3$N$_4$ hybrid under visible light irradiation. *Ecotoxicology and Environmental Safety* **2017,** *136*, 40-45.

22. Dai, K.; Lu, L.; Liu, Q.; Zhu, G.; Wei, X.; Bai, J.; Xuan, L.; Wang, H., Sonication assisted preparation of graphene oxide/graphitic-C$_3$N$_4$ nanosheet hybrid with reinforced photocurrent for photocatalyst applications. *Dalton Transactions* **2014,** *43* (17), 6295-6299.

23. Yao, L. H.; Wei, D.; Ni, Y. M.; Yan, D. P.; Hu, C. W., Surface localization of CdZnS quantum dots onto 2D g-C3N4 ultrathin microribbons: highly efficient visible light-induced H2-generation. *Nano Energy* **2016,** *26*, 248-256.

24. Zhang, L.; Jin, Z.; Huang, S.; Huang, X.; Xu, B.; Hu, L.; Cui, H.; Ruan, S.; Zeng, Y.-J., Bio-inspired carbon doped graphitic carbon nitride with booming photocatalytic hydrogen evolution. *Applied Catalysis B: Environmental* **2019,** *246*, 61-71.

6 Summary and Recommendations

6.1 Summary

In this thesis, the syntheses and structural characterization of PTET-T-COOH powder, PTET-T-COOH/PU coating and g-C$_3$N$_4$ based photocatalysts are reported. The photocatalytic antibacterial performance and mechanism of these three systems towards S. *aureus* were investigated. The main conclusions are listed as follows:

A novel polythiophene derivative, PTET-T-COOH, was designed and synthesized. The chemical structure of PTET-T-COOH was confirmed by FTIR, NMR, SEM and XPS techniques. PTET-T-COOH exhibited potent photocatalytic disinfection activity against gram-positive bacteria S. *aureus* and S. *suis*. Upon 2 h visible light exposure, 99.99 % of both bacteria were killed by PTET-T-COOH powder in solution with a very low concentration of 0.1 mg/mL. PTET-T-COOH demonstrated 5.9-log and 5.1-log inactivation of S. *aureus* and S. *suis* concentration, respectively. Rabbit plasma test and fluorescence microscopy observation were used to evaluate the disinfection effects of PTET-T-COOH against S. *aureus.* Electrons and singlet oxygen played vital roles in photocatalytic antibacterial process which was confirmed by trapping experiments and ESR measurements. This result provided neutral polythiophene derivative with promising photocatalytic disinfection application prospect.

Efficient and stable photocatalytic antimicrobial bilayer coatings were designed and fabricated. The protective layer of PU and photoactive layer of PTET-T-COOH/PU were both fabricated by spin coating on glass substrate in sequence. The formation of chemical bonding between carboxyl groups from PTET-T-COOH and isocyanate groups from pre-polyurethane was confirmed by ATR-FTIR and XPS techniques. Antimicrobial coatings can kill S. aureus completely with 7-log inactivation of S. *aureus* concentration upon 4 h light exposure for the first three recycling runs. The transparent antimicrobial bilayer coating was achieved by optimizing the fabrication process and behaved 5.1-log inactivation against S. *aureus* upon 4 h visible light exposure. This work could be of great

significance for exploring highly efficient antimicrobial coatings for their practical applications.

To further improve the photocatalytic disinfection performance of bulk g-C$_3$N$_4$, g-C$_3$N$_4$-NH$_2$ nanosheets with rich amino groups was fabricated by thermal polymerization. As expected, g-C$_3$N$_4$-NH$_2$ nanosheets demonstrated better antibacterial performance than bulk g-C$_3$N$_4$ owing to its high crystallinity and efficient separation and transportation of charge carriers which were confirmed by XRD, fluorescent emission, photocurrent and EIS measurements. Most importantly, this work could provide a strategy for fabricating stable g-C$_3$N$_4$ based coatings because NH$_2$- in g-C$_3$N$_4$-NH$_2$ can react with isocyanate groups in pre-polyurethane to form urea at low temperature.

6.2   Recommendations

Some suggestions for future work are listed as follows:

Polymer PTET-T-COOH powder and PTET-T-COOH/PU coating exhibit high photocatalytic antimicrobial activation against gram-positive bacteria such as *S. aureus* and *S. suis,* other gram-positive bacteria such as diplococcus and bacillus anthracis should be chosen to testify whether these two systems are effective to all gram-positive bacteria. In addition, these two systems have no effect on *E. coli*. Other gram-negative bacterial can be tested and the mechanism of selectively photocatalytic disinfection can be examined.

Swelling problems appeared after PTET-T-COOH/PU coating was applied in solution. So, the fabrication process of PU can be further optimized to obtain stable antimicrobial coating without deformation.

G-C$_3$N$_4$-NH$_2$ possesses rich -NH$_2$ groups and incorporation of g-C$_3$N$_4$-NH$_2$ with polyurethane via generation of urea to fabricate stable photocatalytic antibacterial coating can be followed. In addition, its photocatalytic disinfection performance needs to be further improved by modification such as quantum dots.

In addition, future directions for research can be expanded to antibacterial or antiviral applications in areas where LED or indoor lighting can be used as irradiation source.

Curriculum Vitae

Name: Chunbo Liu

Post-secondary   Jilin Normal University
Education and   Siping, Jilin, China
Degrees: 1993-1997 B.A.

Jilin Normal University
Siping, Jilin, China
2002-2004 M.A.

Changchun Institute of Optics, Fine Mechanics and Physics,
Chinese Academy of Science
Changchun, Jilin, Chian
2004-2007 Ph.D.

University of Western Ontario
London, Ontario, Canada
2018-2020 M.E.Sc.